Characterization of Nanofiltration membranes

J.M.M. Peeters

39

CHARACTERIZATION

OF

NANOFILTRATION MEMBRANES

PROEFSCHRIFT

ter verkrijging van
de graad van doctor aan de Universiteit Twente,
op gezag van de rector magnificus,
prof. dr. F.A. van Vught,
volgens besluit van het College van Promoties
in het openbaar te verdedigen
op vrijdag 31 januari te 16.45 uur.

door

Johanna Mathea Maria Peeters

geboren op 17 juli 1967
te Stramproy

Dit proefschrift is goedgekeurd door de promotores prof. dr. ir. H. Verweij en prof. dr. H. Strathmann en de assistent-promotor dr. ing. M.H.V. Mulder.

Dankwoord

Zonder andere mensen tekort te willen doen, wil ik een aantal mensen in het bijzonder bedanken voor hun steun tijdens mijn promotieonderzoek:
Prof. Henk Verweij en prof. Heiner Strathmann voor de begeleiding op wetenschappelijk gebied en voor het vasthouden van de grote lijnen,
Marcel Mulder en Klaas Keizer voor de 'dagelijkse' begeleiding en alles wat daar nog bij kwam,
José Nolten voor al die dagen, weken en maanden van metingen doen, waarvan heel wat resultaten in dit proefschrift te vinden zijn,
Bert Damink, Carla Koopman, Simona Mesaric, Jasper de Mos, Niklas Olsson en Carla Reitsma voor de grote bijdrage van hun afstudeer- of stagewerk aan mijn promotieonderzoek,
Jeroen Boom voor het onvermoeibaar schrijven van en schaven aan het computerprogramma waarmee berekingen uit hoofdstuk 2 en 6 gedaan zijn,
Chantal van Dinteren, Bert Pennings, Elise Römer en Mirjam Verbruggen, die als vrijwilliger soms kort en soms behoorlijk lang aan mijn onderzoek meehielpen, en gelukkig allemaal aan een baan kwamen,
Jeroen van Beckum, Edwin van der Steeg, Bart Velner, Marieke ten Have, Peter Paauw, John Glorie en Maikel van Bree voor het praktische werk in het kader van de technische opdracht van de studie Technische Bedrijfskunde,
Astrid Bulte, Warner Nauta en Josef Thesing voor alle zakelijke en niet-zakelijke gesprekken die op kamer CT2160 gevoerd werden,
Jeroen Boom, Thonie van den Boomgaard en Antoine Kemperman voor het plezierig samen organiseren van het PMST'94,
Greet van der Voort voor de gezamenlijke afhandeling van alle administratieve zaken die met dit congres te doen hadden,
Antoine Kemperman, Carla Koopman en Warner Nauta voor het kritisch lezen van het manuscript,
John Heeks voor het verrichten van hand- en spandiensten,
de leden van de vakgroepen Membraantechnologie en Anorganische Materiaalkunde voor de plezierige samenwerking,
Karin voor het meedenken over de lay-out,
pap en mam voor de noodzakelijke basis en de onvoorwaardelijke steun
en
Tony voor ... alles!

Acknowledgement

The European Commission is highly acknowledged for supporting the work described in this thesis in the framework of the 'Science' programme (no.EBRSCI*CT920805).

Peeters, Johanna Mathea Maria

Characterization of nanofiltration membranes/ Johanna Mathea Maria Peeters. -[S.l. : s.n.]. - Ill.
Thesis Enschede. - With Ref. - With Summary in Dutch.
ISBN 90 365 09157

Summary

Nanofiltration is a pressure-driven process which is used to separate multi-valent ions and small organic molecules from water. The driving force for this process is a hydrodynamic pressure difference. Although the applications of nanofiltration membranes cover a broad field, like for instance water softening and the instantaneous concentration and desalting of cheese whey, the separation mechanism of these membranes is not exactly known. Most probably, charge, affinity and size effects play a role in the separation.

In this thesis the separation mechanism of nanofiltration membranes has been investigated using different characterization techniques. Both polymeric and ceramic membranes have been used.

In Chapter 1 of this thesis an overview is given of characterization methods that may be used for nanofiltration membranes. Retention measurements are often used as characterization method, in which the separation of a model solute is determined. Both charged and uncharged solutes can be used as a model solute. In case of charged solutes the charge as well as the size of the solutes influence the separation, whereas in case of uncharged particles the solute size and affinity between membrane and solute play a role. The separation of charged solutes is determined by the membrane charge as well. To quantify the membrane charge characterization techniques like titration, electrokinetic measurements and membrane potential measurements can be used.

In Chapter 2 both the distribution of solutes between membrane and solution and a theoretical description of transport of solutes through the membrane have been described. The concentration of solutes in the membrane may be different from that in the solution because of steric hinderance and affinity effects. For charged systems, the Donnan potential can induce a distribution between membrane and solution as well.

To describe the solute transport theoretically, the extended Nernst-Planck equation can be used. This phenomenological equation does not require any assumption on membrane morphology. Some numerical calculations have been performed with this equation to show the influence of model parameters like the membrane charge, the membrane thickness and the diffusion coefficients of the various components in the solution.

Chapter 3 describes the experimental data of retention measurements with different salt solutions for various nanofiltration membranes. Retention measurements with single salt solutions show that the nanofiltration membranes investigated can be divided in two categories, i.e., membranes for which the charge effects determine the salt separation and membranes for which charge effects determine partially the separation, besides size effects. The first category has been subdivided in positively and negatively charged membranes. Measurements with salt mixtures that consist of a mono-valent and bi-valent anion with a common cation or of a mono-valent and bi-valent cation with a common anion show that with increasing concentration of the bi-valent ion, the lower the retention of the mono-valent ion with the same valency will be. Even negative retentions for these mono-valent ions have been found, both for the anion and for the cation mixtures.

Retention measurements with saccharides and dendrimers have been described in Chapter 4. Both solutes have been chosen as uncharged model solutes. Dendrimers, which are a new type of molecules with a spherical shape, appear to be not very well applicable as model solutes for separation measurements with nanofiltration membranes. This is mainly caused since their size is pH-dependent.

Chapter 5 describes the results of streaming potential measurements that have been performed to determine the surface charge of the membranes. These have been carried out along the membrane surface and result in zeta potentials. The zeta potentials decrease at increasing electrolyte concentration, whereas the kinetic surface charge densities of the membranes, which is dependent on both the zeta potential and the ionic strength, increases. The increase of the kinetic surface charge density can be described by assuming that ions adsorb at the membrane surface according to a Freundlich isotherm. The fixed membrane charge that has been calculated by this model is for all membranes small compared to the adsorbed charge.

The membrane surface charge has been estimated by titrations of the membrane toplayer as well. All membranes contain small amounts of (weak) acidic groups.

Chapter 6 compares the experimental results of the retention measurements with saccharides (Chapter 4) and salts (Chapter 3) and the theoretical calculations with these solutions. The results of the saccharide retention measurements can be described well by the phenomenological equation of Kedem and Katchalsky. However, it is not possible to determine membrane pore sizes from the calculated parameters.

The experimental results of the salt retention measurements with both single salt solutions and salt mixtures can be modeled well by the extended Nernst-Planck equation. The modeling results in a membrane charge and a membrane thickness. The negative retentions of chloride ions in an anion mixture can be described by the model, however, the negative retentions of sodium ions in a cation mixture cannot.

The final chapter evaluates the different characterization methods from this thesis by comparing the properties and parameters that have been determined by these techniques.

Samenvatting

Nanofiltratie is een drukgedreven membraanproces dat toegepast wordt om multivalente ionen en kleine organische moleculen uit water te verwijderen. Hoewel nanofiltratie talrijke toepassingen kent, variërend van waterontharding tot de verwijdering van oliedruppels uit het spoelwater van een boorplatform, is het precieze werkingsmechanisme van deze membranen niet bekend. De scheiding vindt plaats op grond van verschillende mechanismen zoals een zeefmechanisme, een oplos-diffusie-mechanisme en ladingseffecten, afhankelijk van het membraan en de te scheiden opgeloste stoffen.

Het doel van het in dit proefschrift beschreven onderzoek is om het scheidingsmechanisme van nanofiltratiemembranen te doorgronden door deze membranen op verschillende manieren te karakteriseren. Hierbij zijn zowel polymere als keramische membranen gebruikt.

In het eerste hoofdstuk van dit proefschrift wordt een overzicht gegeven van mogelijke karakteriseringsmethoden. Retentiemetingen zijn een veel gebruikte karakteriseringstechniek waarbij de mate van de scheiding van modelstoffen door een membraan bepaald wordt. Als modelstof kunnen zowel geladen als ongeladen deeltjes gebruikt worden. In het eerste geval zijn de lading en de grootte van belang voor de scheiding. Ook de op het membraan aanwezige lading speelt hierbij een rol. Om de grootte van deze lading te bepalen kunnen verschillende methoden ingezet worden, zoals titratie, elektrokinetische metingen en membraanpotentiaal-metingen. Voor het tweede geval zijn de grootte van de deeltjes en de affiniteit tussen de deeltjes en het membraan van belang.

In Hoofdstuk 2 worden zowel de verdelingsevenwichten van deeltjes tussen het membraan en de oplossing als de theoretische beschrijving van het deeltjestransport door het membraan behandeld. De concentratie van deeltjes in het membraan kan afwijken van die in de oplossing door het optreden van sterische hindering, door een verschil in affiniteit of door de Donnan potentiaal die optreedt in het geval van geladen systemen. Om het deeltjestransport door een nanofiltratiemembraan theoretisch te beschrijven kan de uitgebreide Nernst-Planck vergelijking gebruikt worden. Het gebruik van deze fenomenologische vergelijking impliceert geen vooronderstellingen over de morfologie van het membraan. Met deze vergelijking is een aantal theoretische berekingen uitgevoerd om de invloed van parameters zoals de dikte van het membraan, de lading van het membraan en de diffusiecoëfficiënten van de verschillende componenten te onderzoeken.

In Hoofdstuk 3 worden experimentele resultaten van retentiemetingen met verschillende zoutoplossingen voor een aantal nanofiltratiemembranen beschreven. Op grond van metingen met een enkel zout, zijn de onderzochte nanofiltratiemembranen in twee categorieën verdeeld: i) membranen waarbij ladingseffecten bepalend zijn voor de zoutscheiding, ii) membranen waarvoor ladingseffecten slechts mede bepalend zijn, naast de grootte-effecten. De eerste categorie is verder opgesplitst in positief en negatief geladen membranen. Metingen met zoutmengsels, bestaande uit een één- en tweewaardig anion met een gemeenschappelijke kation, danwel een één- en tweewaardig kation met een gemeenschappelijke anion, wijzen uit dat met toenemende concentratie tweewaardige ionen in het mengsel, de retentie van het

éénwaardige ion met eenzelfde valentie afnam. Zelfs negatieve retenties voor deze éénwaardige ionen zijn gevonden, zowel in het geval van het anion- als in het geval van het kationmengsel.
Retentiemetingen met sacchariden en dendrimeren worden in Hoofdstuk 4 beschreven. Beide stoffen zijn gekozen als modelstof voor ongeladen moleculen. Dendrimeren, een nieuwe klasse van moleculen met een bolvormige structuur, blijken niet geschikt te zijn als modelstof voor scheidingsmetingen met nanofiltratiemembranen. Dit wordt vooral veroorzaakt doordat de grootte van deze moleculen afhankelijk is van de pH.
In Hoofdstuk 5 worden de resultaten van stromingspotentiaalmetingen besproken op basis waarvan de oppervlaktelading van de onderzochte membranen bepaald kan worden. De stromingspotentiaalmetingen zijn uitgevoerd langs het membraanoppervlak en resulteren in zeta-potentialen. Voor de zeta-potentialen geldt dat hoe hoger de zoutconcentratie des te lager de zeta-potentiaal. Voor de kinetische oppervlaktelading, die afhankelijk is van de zeta-potentiaal en de zoutconcentratie, geldt dat deze juist groter wordt met toenemende zoutconcentratie. De afhankelijkheid van de kinetische oppervlaktelading van ionsterkte is beschreven door aan te nemen dat ionen aan het membraanoppervlak geadsorbeerd worden volgens een Freundlich-isotherm. De vaste membraanlading, die met behulp van dit model berekend is, is voor alle membranen klein ten opzichte van de geadsorbeerde lading.
De lading van de polymere membranen waarmee stromingspotentiaalmetingen uitgevoerd zijn is ook bepaald met titraties van de toplaag van het membraan. Op alle membranen blijken (zwak) zure groepen aanwezig te zijn, maar steeds in lage concentraties.
In Hoofdstuk 6 zijn de experimentele resultaten van de retentiemetingen met sacchariden (Hoofdstuk 4) en zouten (Hoofdstuk 3) naast theoretische berekeningen aan deze systemen gelegd. De resultaten van de saccharide-retentiemetingen kunnen goed beschreven worden met de fenomenologische vergelijking van Kedem en Katchalsky. Het is echter niet mogelijk om poriegrootten van de membranen af te leiden uit de berekende parameters.
De experimentele resultaten van de zoutscheidingsmetingen kunnen goed gemodelleerd worden met de uitgebreide Nernst-Planck vergelijking. Dit geldt voor zowel de metingen aan zoutoplossingen met een enkel zout als voor die met mengsels. De modellering resulteert in een lading van het membraan en in een membraandikte. De negatieve retenties van chloride-ionen in een anionmengsel kunnen met behulp van het model beschreven worden, de negatieve retenties van natrium-ionen in een kationmengsel echter niet.
Het afsluitende hoofdstuk evalueert de verschillende karakteriseringsmethoden, die in dit proefschrift beschreven zijn, door de bepaalde eigenschappen en parameters van de nanofiltratiefiltratiemembranen met elkaar te vergelijken.

Contents

CHAPTER 1

Characterization of nanofiltration membranes

ABSTRACT

Nanofiltration membranes can be used to separate multivalent ions and small organic molecules from a solvent. The separation of these membranes is thought to be achieved by a combination of size and charge effects.

Characterization of nanofiltration membranes can be performed by the investigation of the separation mechanism, which may result in knowledge of the membrane morphology and membrane charge. Retention measurements are a valuable tool to reveal the separation characteristics of membranes. For this purpose both uncharged molecules and salts can be used as model solutes. The pore size of the mesoporous membranes can be determined by permporometry. The most important techniques to investigate the membrane charge are titration, membrane potential measurements and electrokinetic measurements.

1.1 INTRODUCTION

Membranes are selective barriers that can be used to separate mixtures, e.g., of liquids or gases, into a concentrated and a diluted stream. The driving force for membrane separation is a chemical potential difference between the two phases at each side of the membrane. This potential difference can be the result of a pressure difference, a concentration difference, a temperature difference, a difference in electrical potential or a combination of each. The driving force is often used to classify membrane processes.
Liquid separation can be carried out by pressure-driven processes, like microfiltration, ultrafiltration and reverse osmosis. These techniques have reached maturity and are state-of-the-art technologies. A relatively new pressure-driven process is nanofiltration, which separates organics with a low molecular weight and multivalent ions from a solvent. Although nanofiltration membranes have been applied in several areas, such as in the field of water softening, in the dairy and metal industry, the transport mechanism of these membranes has not been fully understood yet [1,2].

In this chapter, firstly, the properties of nanofiltration membranes will be described. Then, characterization methods for nanofiltration membranes will be discussed, which can give insight in the mechanism of solute separation of these membranes.

1.2 PRESSURE-DRIVEN MEMBRANE PROCESSES

Membrane processes for liquid separation that use a pressure difference as a driving force can be subdivided into four categories, i.e., microfiltration (MF), ultrafiltration (UF), nanofiltration (NF) and reverse osmosis (RO). Although these separation techniques are related to each other, each of them has its specific characteristics. The main features of the four pressure-driven processes are summarized in Table 1.1.

***Table 1.1:** Characteristics of pressure-driven membrane processes*

process	pore size	species to be retained	type of transport
MF	0.05-10 μm	bacteria, yeast	convective
UF	2-100 nm	macromolecules, colloids	convective
NF	0.5-3 nm	low molecular organics, multivalent ions	convective/diffusive
RO	not relevant	ions	convective/diffusive

Nanofiltration forms an intermediate process between ultrafiltration and reverse osmosis. A

schematic drawing of the separation characteristics of nanofiltration membranes is given in Figure 1.1.

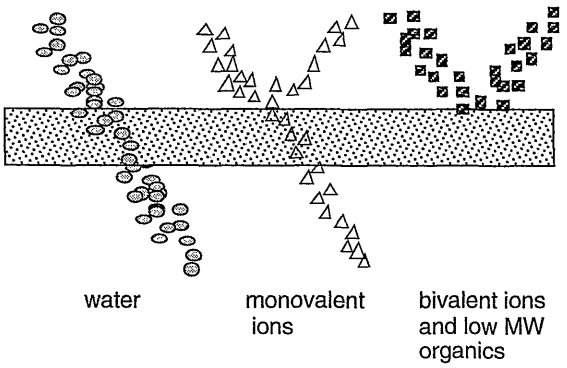

Figure 1.1: *Schematic drawing showing the separation characteristics of nanofiltration membranes*

Ultrafiltration membranes are porous membranes, which means that they have a distinct, permanent porous network through which transport occurs [3]. Polymeric reverse osmosis membranes have no macroscopic pore structure, but consist of a polymer network in which solutes can be dissolved [4]. This solvent-swollen network may be considered as a porous system comparable to dialysis membranes, although the structure of the latter is more loose than that of nanofiltration membranes. Because of the flexibility of the polymer chains, the pores in these membranes are neither fixed in place nor in time.
All ceramic and some polymeric nanofiltration membranes (for instance the cellulose acetate-based nanofiltration membranes which are formed by annealing of ultrafiltration membranes) are considered as porous, but several polymeric nanofiltration membranes are regarded as 'dense', which means that no fixed pores are present in the membrane. The latter membranes consist of a network structure, that can be either charged or uncharged [5,6].
In several transport models for nanofiltration the pore size is used as parameter to describe the morphology of the membrane [7-10]. However, this concept of pores may be considered as hypothetical for several polymeric nanofiltration membranes [9]. Bowen and Mukthar mentioned that the determination of an effective pore size by transport models should not mean that those pores really exist in nanofiltration membranes. The hinderance to transport is the same for ions passing through the polymer network of a specific membrane as for ions passing through pores having these effective sizes.

1.2.1 Nanofiltration

Nanofiltration is a recently introduced term in membrane separation. In 1988, Eriksson was one of the first authors using the word 'nanofiltration' explicitly [11]. Some years before, FilmTec started to use this term for their NF50 membrane which was supposed to be a very

loose reverse osmosis membrane or a very tight ultrafiltration membrane [12]. Since then, this term has been introduced to indicate a specific domain of membrane technology in between ultrafiltration and reverse osmosis. But the history of nanofiltration goes back further in time.
In 1970 Cadotte showed that reverse osmosis membranes could be made out of polyethyleneimine and toluenediisocyanate, forming a polyurea. The NS100 membrane he made was different in several aspects from the then existing reverse osmosis membranes. It was the first reverse osmosis membrane not made by a phase inversion process using cellulose acetate or polyamide. Furthermore, it was the first membrane showing a high salt retention formed by interfacial polymerization. Compared to the cellulosic acetate reverse osmosis membranes, the NS100 membrane showed a higher retention for small organic molecules and a higher water permeability as well [13].
Other combinations of reactants resulted in the formation of interfacially polymerized polyamide membranes with high water fluxes and high salt permeabilities as well. Riley and co-workers at Fluid Systems UOP developed two polymeric membranes from polyepiamine, that were both commercialized, one which was reacted with isophtaloyl chloride and the other with toluenediisocyanate [14,15].
Later, membranes made out of piperazine, an amine *mono*mer, combined with acylchlorides showed good salt separation. Membranes formed from piperazine and different ratios of isophtaloyl chloride (IPC)/trimesoyl chloride (TMC), were used for test runs with sea water (3.5% NaCl, 102 atm., 25°C) and with brackish water (0.5% $MgSO_4$, 13.6 atm., 25°C). The results of these experiments are shown in Table 1.2.
As can be seen from this table, the change in the ratio diacyl/triacyl chloride had hardly any influence on the salt retention of $MgSO_4$, whereas the retention of NaCl dropped when the molar fraction of isophtaloylchloride was decreased. The permeate flux showed a maximum as a function of the ratio diacyl/triacyl chloride.

***Table 1.2:** Flux and retention data of different polypiperazineamide membranes [13]*

Acyl halogene		Sea water[a)]		Brackish water[b)]	
fraction IPC	fraction TMC	Flux (m^3/m^2.day)	Salt retention (%)	Flux (m^3/m^2.day)	Salt retention (%)
1	0	1.0	98	0.2	99.2
0.9	0.1	1.3	96	0.7	99.0
0.8	0.2	3.0	78	2.4	99.9
0.67	0.33	3.8	65	3.1	99.6
0.5	0.5	3.9	64	1.3	99.9
0	1	3.3	68	1.1	99.3

a) c_{NaCl} =3.5 w%; ΔP=102 atm.; T=25°C
b) c_{MgSO4} =0.5 w%; ΔP=13.6 atm.; T=25°C

The membrane made of only piperazine and trimesoylchloride exhibited low retentions for monovalent anions (chloride) and high retentions for bivalent anions (sulphate), whereas no

difference was found in retention between monovalent cations (sodium) and bivalent cations (magnesium). This indicated that the NS300 membrane, as the membrane was called, was selective for anions, caused by the negatively charged polypiperazine toplayer. According to Cadotte, this negative charge could be the result of a partial hydrolysis of acylchloride into carboxylic groups. The chemical structure of the NS300 membrane is shown in Figure 1.2.

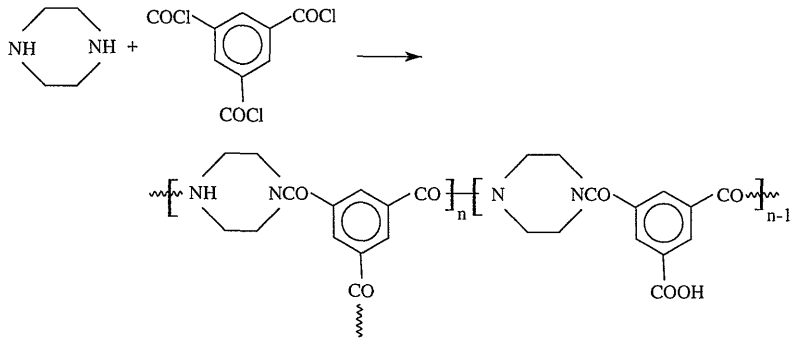

Figure 1.2: *Chemical structure of NS300 membrane, from piperazine and trimesoylchloride [13]*

Some of the earliest nanofiltration membranes, like the NF40 membrane of FilmTec, the NTR7250 of Nitto-Denko and the UTC20 and UTC60 of Toray, are formed by a comparable synthesis route as the NS300 membrane [6,13].

In general, interfacially polymerized membranes are made by impregnating a porous ultrafiltration membrane, most often polysulfone, with a solution containing a monomeric amine (liquid1 + reactant A). Then, the substrate is put in contact with an organic solution containing the acylchlorides (liquid2 + reactant B). By interfacial polycondensation a thin layer is formed, the actual membrane. A schematic drawing of this process is shown in Figure 1.3.

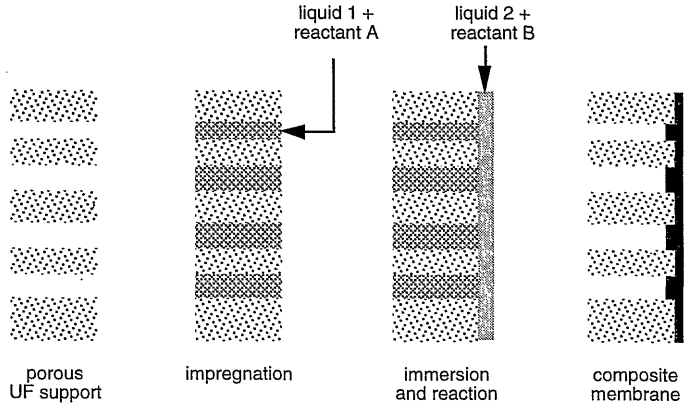

Figure 1.3: *Schematic illustration of interfacial polymerization method*

Not only Cadotte, but also Jonsson and Kurihara described already in the seventies and early eighties the characteristics of what is now called nanofiltration membranes [16-18]. They classified these membranes as 'open', 'medium tight' or 'low pressure' reverse osmosis membranes. The charged ultrafiltration membranes described by Bhattacharyya, Tsuru and co-workers, Jitsuhara and Kimura showed at least in case of salt retention measurements the same features as nanofiltration membranes [19-23]. All these membranes will be classified in this thesis as nanofiltration membranes.

In the field of inorganic membranes, high water fluxes combined with moderate NaCl retentions have been obtained by dynamically formed ZrO_2 membranes and by glass membranes. Except for one case in which a dynamically formed zirconia layer was coated and stabilized by a polyacrylic acid, these membranes were never used on a large scale [13,24-26]. Only recently, ceramic composite membranes with nanofiltration characteristics are available. These membranes are reported to have pore sizes in the range of 0.5 to 2 nm, showing high retentions for organics with a molecular weight larger than 500 g/mol, high retentions for bivalent ions, and moderate retentions for monovalent ions [27-29]. The salt retentions are resulting from charge interactions between the ions and the ceramic membrane, which consists of charged particles with a surface potential dependent on the pH of the solution [30]. The water permeabilities of these ceramic membranes are relatively low compared to the polymeric nanofiltration membranes.

Ceramic membranes have a porous structure, which remains stable irrespective of its environment. Under moderate conditions, the size and amount of the pores is fixed, contrarily to the swelling of a polymeric membrane which may depend on factors like electrolyte strength and solvent type.

Ceramic nanofiltration membranes are composite membranes, consisting of a macroporous support, with pores larger than 50 nm, and a microporous toplayer, i.e., pores smaller than 2 nm. Sol-gel processing is the main technique to make the ceramic toplayer. By this technique, it is possible to make layers of orderly packed particles with a uniform size. These layers are formed out of suspensions of precursor materials, sols, that are often electrochemically stabilized [31]. Thin colloidal films can be formed by dipcoating or filmcoating. When drying such a film, gelation will occur and after calcination, a membrane will result. Sol-gel membranes can be made out of, e.g., alumina, zirconia, titania and silica [32].

Nanofiltration membranes are being used in several areas, e.g., in water treatment, in food, textile and mining industries, see for instance [1,11,12,33-38]. Several membrane manufacturers produce nanofiltration membranes. In Table 1.3 an overview of nanofiltration membrane manufacturers is given, the membrane materials they use and the module configuration they provide [39]. As shown in this table, manufacturers supply both polymeric and ceramic nanofiltration membranes.

Table 1.3: *Nanofiltration membrane manufacturers, membrane materials and configuration [39]*

Manufacturer	membrane material	configuration
Advanced Membrane Technology	SPSf/composite	sw
Celfa	CA/comp. of PA-PSf	flat sheet
Desalination Systems	CA/PA	sw
Dow	PA	sw
Fluid Systems	CA/PA	sw
Hoechst	CA/PES	flat sheet/sw
Hydranautics	composite	sw
Membrane Systems Kiryat Weizmann	composite	flat sheet/sw/tubular
Millipore	PA	flat sheet/sw
North Carolina SRT	several materials	flat sheet
NWW Acumem	PSf	sw
Osmonics	CA/PA/propr.polymer	sw
Osmota	composite	flat sheet/sw/tubular
PCI	several polymers, ceramics	tubular
Sempas	PSf/PA	sw
Stork Friesland	PA	tubular
TechSep	zirconia	
Toray	PA, PES	sw
Tri-Sep	PA	sw
US Filter SCT	titania	tubular
Wheelabrator	PVDF/PSf/PAN/ceramics	tubular
X-Flow	PES	sw

membrane material: CA: cellulose acetate, PA: polyamide, PAN: polyacrylonitrile, PES: polyethersulfon, PSf: polysulfon, PVDF: polyvinylidenefluoride, SPSf: sulfonated polysulfon, *configuration:* sw: spiral wound

1.3 CHARACTERIZATION OF NANOFILTRATION MEMBRANES

Different characterization methods can be used to compare nanofiltration membranes. These methods provide information on structure and performance related properties of the membranes. One of the aims of membrane characterization is to relate the morphological properties of the membranes to their separation characteristics, although this often appears to be difficult. When this relationship is known, the morphology of the membranes can be changed to obtain better separation characteristics or to be adapted for specific applications.
Accurate characterization of membranes often poses problems because, in the first place, the parameters determined may depend on the characterization method and on the process conditions used and, in the second place, often a model for the membrane morphology is used to interpret the experimental data, implying a certain membrane structure.

A difference should be made between polymeric and ceramic nanofiltration membranes, when

selecting appropriate characterization methods for nanofiltration membranes. In case of a ceramic membrane, the morphology remains unchanged, irrespective of its wet or a dry state. In case of a polymeric membrane, a morphological change takes place due to swelling when a dry membrane is immersed in water. When drying the swollen membrane, the morphology may change again and often this occurs irreversibly, because of the high capillary forces that play a role upon drying. Because of the dependence of the morphology of polymeric nanofiltration membranes on their environment, these membranes should be preferably investigated in the same state as in which they are applied, i.e., in the wet state. For ceramic membranes, there is no preference for either wet or dry state characterization.

Nanofiltration membranes can be divided into two categories concerning their structures, as mentioned before, i.e., porous membranes and membranes with a swollen-network structure. Both types can be either charged or uncharged, although no uncharged porous membranes are known that show nanofiltration properties.
The porous and the network-swollen nanofiltration membranes have the same separation performance, although their mechanism is different. Uncharged solutes will be separated by a sieving mechanism in case of porous membranes, whereas in case of a swollen network a solution-diffusion type of mechanism will determine the transport. This is schematically shown in Figure 1.4.

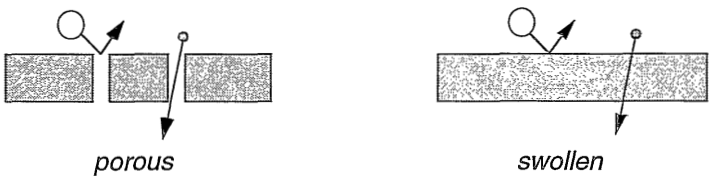

Figure 1.4: *Schematic drawing of separation of uncharged molecules by nanofiltration membranes. At the left-hand side a porous membrane and at the right-hand side a membrane with a network swollen structure*

A charged porous membrane will retain charged solutes by repulsion between the membrane and the solute and, possibly, by sieving. In case of a swollen network, again a solution-diffusion type of mechanism will cause separation, which is for a charged swollen network combined with charge effects (see Figure 1.5).

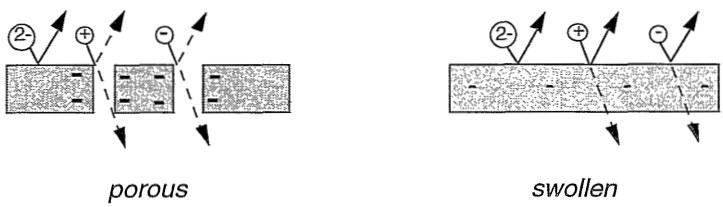

Figure 1.5: *Schematic drawing of separation of ions by nanofiltration membranes. At the left-hand side a (negatively) charged porous membrane and at the right hand-side a negatively charged membrane with a network swollen structure*

Because of the possible variations in membrane structure, the characterization of nanofiltration membranes has similarities to both the characterization of (charged) ultrafiltration and reverse osmosis membranes. In case of ultrafiltration membranes an important characteristic parameter is the cut-off value, which indicates the molecular mass of molecules that are retained for more than 90% by the membrane. For charged ultrafiltration membranes the surface charge density or the ion exchange capacity are important parameters as well. Reverse osmosis membranes are mostly characterized by performance related properties, of which the (overall) salt retention is the most important. With respect to salt retention characteristics, nanofiltration membranes can be classified as reverse osmosis membranes with a low retention. This retention is highly dependent on the feed concentration, unlike in reverse osmosis.
To be able to compare different nanofiltration membranes, characterization techniques should be used that can be applied for both porous charged membranes and membranes with a charged or uncharged swollen network structure.

As the effective pore size of nanofiltration membranes is very small, at least smaller than 3 nm, the interactions between molecules and pore walls become important. At this small scale it should be noted that several macroscopic laws cannot be used anymore. For instance, the law used to describe capillary condensation (Kelvin's law) becomes without meaning if the pores which are filled by condensate have dimensions smaller than the condensate molecular size. Furthermore, if the Debije length of a certain electrolyte solution (which is a measure for the distance over which the electric potential of ions extends with appreciable strength) is about as large as the pore size, the equation which is used to relate electrokinetic phenomena to the potential of a surface, the Helmholtz-Smoluchowski equation, cannot be used anymore. Even the equation which is used to relate the solvent flux to different morphological membrane parameters, the Poisseuille equation, cannot be used without assuming that the liquid viscosity in these small membrane pores equals the bulk viscosity of the solvent.

Although the use of nanofiltration membranes has grown very fast during last years, until now no extended studies have been carried out on characterization methods for these membranes. Therefore, in this thesis several characterization techniques were compared and related to each other, to obtain parameters describing or influencing the separation behavior of nanofiltration membranes, irrespective of their morphological structure.

1.3.1 Characterization methods

In Table 1.4 a summary is given of characterization techniques available for nanofiltration membranes with a different morphology. They will be discussed further in this section.

Table 1.4: Characterization methods for nanofiltration membranes

Characterization method	***Characteristic***	
	porous charged membranes	*swollen networks*
solvent flux measurements	ratio of porosity and membrane thickness	solvent permeability
retention measurements with		
* uncharged molecules	pore size	solute permeability size hinderance factor
* electrolyte solutions	pore size membrane charge	solute permeability size hinderance factor charge hinderance factor membrane charge
(FE)SEM, AFM	pore size porosity	overall structure defects
permporometry	pore size porosity	-
gas adsorption/desorption	pore size surface area	surface area
charge determining method		
* titration	membrane charge (bulk)	membrane charge (bulk)
* electrokinetic measurements		
- along membrane surface	membrane charge (surface)	membrane charge (surface)
- through membrane	pore wall charge (surface)	membrane charge (bulk)
* membrane potential	membrane charge (bulk)	membrane charge (bulk)
* membrane resistance	membrane resistance (bulk)	membrane resistance (bulk)

Retention measurements

The most often used characterization method for nanofiltration membranes are retention measurements. Retention is a measure for the ability of a membrane to retain a certain solute and is expressed as retention coefficient or rejection coefficient (symbol: R). A retention coefficient of 1 refers to total exclusion, whereas a retention coefficient of 0 means that no solute has been retained:

$$R = 1 - \frac{c_p}{c_f} \qquad \{1.1\}$$

with c_p being the permeate concentration and c_f the feed concentration.
Retention measurements can be carried out with different solutes and at different process conditions. As nanofiltration membranes are applied for both the separation of (multivalent) ions and that of low-molecular uncharged organics, retention measurements are often carried out with model species representing these two categories. In case of ionic solutions either single salt solutions or salt mixtures are used. Saccharides or polyethyleneglycols of different molecular weight are often used as model solutes for uncharged species.
The retention of a solute may be affected by process parameters as well. Important parameters are the concentration of the solute and the pressure applied.

Uncharged solutes
Porous nanofiltration membranes behave in case of separation of uncharged molecules like ultra- or microfiltration membranes. The separation takes place because of a sieving mechanism and large particles can be separated from smaller ones. In case of nanofiltration membranes with a swollen network structure a solution-diffusion mechanism will favor the transport of smaller solutes above that of larger ones as well because their diffusion coefficient is higher, resulting in a higher retention for the larger components.
The molecular weight cut-off may be used as a characteristic for nanofiltration membranes, which has values in between 200 and 1000 g/mol. This cut-off value is defined as a parameter that represents the molecular weight of the components that are retained for 90% by the membrane [40]. This parameter is often used, especially for ultrafiltration membranes, but it cannot be considered as an absolute parameter. The molecular weight cut-off varies with the pressure applied, with the concentration of the solute and with the nature of the solute. The influence of the type of solute on the retention was for instance shown by differences in retentions between pesticides, between dextranes and polyethyleneglycols (PEGs) and between polysaccharides and PEGs with similar molecular weight [41-43]. The different pesticide retentions were attributed to the molecular shapes of these molecules, whereas the difference between PEG and polysaccharides was caused by adsorption of the PEG molecules by the membrane tested, while the polysaccharides were repelled by the membrane.

Retention measurements with molecules of different size but with similar interaction towards the membrane can be used to determine a membrane pore size distribution. This (elaborate) method was mainly used for ultrafiltration membranes, for instance by Nobrega, Aimar and co-workers [44,45]. In case of nanofiltration membranes, generally, the mean pore size is determined by this type of measurements and not its distribution [7,46,47].
Guizard and Larbot used retention measurements with dyes to determine the pore size [48,49]. In case of a dye retention of 100%, they concluded that all pores in the membrane were smaller than the size of the retained solute. As the solvent fluxes remained constant, no adsorption was thought to occur.

Pressure dependence
By increasing the operating pressure difference, the retention will increase until it reaches a

plateau value. This is because the solvent flux through the membrane is linearly related to the pressure difference applied, whereas the solute flux is both dependent on the concentration difference over the membrane and on the solvent flux. When increasing the pressure difference, the solvent flux increases relatively more than the solute flux. This causes a decreasing permeate concentration and an increasing retention.
A schematic drawing of the limiting behavior of the retention, R, as a function of the pressure difference applied, ΔP, is shown in Figure 1.6. The upper line in this figure (a) represents a system with a maximum retention of 1, whereas in case of line (b) the plateau value of the retention is lower than 1.

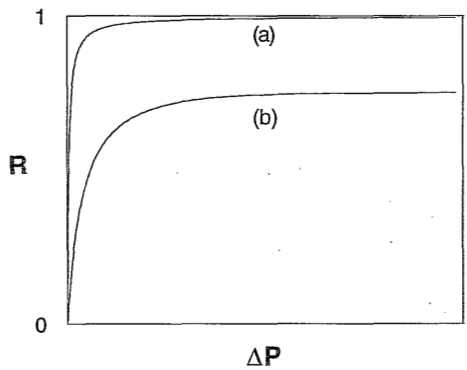

Figure 1.6: *Schematic drawing of the dependence of the retention on the pressure difference applied, ΔP*

Concentration dependence
Several theoretical models predict different behavior of the retention dependence for uncharged molecules on the concentration. A simple solution-diffusion model that is often used for transport through reverse osmosis membranes does not predict any concentration dependence of the solute retention. In this model it is assumed that the solute concentrations in the membrane are small and therefore, coupling effects between the solvent and the solute flux can be neglected.
In case of an extended solution-diffusion model, in which both solvent and solute fluxes are coupled, the retention decreases with increasing solute concentration, although this decrease is only small [50]. These theoretical distinctions between the separation behavior were observed experimentally as well. Schirg observed no concentration dependence of the retention for some polysaccharides in the concentration range of 0.8 to 4 g/l [46]. However, Schneider determined a concentration-dependent retention for organic components, like methanol, ethanol and different glycols in the concentration range 1 to 170 g/l [50]. The relation between solute concentration and retention could be described by the extended solution-diffusion model. Most probably, these different relations between retention and solute concentration are caused by the different solute concentration ranges.

Electrolyte solutions

Whereas the sieving features of a nanofiltration membrane are important for the separation of uncharged molecules, in case of ions both sieving features and the electrostatic repulsion between the charged membrane and the solute may become important. Differences in retentions of ions of comparable size will be determined by charge effects. Bi- or tri-valent ions with the same sign of charge as the membrane surface will be more effectively repelled than monovalent ions. The retention is mainly determined by the co-ion, i.e., the ion with a similar charge as the membrane. In case of different counter-ions, i.e., ions with a charge opposite to the membrane charge, the counter-ion with the lowest charge will show the highest retention.

Concentration dependence

Mostly, the retention of salts of nanofiltration membranes is strongly affected by the concentration of the feed, see e.g., [7,18,51-54]. The higher the concentration of ions, the lower the retention, which is characteristic for charged membranes [21]. The decrease in retention is caused by a different equilibrium distribution of ions between membrane and adjacent solution at higher ionic concentrations. This so-called Donnan equilibrium will be discussed in more detail in Chapter 2.

Some nanofiltration membranes show a nearly constant retention as a function of salt concentration. In this case rather steric than charge effects will be rate determining [52].

Pressure dependence

The influence of the pressure difference on the retention for salt solutions is similar to that for the uncharged solutes, since the Donnan equilibrium is not affected by pressure difference applied. The retention will asymptotically increase with an increase in operating pressure difference, until a limiting value is reached as shown in Figure 1.6.

Salt mixtures

In a salt mixture the specific characteristics of nanofiltration membranes become apparent. Several authors showed that in case of salt mixtures with various co-ions, the retention of the co-ion with the lowest charge decreased considerably compared to the retention in case of a single salt solution, whereas the retention of the co-ion with the highest charge remained almost constant [9,19,55-58]. However, in these cases not only the charge of the ions determined the separation, but the differences in mobility of the ions played a role as well. The ion with the lowest mobility was retained best. Both the influence of the charge and that of the mobility influence the separation in the same direction.

At high concentrations of the highest charged ions even negative retentions of the lower charged ions were observed. This means that when these latter ions are transported from the feed to the permeate solution side, they move opposite to their concentration gradient, i.e., from a low to a high concentration. In retention experiments using mixtures with different counter-ions, the ionic mobilities in the membrane determine the selectivity of the process [59].

Retention measurements with single salt solutions and salt mixtures may be interpreted in terms

of morphological membrane parameters like the porosity-membrane thickness ratio, the membrane charge density and the effective pore size [8,9,20,21]. Furthermore, retention measurements with salt mixtures can give qualitative information on the separation mechanism.

Permporometry

Permporometry is a method which allows to determine the pore size distribution and the mean pore size of a membrane [60,61]. By this technique only the active pores are determined. In a permporometry measurement, the principle of capillary condensation is combined with the diffusive transport of gases through the open pores of a membrane. Capillary condensation is a phenomenon taking place in pores of a certain size, when the vapor pressure exceeds a certain value. The relation between the vapor pressure and the radius of a capillary pore when evaporation from a curved surface starts is given by the Kelvin equation:

$$\ln \frac{P}{P_0} = -\frac{2\gamma V_{mol}}{R\,T\,r_k}\cos\theta \qquad \{1.2\}$$

where P and P_0 are the actual pressure and the saturation condensation pressure at temperature T and 1 atm., respectively, γ the surface tension between liquid and air, V_{mol} the molar volume of the liquid, θ the contact angle, R the gas constant, T the temperature and r_k the Kelvin-radius.

In Figure 1.7 a schematic drawing of capillary condensation is shown. At a relative pressure of zero, the pore will be open (a). An increase of this relative vapor pressure results in monolayer adsorption at the pore wall (b). This mono layer is called the t-layer. Increasing the relative vapor pressure even further, condensation will occur first in the largest pores (c). At a relative vapor pressure of unity all pores will be filled with condensate (d).

By applying a partial pressure difference of a gas (mostly oxygen is used) over the membrane, the transport of the gas will depend on the relative vapor pressure of the condensable liquid. At low vapor pressures most pores will be opened and gas transport can occur. At higher vapor pressures, some pores will be blocked by the condensate and as a result the amount of gas passing the membrane will diminish.

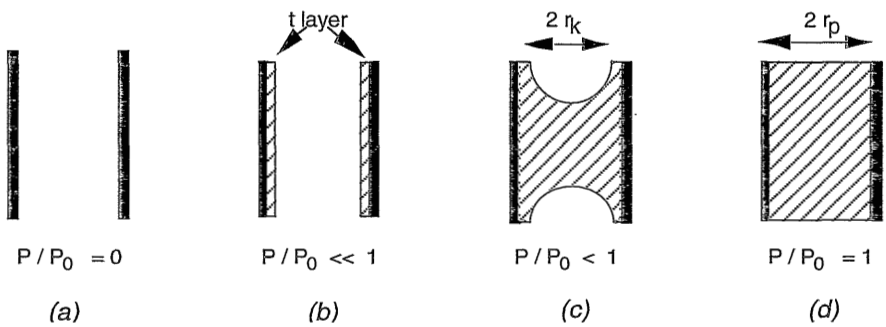

Figure 1.7: Schematic drawing of different stages of capillary condensation

The condensable gas used in the permporometry experiments can be any gas, provided that it has negligible interaction with the membrane, that it has a reasonable vapor pressure and a high evaporation rate [61]. Cyclohexane, which can be considered as a Van der Waals-gas consisting of hard spherical molecules, is often used as condensable gas [62].
By a permporometry measurement, the maximum pore size of the membrane can be determined. Furthermore, qualitative information on the pore size distribution can be obtained as well. An example of a pore size distribution obtained by permporometry is shown in Figure 1.8. On the y-axis at the left, the total amount of oxygen diffusing through the membrane is shown as a function of the pore size, r_k. By differentiating this curve a pore size distribution can be obtained, which is shown by the other curve.

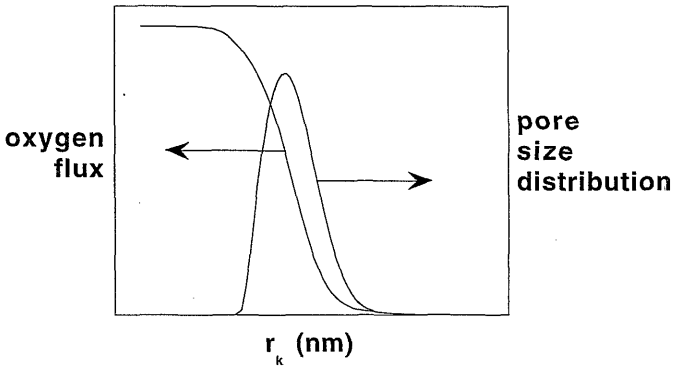

Figure 1.8: *Schematic illustration of the cumulative oxygen flux through a membrane as a function of the pore size and the resulting pore size distribution, obtained by permporometry*

In case of polymeric membranes, permporometry may cause some problems, because during the experiment the morphology of the membrane may change due to swelling [63].
Permporometry can be used to determine pores with radii down to about 1.5 nm. In case of smaller pores, no quantitative interpretation of the data can be carried out, as the Kelvin law cannot be applied anymore in the range of these small pore sizes.

Gas adsorption-desorption

Gas adsorption-desorption can be considered as a standard characterization technique for porous inorganic materials. This method determines the pore area within a sample and from that a mean pore size and a pore size distribution can be determined. Both the active and inactive pores, i.e., pores that do and do not contribute to the transport through the membrane, are measured by gas adsorption-desorption. The method has only been used for unsupported ceramic membranes, i.e., gel films which have been calcined.
Gas adsorption-desorption is based on the difference between the vapor pressure above a curved surface and that above a flat surface. Because of this difference a gas can condense in

small pores at relative pressures lower than one. The volume of gas adsorbed at various vapor pressures is measured in both the adsorption and desorption mode and the pore size and pore size distribution can be calculated. Nitrogen is most often used as condensation gas at the temperature of boiling nitrogen, i.e., 77K at 1 bar, although other gases, as argon and carbondioxide, may be used as well, see e.g., [64-68]. Usually, hysteresis occurs between the adsorption and desorption isotherm, because capillary condensation in the adsorption mode is different from desorption. Due to a curved meniscus in the desorption mode (see Figure 1.7), the condensate evaporates at lower pressures than it would condensate. The solvent curvature causes a lowering of the relative vapor pressure above the meniscus. A typical isotherm for a porous material with a uniform pore size distribution is given in Figure 1.9.

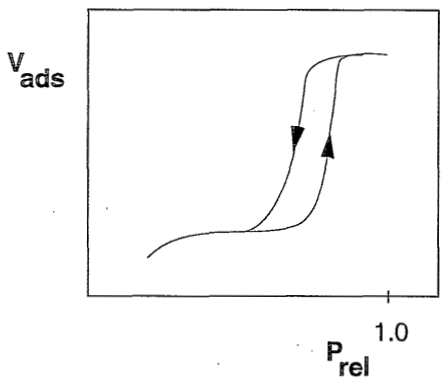

Figure 1.9: *Schematic drawing of an adsorption-desorption isotherm for a macroporous material with a uniform pore distribution*

The adsorption isotherm of materials containing pores with radii smaller than about 1 nm significantly differs from the isotherm shown in Figure 1.9, as isotherms of systems with very small pores do not show hysteresis, because of the absence of capillary condensation.
As the Kelvin equation cannot be used for the calculation of pore radii smaller than 1.5 nm, other methods have been developed to determine smaller pore sizes, like the Dubinin and Radushkevich method and the Horváth and Kawazoe method which are both based on the adsorption potential in micropores [69-71].
Besides mathematical and physical problems to interpret nitrogen adsorption-desorption measurements for materials with pore radii smaller than 1.5 nm, it should be considered that the membrane samples have to be dry, what may be a serious draw-back in the case of polymeric membranes. In literature, some gas adsorption-desorption measurements have been described for the characterization of asymmetric polymeric membranes [72,73]. Since it is not possible, like in case of ceramic membranes, to measure only the toplayer of an asymmetric polymeric membrane, most surface area determined by gas adsorption is present in pores of the sublayer, which pores do not have a large influence on the membrane performance [73].
Comparison of the mean pore sizes and pore size distributions obtained by gas adsorption-desorption measurements of unsupported ceramic membranes and by permporometry

measurements of supported membranes resulted in identical data [61]. These showed that gas adsorption measurements of unsupported systems may give a good indication of the pore size of supported ceramic membranes.

Microscopy

In general, microscopic techniques visualize the membrane structure and give information on morphological aspects like surface pore shape and size, their distributions, the porosity and the cross-sectional structure [74].
In Scanning Electron Microscopy (SEM) a three-dimensional image of the sample is obtained by radiation of the sample with an electron beam. The image is determined by the reflected, secondary electrons. The resolution limit of SEM is about 5 nm. However, this is dependent on the voltage of the high energy electron beam used and on the mass of molecules present in the sample. Especially for polymeric membranes, low voltages should be applied to avoid damage of the sample surface which, consequently, result in lower resolution.
Using SEM, the membrane surface should be conductive, because, otherwise, the electron beam will charge the membrane material or even burn the sample. Therefore, a conductive coating is applied, which may obscure the finer details in the picture [75]. In case of nanofiltration membranes, SEM will only give information on the macroscopic structure of the membranes, because the resolution of the method is too low to observe any pores, if present. Defects in the toplayer may be observed as well.
Furthermore, because SEM is a vacuum technique, the sample is observed in a dry state, and in case of some polymeric nanofiltration membranes the possibility of a morphological change of the dried sample compared to the liquid-swollen membrane should be taken into account.

Field Emission SEM achieves high resolutions (to about 1 nm) at relatively low beam energies. This technique is until now not frequently used for nanofiltration membranes, most probably because FESEM is a vacuum technique as well.

A relatively new microscopic technique is Atomic Force Microscopy (AFM). This method can be applied to investigate the surface roughness of a membrane by scanning the sample surface with a sharp tip at the end of a flexible cantilever. By moving this tip at a constant force or a constant distance over the membrane surface, an image of the surface can be obtained. Unlike (FE)SEM, AFM does not require a vacuum and samples can be measured in air or even in a liquid. AFM has been mainly used to investigate the surface morphologies of ultrafiltration membranes [76-80]. Most probably the size of the tip with a radius of 10 to 40 nm restricted the resolution of this technique and, therefore, AFM has not been often used for the characterization of nanofiltration membranes. Examination of AFM pictures may result in a pore size distribution of a porous nanofiltration membrane, by determination of the diameters of the pores at the membrane surface [81]. To obtain reliable information from AFM pictures a good method should be used to distinct between pores and the surface roughness.

Characterization methods related to the membrane charge

Different characterization methods for nanofiltration membranes can be applied which focus on the membrane charge or related properties. Techniques to obtain information on the membrane charge, its zeta potential or its electrical resistance are, for instance, membrane titration, electrokinetic measurements, membrane potential measurements and electrical impedance measurements.

Titration measurements

Membranes with fixed charged groups can be considered as insoluble acids or bases [82]. Titration is a way to obtain the concentration of charged groups in the membrane. The amount of, for instance, fixed negatively charged groups is determined by adding a strong acid to the membrane, bringing it in acidic form. Then, the membrane is titrated back by a strong base. As titration is a bulk technique, all fixed charged groups in the membrane will be determined.

Membrane potential measurements

The membrane potential arises when a membrane separates two electrolyte solutions with different concentrations. The potential is the sum of three separate potentials, i.e., two Donnan potentials at both membrane-solution interfaces and the diffusion potential across the membrane as shown in Figure 1.10. In this figure the potentials in a system with a symmetric membrane in contact with two solutions is schematically drawn. Here it is assumed that the Donnan equilibrium exists at the two interfaces of membrane and solution.
By a membrane potential measurement the permselectivity of a membrane can be measured. Furthermore, insight can be obtained in membrane properties such as transport numbers of ions [83-85], ionic diffusion coefficients [86,87] and membrane charge densities [20,85,88].

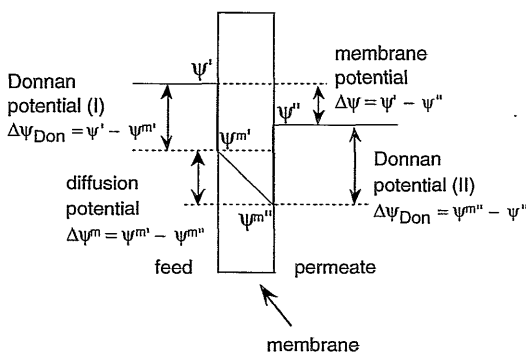

Figure 1.10: Schematic drawing of various potentials in a symmetric membrane in contact with two electrolyte solutions with different concentrations

If parameters like transport number and diffusion coefficients are determined from membrane potential measurements with asymmetric membranes, a correction should be made for the influence of the support layer. Pusch showed that the diffusion potential in the support layer

may dominate the membrane potential [88]. The influence of the support layer was shown in experiments of Jonsson and Benavente as well [83].

Electrokinetic measurements

If charged groups are present at a surface, the ions in the adjacent electrolyte solution will arrange in a specific way near the charged surface, causing an electrical double layer that contains mainly counter-ions. Electrokinetic measurements can be carried out by which the zeta potential can be determined, which is the potential at the shear plane between the solution and the membrane. In case of the characterization of nanofiltration membranes, two of these electrokinetic measurements are frequently applied, i.e., electro-osmotic and streaming potential measurements. In case of electro-osmotic measurements an electrical potential difference is applied along a double layer, thereby inducing a solution flow. In case of streaming potential measurements a liquid flow generates an electrical potential difference. Electrokinetic phenomena can be generated both through and along a charged surface, i.e., the charge at a pore wall or the charge at the membrane surface can be determined.

Electro-osmosis

Electro-osmosis is the transport of a liquid relative to a charged surface by an electric field [89]. The amount of transported liquid is proportional to the potential applied. The electro-osmotic flow rate can be related to the zeta potential of the charged surface. This zeta potential is the potential at the shear plane at a certain distance from the membrane surface, at about the transition between the fixed adsorbed ions and the mobile ions (Stern plane). A schematic drawing of the potential decrease within an electrolyte solution as a function of the distance from the charged surface is shown in Figure 1.11.

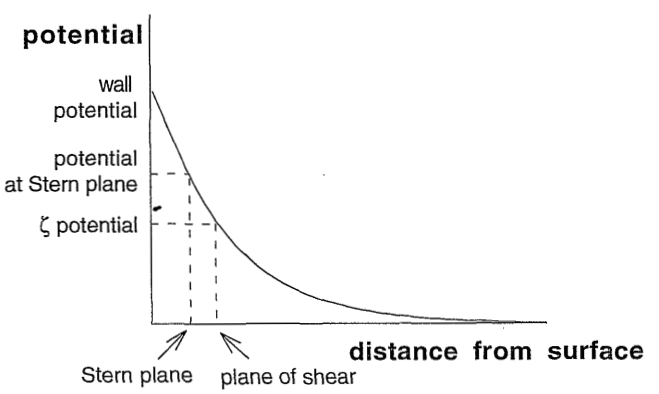

Figure 1.11: *Potential decrease within a solution near a charged wall*

Streaming potential measurements

A streaming potential is induced when ions within an electrical double layer are forced to move along with a flow, thereby generating a potential difference. This potential, the streaming

potential E_{str}, is a linear function of the force applied, ΔP, as described by the Helmholtz-Smoluchowski equation (e.g., [90,91]):

$$\frac{\Delta E_{str}}{\Delta P} = \frac{\varepsilon \zeta}{\eta \lambda_0} \qquad \{1.3\}$$

where ζ is the zeta potential, ε the permittivity of the medium, η the viscosity, λ_0 the bulk conductivity and r the radius of the pore or capillary. From equation {1.3} the zeta potential can be obtained. Streaming potential measurements can be carried out both *through* the membrane and *along* the membrane surface. In the former case, the charged pores of the membrane can be considered as streaming channels for the electrolyte solution and, consequently, pore characteristics are determined [92-94]. In the latter case, surface characteristics are measured [95-97].
Investigation of the pH dependence of the zeta potential gives information on the acidic and basic strength of the surface charge groups [92,98-100]. The dependence of the zeta potential on the electrolyte concentration can provide information on the free energy of adsorption of ions at the membrane surface and the preferential adsorption of ions at the surface [98-100]. These are dependent on the surface properties of the polymer, the type and kind of electrolyte and the adsorption behavior of the solvent.
The interpretation of streaming potential measurements *through* the membrane is difficult in case of nanofiltration membranes, firstly, because the Helmholtz-Smoluchowski equation which is used to calculate the zeta potential from the streaming potential does not hold for pore sizes as small as 1 nm, like in nanofiltration membranes, and, secondly, because the influence of the support layer is not well incorporated.
The zeta potential is a well-defined parameter in case of a smooth surface [101]. In case of roughness of the surface, like in case of a membrane surface, problems may occur in the interpretation of the electrokinetic results, because of disturbances of the electrical double layer [102].

Electrical resistance measurements
Electrical resistance measurements, both direct and alternating current measurements, can be performed to determine the electrical resistance to ionic transport [83,86,103].

1.4 OUTLINE

The main objective of this thesis is the characterization of both polymeric and ceramic nanofiltration membranes by different techniques. Since nanofiltration membranes can have various structures, characterization techniques are elaborated that can be used for uncharged as well as for charged nanofiltration membranes, with either a porous or a swollen network structure. This implies that techniques elucidating the membrane performance will have a central role.
Chapter 2 describes the theory of solute transport through nanofiltration membranes. The

extended Nernst-Planck equation is mainly used for this description.
In the experimental part emphasis is put on the separation of ions, polysaccharides and dendrimers with nanofiltration membranes. *Chapter 3* contains the retention measurements with single salt solutions and salt mixtures, whereas in *Chapter 4* saccharides and dendrimers, which are molecules with a well-defined shape, are used as model solutes for the membrane characterization. In case of the uncharged saccharides, the size of the molecules can be related to the pore size or the density of the membrane matrix. The separation of ions is thought to be affected by both size effects and by electrostatic interactions between membrane and ions. To investigate this latter effect, the zeta potentials and surface charge densities of the membranes are determined by streaming potential measurements as described in *Chapter 5*. The membrane charge was measured by titration measurements as well.
In *Chapter 6* the experimental results of the retention measurements with both electrolyte and saccharide solutions are modeled by the theoretical concepts as shown in Chapter 2.
Finally, in *Chapter 7* general conclusions from the different characterization techniques are drawn.

SYMBOLS

c:	concentration	(mol/l)
E_{str}:	streaming potential	(V)
P:	pressure	(bar)
P_0:	vapor condensation pressure at temperature T and 1 atm.	(bar)
r:	pore radius	(m)
r_k:	Kelvin radius	(m)
R:	retention	(-)
R:	gas constant	(J/mol.K)
T:	temperature	(K)
V_{mol}:	molecular volume	(m^3/mol)
γ:	surface tension	(N/m)
ε:	permittivity of the medium	(A.s/V.m)
ζ:	zeta potential	(V)
η:	viscosity	(Pa.s)
θ:	contact angle	(-)
λ_0:	bulk conductivity	(Ω^{-1}/m)

subscripts:

f:	feed
p:	permeate

REFERENCES

[1] Raman, L. P., Cheryan, M., Rajagopalan, N., *Consider nanofiltration for membrane separations*, Chem. Eng. Progress, 3 (1994) 68

[2] Rautenbach, R., Gröschl, A., *Separation potential of nanofiltration membranes*, Desalination, 77 (1990) 73-84

[3] Broek, A., Characterization of hemodialysis membranes: membrane structure and function, Thesis, University of Twente, Enschede, The Netherlands, 1993

[4] Strathmann, H., Trennung von molekularen Mischungen mit Hilfe synthetischer Membranen, Steinkopff, Darmstadt, 1979

[5] Cadotte, J., Forester, R., Kim, M., Petersen, R., Stocker, T., *Nanofiltration membranes broaden the use of membrane separation technology*, Desalination, 70 (1988) 77

[6] Kurihara, M., Himeshima, Y., *The major developments of the evolving reverse osmosis membranes and ultrafiltration membranes*, Polym. J., 23 (1991) 513-520

[7] Wang, X.-L., Tsuru, T., Togoh, M., Nakao, S.I., Kimura, S., *Evaluation of pore structure and electrical properties of nanofiltration membranes*, J. Chem. Eng. Jap., 28 (1995) 186-192

[8] Wang, X.-L., Tsuru, T., Togoh, M., Nakao, S.I., Kimura, S., *Transport of organic electrolytes with electrostatic and steric-hindrance effects through nanofiltration membranes*, J. Chem. Eng. Jap., 28 (1995) 372-380

[9] Bowen, W. R., Mukthar, H., *Characterisation and prediction of separation performance of nanofiltration membranes*, J. Membrane Sci., 112 (1996) 263-274

[10] Smit, J. A. M., *Reverse osmosis in charged membranes: analytical predictions from the space-charge model*, J. Coll. Int. Sci., 132 (1989)

[11] Eriksson, P., *Nanofiltration extends the range of membrane filtration*, Env. Progress, 7 (1988) 58

[12] Conlon, W. J., *Pilot field test data for prototype ultra low pressure reverse osmosis elements*, Desalination, 56 (1985) 203

[13] Petersen, R. J., *Composite reverse osmosis and nanofiltration membranes*, J. Membrane Sci., 83 (1993) 81

[14] Riley, R. L., Fox, R.L., Lyons, C.R., Milstead, C.E., Seroy M.W., Tagami, M., *Spiral-wound poly(ether/amide) thin-film composite membrane systems*, Desalination, 19 (1976) 113-126

[15] Riley, R. L., Milstead, C.E., Lloyd, A.L., Seroy M.W., Tagami, M., *Spiral wound thin-film composite membrane systems for brackish and seawater desalination by reverse osmosis*, Desalination, 23 (1977) 331-355

[16] Jonsson, G., Boesen, C.E., *Water and solute transport through cellulosic acetate reverse osmosis membranes*, Desalination, 17 (1975) 145

[17] Jonsson, G., *Coupling of ion fluxes by boundary-diffusion and streaming potentials under reverse osmosis conditions*, 7th International Symposium on Fresh water from the sea, 1980, p. 153

[18] Kurihara, M., Uemura, T., Nakagawa, Y., Tonomura, T., *The thin-film composite low-pressure reverse osmosis membranes*, Desalination, 54 (1985) 75-88

[19] Bhattacharyya, D., McCarthy, J.M., Grieves, R.B., *Charged membrane ultrafiltration of inorganic ions in single and multi-salt systems*, AIChE J., 20 (1974) 1206

[20] Tsuru, T., Nakao, S.I., Kimura, S., *Effective charge density and pore structure of charged ultrafiltration membranes*, J. Chem. Eng. Jap., 23 (1990) 604

[21] Jitsuhara, I., Kimura, S., *Structure and properties of charged ultrafiltration membranes made of sulfonated polysulfone*, J. Chem. Eng. Jap., 16 (1983) 389

[22] Jitsuhara, I., Kimura, S., *Rejection of inorganic salts by charged ultrafiltration membranes made of*

sulfonated polysulfone, J. Chem. Eng. Jap., 16 (1983) 394

[23] Kimura, S., Jitsuhara, I., *Transport through charged ultrafiltration membranes*, Desalination, 46 (1983) 407-416

[24] Shor, A. J., Kraus, K.A., Smith, Jr. , W.T., Johnson, J.S., Jr., *Hyperfiltration studies. XI. Salt-rejection properties of dynamically formed hydrous zirconium (IV) oxide membranes*, J. Phys. Chem., 72 (1968) 2200

[25] Ballou, E. V., Wijdeven, T., Leban, M., *Solute rejection by porous membranes. I Hyperfiltration of sodium chloride and urea feed solutions*, Environ. Sci. Technol., 5 (1971) 1032

[26] Johnson, J. S., Minturn, R.E., Wadia, P.H., *Hyperfiltration XXI. Dynamically formed hydrous Zr (IV) oxide-polyacrylate membranes*, J. Electroanal. Chem., 37 (1972) 267

[27] Larbot, A., Alami-Younssi, S., Persin, M., Sarrazin, J., Cot, L., *Preparation of a γ-alumina nanofiltration membrane*, J. Membrane Sci., 97 (1994) 167-173

[28] Alami-Younssi, S., Larbot, A., Persin, M., Sarrazin, J., Cot, L., *Gamma alumina nanofiltration membrane. Application to the rejection of metallic cations*, J. Membrane Sci., 91 (1994) 87

[29] Sarrade, S., Rios, G.M., Carlès, M., *Dynamic characterization and transport mechanisms of two inorganic membranes for nanofiltration*, J. Membrane Sci., 97 (1994) 155-166

[30] Bhave, R. R., *Liquid filtration and separation with inorganic membranes: operating considerations and some aspects of system design*, in: Inorganic membranes; synthesis, characteristics and applications, ed. by R.R. Bhave, Van Nostrand Reinhold, New York, 1991

[31] Uhlhorn, R. J., Ceramic membranes for gas separation. Synthesis and transport properties, Thesis, University of Twente, Enschede, The Netherlands, 1990

[32] Burggraaf, A. J., Keizer, K., *Synthesis of inorganic membranes*, in: Inorganic membranes; synthesis, characteristics and applications, edited by R.R. Bhave, Van Nostrand Reinhold, New York, 1991

[33] Hagmeyer, G., Gimbel, R., Einsatz- und Entwicklungsmöglichkeiten von Membranverfahren in der öffentliche Wasserversorgung, Eschborn, 1991

[34] Tan, L., Sudak, R.G., *Removing color from a groundwater source*, J. AWWA, 84 (1992) 79

[35] Bhattacharyya, D., Adams, R., Williams, M., *Separation of selected organic and inorganic solutes by low pressure reverse osmosis membranes*, Prog.Clin.Biol.Res., 292 (1989) 453

[36] Berg, P., Hagmeyer, G., Gimbel, R., *Rejection of pesticides and other trace organics by nanofiltration*, Membrane Technology Conference of the AWWA, Reno, Nevada, 1995

[37] Duranceau, S. J., Taylor, J.S., Mulford, L.A., *SOC removal in a membrane softening process*, J.AWWA, 1 (1992) 68

[38] Watson, B. M., Hornburg, C.D., *Low-energy membrane nanofiltration for removal of color organics and hardness from drinking water supplies*, Desalination, 72 (1989) 11

[39] Maaskant, W., Tholen, J., Mulder, M.H.V., Nederlandse membraangids, 1996

[40] Koops, G. H., *Nomenclature and symbols in membrane science and technology*, ESMST, Enschede, the Netherlands, 1995

[41] Hofman, J. A. M. H., Noij, Th.H.M., Kruithof, J.C., Schippers, J.C., *Removal of pesticides and other micropollutants with membrane filtration*, Water supply, 11 (1993) 259

[42] Smolders, C. A., Vugteveen, E., *New characterization methods for anisotropic ultrafiltration membranes*, Pol. Mats Sci. Eng., 50 (1984) 177

[43] Rudie, B. J., Ross, G.S., Harrold, S.J., *Effects of surface force interactions on a NF/UF membrane*, Desalination, 90 (1993) 107

[44] Nobrega, P., de Balmann, H., Aimar, P., Sanchez, V., *Transfer of dextran through ultrafiltration membranes. A study using retention data analysed by gel permeation chromatography*, J. Membrane

Sci., 45 (1989) 17

[45] Aimar, P., Meireles, M., Sanchez, V., *A contribution to the translation of retention curves into pore size distributions for sieving membranes*, J. Membrane Sci., 54 (1990) 321-338

[46] Schirg, P., Charakterisierung von Nanofiltrationsmembranen für die Trennung von wässrigen Farbstoff-Salzlösungen, Thesis, ETH Zürich, 1992

[47] Tsuru, T., Wang, X.-L., Nakao, S.I., Kimura, S., *Transport of neutral and charged solutes through nanofiltration membranes*, International Symposium on Fiber Science and Technology, Yokohama, Japan, 1994

[48] Guizard, C., Ajanka, N., Besland, M.P., Larbot, A., Cot, L., *Heteropolysiloxanes membranes designed for the separation of small molecules*, Key Eng. Mats., Vol 61&62 (1991) 537

[49] Larbot, A., Young, D., Guizard, C., Paterson, R., Cot, L., *Alumina nanofiltration membrane from sol-gel process*, Key Eng. Mats., Vol. 61&62 (1991) 395

[50] Schneider, G., *Trennverfahren von Nanofiltrationsmembranen*, Thesis, RWTH Aachen, 1994

[51] Ikeda, K., Nakano, T., Ito, H., Kubota, T.,Yamamoto, S., *New composite charged reverse osmosis membrane*, Desalination, 68 (1988) 109

[52] Schirg, P., Widmer, F., *Characterization of nanofiltration membranes for the separation of aqueous dye-salt solutions*, Desalination, 89 (1992) 89-107

[53] Comstock, D. L., *Desal-5 membrane for water softening*, Desalination, 76 (1988) 61-72

[54] Freeman, S. D. N., Stocker, T.F., *Comparison of two thin-film composite membranes: low pressure FT-30 to very low pressure NF-40-HF*, Desalination, 62 (1987) 183-191

[55] Boyé, A., Guizard, C., Larbot, A., Cot, L., Grangeon, A., *A polyphosphazene membrane active in nanofiltration*, Key Eng. Mats., Vol.61&62 (1991) 403

[56] Lonsdale, H., Pusch, W., Walch, A., *Donnan-membrane effects in hyperfiltration of ternary systems*, J. Chem. Soc., Faraday Transcriptions I, 71 (1975) 501

[57] Nielsen, D. W., Jonsson, G., *Bulk-phase criteria for negative ion rejection in nanofiltration of multi-component salt solutions*, Sep. Sci. Techn., 29 (1994) 1165

[58] Alami-Younssi, S., Larbot, A., Persin, M., Sarrazin, J., Cot, L., *Rejection of mineral salts on a gamma alumina nanofiltration membrane. Application to environmental process*, J. Membrane Sci., 102 (1995) 123-129

[59] Yaroshchuk, A. E., Vovkogon, Y.A., *Pressure-driven transport of ternary electrolyte solutions with a common coion transport through charged membranes. Numerical analysis*, J. Membrane Sci., 86 (1994) 19

[60] Cuperus, F. P., Smolders, C.A., *Characterization of UF membranes. Membrane characteristics and characterization techniques*, Adv. Coll. Interf. Sci., 34 (1991) 135

[61] Cao, G. Z., Meijerink, J., Brinkman, H.W., Burggraaf, A.J., *Permporometry study on the size distribution of active pores in porous ceramic membranes*, J. Membrane Sci., 83 (1993) 221-235

[62] Cuperus, F. P., Bargeman, D., Smolders, C.A., *Permporometry. The determination of the size distribution of active pores in UF membranes*, J. Membrane Sci., 71 (1992) 57-67

[63] Beerlage, M. A. M., Polyimide ultrafiltration membranes for non-aqueous systems, Thesis, University of Twente, Enschede, The Netherlands, 1994

[64] Leenaars, A. F. M., Keizer, K., Burggraaf, A.J., *The preparation and characterization of alumina membranes with ultra-fine pores. Part 1. Microstructural investigations on non-supported membranes*, J. Mats. Sci., 19 (1984) 1077-1088

[65] Grillet, Y., *Adsorption of carbon dioxide, benzene, nitrogen and argon by microporous carbons: interpretation of isotherms and enthalpies of adsorption and immersion*, in: Characterization of porous

solids, ed. by K.K. Unger, K.S.W. Sing, Elsevier, Amsterdam, 1988

[66] Sheng, G., Chu, L., Zeltner, W.A., Anderson, M.A., *Nanoparticulate alumina, silica and aluminosilicate membranes*, J. Non-Cryst. Solids, 147&148 (1992) 548-553

[67] Kakei, O., Suzuki, Kaneko, *Multi-stage micropore filling of nitrogen and argon by microporous carbon fibers*, in: Characterization of porous solids II, ed. by F. Rodríguez-Reinoso et al., Elsevier, Amsterdam, 1991

[68] Webb, S. W., Conner, W.C., *Sorption of gases on microporous solids: pore size characterization by gas adsorption*, in: Characterization of porous solids II, ed. by F. Rodríguez-Reinoso et al., Elsevier, Amsterdam, 1991

[69] Dubinin, M. M., Plavnik, G.M., Zaverina, E.D., *Integrated study of the porous structure of active carbons from carbonized sucrose*, Carbon, 2 (1964) 261

[70] Dubinin, M. M., Plavnik, G.M., *Microporous structures of carbonaceous adsorbents*, Carbon, 6 (1968) 183

[71] Horváth, G., Kawazoe, K., *Method for the calculation of effective pore size distribution in molecular sieve carbon*, J. Chem. Eng. Jap., 16 (1983) 470

[72] Smolders, C. A., Vugteveen, E., *New characterization methods for asymmetric ultrafiltration membranes*, in: Material science of synthetic membranes; Vol. 269, ed. by D.R. Lloyd, 1985, p. 327

[73] Cuperus, F. P., Characterization of ultrafiltration membranes. Pore structure and top layer thickness, Thesis, University of Twente, Enschede, The Netherlands, 1990

[74] Nakao, S., *Determination of pore size and pore size distribution. 3. Filtration membranes*, J. Membrane Sci., 96 (1994) 131-165

[75] Kim, K.-J., Fane, A.G., *Low voltage scanning electron microscopy in membrane research*, J. Membrane Sci., 88 (1994) 103-114

[76] Fritzsche, A. K., Arevalo, A.R., Moore, M.D., Weber, C.J., Elings, V.B., Kjoller, K., Wu, C.M., *Image enhancement of polyethersulfone ultrafiltration membrane surface structure for atomic force microscopy*, J. Appl. Pol. Sci., 46 (1992) 167-178

[77] Fritzsche, A. K., Arevalo, A.R., Moore, M.D., O'Hara, C., *The surface structure and morphology of PolyAcryloNitrile membranes by atomic force microscopy*, J. Membrane Sci., 81 (1993) 109

[78] Dietz, P., Hansma, P.K., Hermann, K.-H.,Inacker, O., Lehmann, H.D., *Atomic-force microscopy of synthetic ultrafiltration membranes in air and under water*, Ultramicroscopy, 35 (1991) 155

[79] Bowen, W. R., Hilal, N., Lovitt, R.W., Williams, P.M., *Visualisation of an ultrafiltration membrane by non-contact atomic force microscopy at single pore resolution*, J. Membrane Sci., 110 (1996) 229-232

[80] Bowen, W. R., Hilal, N., Lovitt, R.W., Williams, P.M., *Atomic force microscope studies of membranes: surface pore structures of diaflo ultrafiltration membranes*, J. Coll. Int. Sci., 180 (1996) 350-359

[81] Bowen, W. R., Lovitt, R.W., Hilal, N., Williams, P.M., *Atomic force microscope studies of synthetic membranes*, Euromembrane '95, Bath, UK, 1995, ESMST, p. 136-139

[82] Helfferich, F., Ionenaustaucher, Verlag Chemie, Weinheim, 1959

[83] Jonsson, G., Benavente, J., *Determination of some transport coefficients for the skin and porous layer of a composite membrane*, J. Membrane Sci., 69 (1992) 29

[84] Kobatake, Y., Takeguchi, N., Toyoshima, Y., Fujita, H., *Studies of membrane phenomena. I. Membrane potential*, J. Phys. Chem., (1966) 3981

[85] Kimura, Y., Lim, H.-J., Iijima, T., *Membrane potentials of charged cellulosic membranes*, J. Membrane Sci., 18 (1984) 285-296

[86] Benavente, J., García, J.M., de la Campa, J.G., de Abajo, J., *Determination of some electrical parameters for two novel aliphatic-aromatic polyamide membranes*, J. Membrane Sci., 114 (1996) 51-57

[87] Beg, M. N., Siddiqi, F.A., Shya,, R., Altaf, I., Arshad, M., *Transport through inorganic precipitate membranes: application of absolute reaction rate theory and theory of membrane potential*, Ind. Journ. Chem., 20A (1981) 216

[88] Pusch, W., *Membrane potentials of asymmetric cellulose acetate membranes*, in: Charged gels and membranes I, ed. by E. Sélégny, D. Reidel, Dordrecht, 1976, p. 267-276

[89] Bowen, W. R., *Electrochemical aspects of microfiltration and ultrafiltration*, in: Membranes in bioprocessing, theory and applications, ed. by J.A. Howell, V. Sanchez, R.W. Field, Blackie Academic & Professional, London, 1993, p. 265

[90] Lyklema, J., Fundamentals of Interface and Colloid Science, Vol. II: Solid-fluid interfaces, Academic Press, London, 1995

[91] Hunter, R. J., Zeta potential in colloid science. Principles and applications, Academic Press, London, 1981

[92] Nyström, M., Lindström, M., Matthiasson, E., *Streaming potential as a tool in the characterization of ultrafiltration membranes*, Colloids and Surfaces A, 36 (1989) 297-312

[93] Nyström, M., Pihlajamäki, A., Ehsani, N., *Characterization of ultrafiltration membranes by simultaneous streaming potential measurements and flux measurements*, J. Membrane Sci., 87 (1994) 245

[94] Causserand, C., Nyström, M., Aimar, P., *Study of streaming potentials of clean and fouled ultrafiltration membranes*, J. Membrane Sci., 88 (1994) 211

[95] Wagenen, R. A., van, Andrea, J.D., de, Hibbs, J.B. jr., *Streaming potential measurements of biosurfaces*, J. Electrochem. Soc., 123 (1976) 1438

[96] Lukás, J., Richau, K., Schwarz, H.-H., Paul, D., *Surface characterization of polyelectrolyte complex membranes based on sodium cellulose sulfate and poly(dimethyldiallylammonium chloride)*, J. Membrane Sci., 106 (1995) 281-288

[97] Nakamae, K., Miyata, T., Matsumoto, T., *Surface studies on the ultrathin membrane prepared by spreading the polymer solution on a water surface*, J. Membrane Sci., 69 (1992) 121

[98] Börner, M., Jacobasch, H.-J., Simon, F., Churaev, N.V., Sergeeva, I.P., Sobolev, V.D., *Zeta potential measurements with fibre plugs in 1:1 electrolyte solutions*, Colloids and Surfaces A, 85 (1994) 9-17

[99] Jacobasch, H.-J., Schurz, J., *Characterization of polymer surfaces by means of electrokinetic measurements*, Prog. Coll. Pol. Sci., 77 (1988) 40-48

[100] Werner, C., Jacobasch, H.-J., Reichelt, G., *Surface characterization of hemodialysis membranes based on streaming potential measurements*, J. Biomats Sci., Polymer ed., 7 (1995) 61-76

[101] Starov, V. M., Solomentsev, Y.E., *Influence of gel layers on electrokinetic phenomena. I. Streaming potential*, J. Coll. Int. Sci., 158 (1993) 159-165

[102] Wagenen, R. A., van, Andrade, J.D., *Flat plate streaming potential investigations: hydrodynamics and electrokinetic theory*, J. Coll. Int. Sci., 76 (1980) 305

[103] Benavente, J., Jonsson, G., *Transport of Na_2SO_4 and $MgSO_4$ solutions through a composite membrane*, J. Membrane Sci., 80 (1993) 275

CHAPTER 2

Solute transport and distribution equilibria

ABSTRACT

Solute transport through nanofiltration membranes can be described by a combination of the concentration of solutes within the membrane and the solute flux equations.

The distribution equilibria which relate the solute concentration in the solution to that in the membrane are different for uncharged and charged particles. In case of uncharged particles, specific interactions or steric hindrance cause a solute distribution between membrane and solution, whereas in case of charged particles and a charged membrane, the electric interactions between ions and the membrane, or between the ions mutually, influence the distribution of ions in the membrane strongly.

Phenomenological transport equations describe the flux of different components present in the solution as a function of various driving forces, e.g., a concentration difference, a hydrodynamic pressure difference or a electrical potential difference. To describe multicomponent systems, i.e., systems containing three or more solutes, the extended Nernst-Planck equation can be used. Some theoretical calculations were carried out with this model to investigate the influence of membrane parameters, such as membrane charge and charge density and membrane thickness, and solution characteristics, such as the diffusion coefficients of the components.

2.1 INTRODUCTION

The transport of molecules or ions through membranes can be subdivided in various stages. Firstly, the solute should enter into the membrane phase from the feed side. Then, the solute is transported through the membrane and finally, it desorbs at the permeate side.
To describe solvent and solute transport in different membrane structures adequately, different models can be used. For instance, a microfiltration membrane is often modeled as a series of parallel capillaries through which solvent and solute transport occurs. In case of an isotropic membrane, the whole membrane contributes to the resistance to transport. In case of an ultrafiltration membrane, which often has an asymmetric structure, the porous toplayer determines the transport rate through the membrane. A reverse osmosis membrane is often modeled as a barrier showing specific interactions with the permeating species and having a certain resistance to transport. The transport through a reverse osmosis membrane can be described by a solution-diffusion type of mechanism.
Since nanofiltration membranes may have different morphologies, either porous or solvent-swollen, charged or uncharged, ceramic or polymeric, different theories can be used to describe the transport through these membranes. Pore models describe the transport of solvent and solute particles through membranes in terms of morphological membrane parameters, like pore size, porosity, tortuosity and membrane thickness. In case of transport through solvent-swollen systems, the membrane is often treated as a black box which is characterized by the permeability coefficients of solvent and solute and by the extent of coupling between solvent and solute flows.
In a complete description of transport of solutes through a membrane, both the fluxes through the membrane and the distribution of solutes between membrane and adjacent solutions should be considered. In this chapter, various equations to describe distribution equilibria will be presented, followed by a discussion of various transport models. The overall transport of solutes can then be described quantitatively by the use of a proper distribution coefficient which is introduced in the flux equation.

2.2 DISTRIBUTION EQUILIBRIA

At the interfaces between the membrane and the permeate or feed solution, a discontinuity in the concentration may be present as a result of steric or electrostatic effects or of specific interactions, such as hydrophobic or hydrophylic interactions. To calculate the real concentrations within the membrane, the distribution coefficients of the solutes between solution and membrane should be taken into account.
Distribution coefficients resulting from steric effects are related to the decreased effective pore area available for the permeation of solute molecules. The parameters that account for the steric hindrance of solutes entering and passing a membrane are mostly related to the membrane pore size or to the chemical nature of the solutes and the membrane material. The distribution resulting from electrostatic effects is related to the Donnan equilibrium, which is dependent on

the fixed charges which are present at the membrane surface.

2.2.1 Steric hindrance factors

The transport of charged and uncharged solutes through a membrane pore will be susceptible to steric hindrance effects. When the solutes have sizes which are comparable to those of the membrane pores or those of the interstices in the polymer network, their transport will be retarded both by steric hindrance in case of solving into the membrane as well as by frictional forces in case of transport through the membrane. These hindrance factors are of importance to both diffusive and convective flows. This means that two correction factors can be introduced to describe either the diffusive or the convective transport through a membrane: the steric hindrance factor, S_D or S_F, for diffusive or convective transport, respectively, and the wall correction factor, $f(\lambda)$ or $g(\lambda)$. These latter factors are defined as the ratio between the frictional resistance of diffusive transport of a particle through a pore and its free diffusion and the ratio between frictional resistance of convective transport and free convection, respectively.
To describe the hindrance and wall correction factors, the membrane is assumed to be porous, i.e., the membrane can be considered as a bundle of capillaries having all the same radius.

In case of *diffusive transport* the available pore area for transport decreases with increasing solute size, as can be seen from Figure 2.1. The hindrance factor for diffusive transport, S_D, equals the ratio of the available area, A_s, for transport for a solute with size r_s, $A_s = \pi (r_p - r_s)^2$, and the total area for transport, $A_T = \pi r_p^2$:

$$S_D = (1 - \lambda)^2 \qquad \{2.1\}$$

with $\lambda = r_s / r_p$ and r_s is the radius of the solute and r_p the radius of the pore.
According to Haberman and Sayre, the wall correction coefficient, f, as a function of λ, for $\lambda < 0.8$, is given by [1]:

$$f(\lambda) = \frac{1 - 2.105\,\lambda + 2.0865\,\lambda^3 - 1.7068\,\lambda^5 + 0.72603\,\lambda^6}{1 - 0.75857\,\lambda^5} \qquad \{2.2\}$$

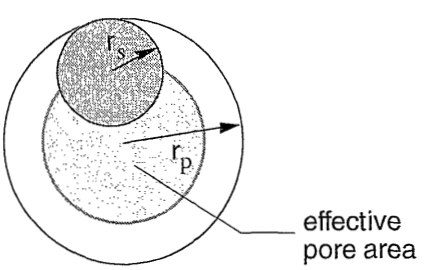

Figure 2.1: *Steric hindrance of a particle for diffusive flow*

In case of *convective* flow the steric hindrance factor, S_F, equals:

$$S_F = 2\,(1 - \lambda)^2 - (1 - \lambda)^4 \qquad \{2.3\}$$

Equation {2.3} could be derived by dividing the convectional flow, ϕ, for a solute with radius r_s within a pore with size r_p:

$$\phi = \int_0^{r_p - r_s} 2\,\pi\, r\, v_0 \left(1 - \frac{r^2}{r_p^2}\right) dr \qquad \{2.4\}$$

by the total convectional flow through this pore:

$$\phi = \int_0^{r_p} 2\,\pi\, r\, v_0 \left(1 - \frac{r^2}{r_p^2}\right) dr \qquad \{2.5\}$$

as shown in Figure 2.2. In these equations v_0 is the velocity of the solution,

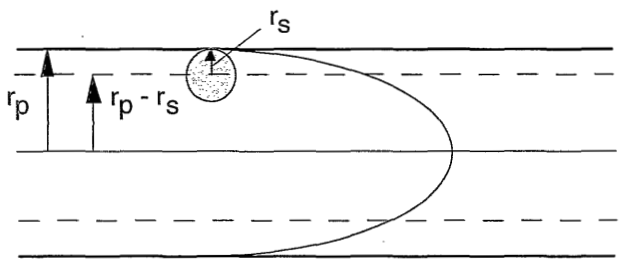

Figure 2.2: *Steric hindrance of a particle for convective, Poisseuille, flow (after [2])*

The wall correction factor for convective transport, $g(\lambda)$, for $\lambda < 0.8$, can be written as [1]:

$$g(\lambda) = \frac{1 - \frac{2}{3}\lambda^2 - 0.20217\,\lambda^5}{1 - 0.75857\,\lambda^5} \qquad \{2.6\}$$

As can be seen from equations {2.1} to {2.3} and {2.6}, the correction factors only depend on the ratio of the particle size and the membrane pore size. This implies that interactions between particle and membrane are not taken into account, neither in the steric hindrance factors, nor in the wall correction factors. In this approach the molecules are treated as rigid balls.

2.2.2 Donnan distribution

The distribution of charged species between membrane and solution will be affected by interactions between the (possible) charge at the membrane surface and the ions in the solution. Furthermore, interactions between the different ions will influence this distribution as well.

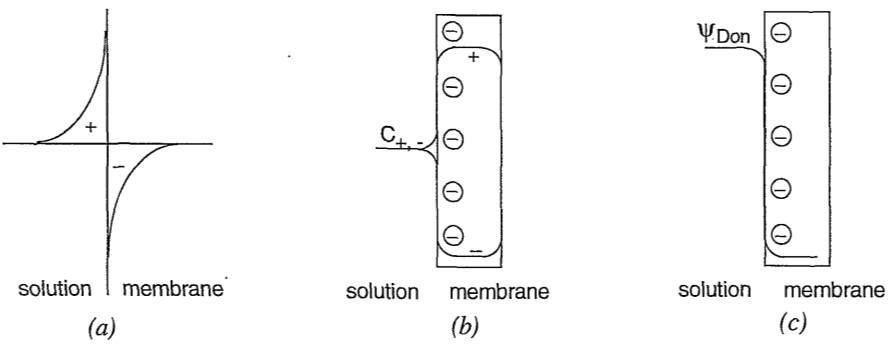

Figure 2.3: *Schematic drawings of (a) the excess of positive and negative charges near the interface of a (negatively charged) membrane and the solution., b) concentration profiles of anions and cations, c_+ and c_-, in the membrane and (c) the Donnan potential, ψ_{Don}, near the interface*

In case of a charged membrane, the concentration of co-ions, i.e., ions with the same charge as the membrane, in the membrane will be lower than that in solution, whereas the counter-ions, which have the opposite charge, have a higher concentration in the membrane than in the solution. Because of this concentration difference of the ions, a potential difference is generated at the interface between the membrane and the solution, which is called the Donnan potential. Because of this potential co-ions are repelled by the membrane, whereas counter-ions are attracted.

Figure 2.3(a) schematically shows the excess of positive and negative charges near the interface of a negative charged membrane and the solution, whereas in Figure 2.3(b) the concentration profiles of the anions and cations within the membrane are shown. In this case the concentration of the anion will be lower than that of the cations. Finally, in Figure 2.3(c) the Donnan potential, which will be negative in case of a negatively charge membrane, is shown.

A charged membrane in contact with a single salt solution

By contacting a charged membrane containing fixed charged groups with an ionic solution containing the strong electrolyte AB, an equilibrium will establish between the membrane and the solution. Assuming a membrane with a negative charge X^m and A being the cation and B the anion, the equilibrium situation is shown in Figure 2.4.

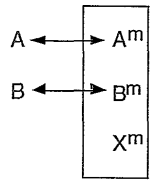

Figure 2.4: *Schematic drawing of the distribution of ions A and B between solution and membrane with charge X^m*

The distribution of ions between membrane and solution can be calculated by comparing the electrochemical potential of the ions in the membrane with that in the solution. In the solution, the electrochemical potential can be described by:

$$\eta_i = \mu_i^0 + R\,T\,\ln a_i + z_i\,F\,\psi \qquad \{2.7\}$$

and that in the membrane:

$$\eta_i^m = \mu_i^{0,m} + R\,T\,\ln a_i^m + z_i\,F\,\psi^m \qquad \{2.8\}$$

where η_i is the electrochemical potential of the ions (J/mol), μ_i^0 the reference state (J/mol), R the gas constant (J/mol.K), T the temperature (K), z_i the valence of the ions, F the Faraday constant (A.s/mol), ψ the electric potential (V) and a the activity of the solutes (-). The superscript m refers to the membrane phase.
In the derivation of the electrochemical potential, the difference in pressure between the solution and the membrane is neglected. This assumption can be justified if the swelling of the membrane is only small.

In equilibrium, the electrochemical potentials of the ions in the solution and in the membrane should be equal, hence:

$$\eta_i = \eta_i^m \qquad \{2.9\}$$

Because of the presence of the fixed membrane charge X^m, the ionic concentrations in the solution will not be equal to those in the membrane. These concentration differences between solution and membrane lead to a chemical potential difference across the membrane interface and this difference will, on its turn, be compensated by an additional electrical potential across the interface, the Donnan potential. As it is assumed that the reference chemical potentials of solution and membrane are equal, the electrical potential difference between solution and membrane, which is called the Donnan potential, ψ_{Don}, can be written as by a combination of equations {2.5}, {2.6} and {2.7}:

$$\psi_{Don} = \psi^m - \psi = \frac{R\,T}{z_i\,F} \ln \frac{a_i}{a_i^m} = \frac{R\,T}{z_j\,F} \ln \frac{a_j}{a_j^m} \qquad \{2.10\}$$

with the subscripts i and j being the components i and j in the solution.
As the Donnan potential for the components in a certain solution is equal, it can be derived from equation {2.10} that for a solution containing solutes A and B:

$$c_A^{\nu_+} * c_B^{\nu_-} = (c_A^m)^{\nu_+} * (c_B^m)^{\nu_-} \qquad \{2.11\}$$

assuming diluted solutions, so $a_i \approx c_i$. In equation {2.11} ν_- and ν_+ are the stoichiometric numbers of the anion and cation, respectively. The relation between the stoichiometric numbers and the valencies of the ions can be written as:

$$|z_A|\,\nu^+ = |z_B|\,\nu^- \qquad \{2.12\}$$

The conditions of electroneutrality in the solution and in the membrane are:

$$|z_A|\,c_A = |z_B|\,c_B \qquad \{2.13\}$$

$$|z_A|\,c_A^m = |z_B|\,c_B^m + |z_X|\,c_X^m \qquad \{2.14\}$$

where the concentration of the fixed membrane charge is indicated by c_X^m and its valency by z_X.
Combining {2.11} with {2.13} and {2.14}, a relation between the distribution of co-ions B^- between the solution and the membrane can be derived as a function of the concentration of the fixed membrane charge X^m [3]:

$$\frac{c_B^m}{c_B} = \left(\frac{|z_B|\,c_B}{|z_B|\,c_B^m + |z_X|\,c_X^m} \right)^{(|z_B|/|z_A|)} \qquad \{2.15\}$$

The ratio $\frac{c_B^m}{c_B}$ will be called the distribution coefficient of B.
More specifically, in cases of a mono-monovalent salt (such as NaCl), a bi-monovalent (counter-co-ion) salt (such as $CaCl_2$ in case of a negatively charged membrane) and a mono-bivalent salt (such as Na_2SO_4 in case of a negatively charged membrane), respectively, the Donnan equilibria can be written as:

(1-1) $$\frac{c_B^m}{c_B} = \frac{c_B}{c_B^m + c_X^m} \qquad \{2.16\}$$

(2-1) $$\frac{c_B^m}{c_B} = \left(\frac{2\,c_B}{2\,c_B^m + c_X^m} \right)^2 \qquad \{2.17\}$$

(1-2) $$\frac{c_B^m}{c_B} = \sqrt{\frac{c_B}{c_B^m + c_X^m}} \qquad \{2.18\}$$

Figure 2.5 shows the differences in co-ion distribution as a function of the feed salt concentration, represented by equations {2.16} to {2.18}. For these calculations the concentration of the negative fixed charges was chosen to be 10^{-2} mol/l.
As can be seen from this figure, a higher valence of the co-ion will cause a lower distribution coefficient of the co-ion B between membrane and solution, whereas a higher valence of the counter-ion will cause a higher distribution coefficient.

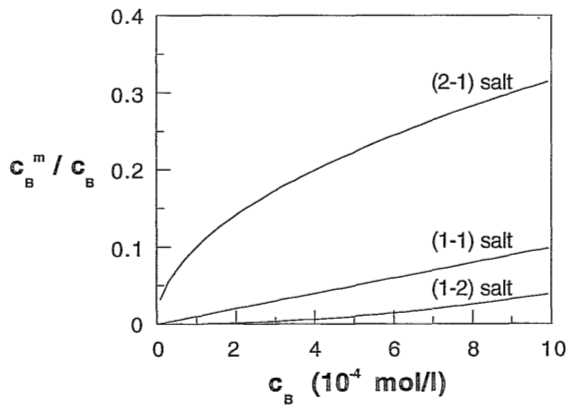

Figure 2.5: *Distribution coefficient of co-ions between membrane and solution in case of a negatively charged membrane, with $c_X^m = 10^{-2}$ mol/l, as a function of the co-ion concentration in the feed*

Summarizing, it can be seen from equation {2.15} that the Donnan equilibrium is dependent on the following factors:
* salt concentration
* fixed charge concentration in the membrane
* valence of the co-ion
* valence of the counter-ion

With an increase in salt concentration in the solution and a decrease of the fixed membrane charge, the concentration of the co-ion B in the membrane increases. This decrease of co-ion exclusion from the membrane often leads to a lower rejection of the salt, as the rejection of the co-ion determines the rejection of the salt. The co-ion concentration in the membrane will increase with increasing counter-ion valence and decreasing co-ion valence.

A charged membrane in contact with a salt mixture
In case of salt mixtures, the description of the Donnan equilibrium becomes much more complex than for the single salt solutions which has been described above. However, a hypothetical case in which an electrolyte AC is added to a salt solution AB may illustrate the

influence of some parameters on the Donnan equilibrium, assuming that the co-ion C cannot enter the charged membrane. In Figure 2.6 this system is schematically drawn.

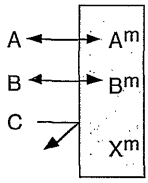

Figure 2.6: *Schematic drawing of the distribution of ions A and B between a solution and a charged membrane. The solution contains the impermeable ion C, the membrane has charge* X^m

To determine the Donnan equilibrium in this case, equation {2.11} and {2.14} can be used, as both the relation of electroneutrality in the membrane will not change compared to the case of the single salt electrolyte solution and the chemical potentials of the ions A and B in the membrane and the solution will be equal, only equation {2.13} changes. The resulting equation for the Donnan equilibrium is:

$$\frac{c_B^m}{c_B} = \left(\frac{|z_A| c_A}{|z_B| c_B^m + |z_X| c_X^m} \right)^{(|z_B|/|z_A|)} \qquad \{2.19\}$$

The addition of AC to a solution of AB will cause an increase of the concentration of counter-ions A in the solution, whereas the concentration of B in the feed solution remains constant. As can be seen from equation {2.19}, this will cause a higher concentration of B ions in the membrane and the Donnan exclusion will be less effective for component B. It is even possible that the concentration of B in the membrane becomes higher than that in the solution which may lead to negative rejections for B. Then, the ratio $c_B{}^m / c_B > 1$. When it is assumed that the co-ion concentration in the permeate equals the co-ion concentration in the membrane and that the valency of components A and B equals 1, negative retentions of component B can be found if the concentration of A in the solution is much higher than the concentration of the fixed charges.

Figure 2.7 and 2.8 show the distribution coefficient of B ions between solution and membrane as a function of the concentration of B^- in the solution for different concentrations of A and for different concentrations of fixed membrane charge, respectively. The distribution coefficient is calculated by equation {2.19}, assuming $|z_A| = |z_B| = 1$.
As can be seen from Figure 2.7, the higher the concentration of A in the electrolyte solution, the higher the ratio of the concentration of B ions between the membrane and the feed will be. Low feed concentrations of B result in higher ratios of B ion concentrations between membrane and solution as well. The fixed membrane charge is $1*10^{-3}$ mol/l.

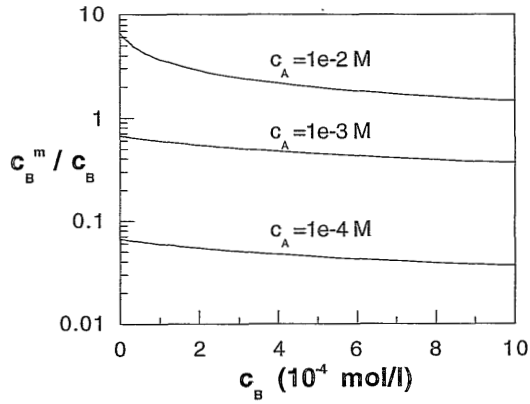

*Figure 2.7: Distribution coefficient of co-ions B between membrane and solution as a function of the co-ion concentration in the feed in case of a salt mixture with different concentrations of counter-ions A and a charged membrane with c_X^m = 1*10^{-3} mol/l, calculated according to equation {2.19}.* $|z_A| = |z_B| = 1$

The ratio of B ions between membrane and solution is shown in Figure 2.8 for different concentrations of the membrane charge. The concentration of A is fixed at 1*10^{-3} mol/l.

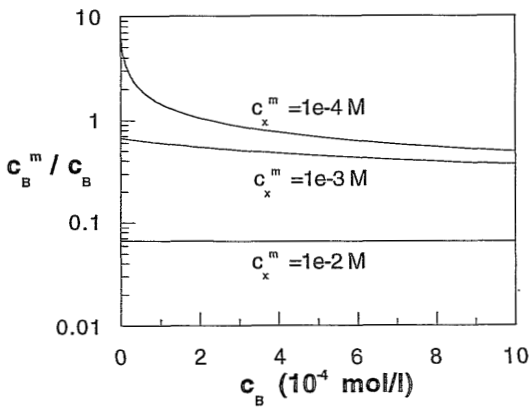

*Figure 2.8: Distribution coefficient of co-ions B between membrane and solution as a function of the co-ion concentration in the feed in case of a salt mixture with different concentrations of fixed membrane charges, c_X^m, and a fixed concentration counter-ions A, c_A = 1*10^{-3} mol/l, calculated according to equation {2.19}.* $|z_A| = |z_B| = 1$

This figure shows that the distribution coefficient of B ions between membrane and solution becomes higher in case of lower B concentrations in the solution, except for the highest membrane charge, $c_X^m = 10^{-2}$ mol/l. Furthermore, a lower membrane charge results in higher ratios of B between membrane and solution as well.
In conclusion, it can be stated that in case of a salt mixture, with the counter-ion A and the co-

ions B and C, in contact with a charged membrane, a high distribution coefficient of the permeable co-ion B between membrane and solution is enhanced by:
* low solution concentrations of B
* high solution concentrations of counter-ion A
* low membrane charge

An uncharged membrane in contact with a salt mixture
From Figure 2.8 it could be seen that the membrane charge strongly influences the distribution coefficient of B. This coefficient becomes higher when the charge of the membrane decreases. This means that in the limiting case of an uncharged membrane in contact with a salt mixture, containing the permeable ions A and B and the impermeable ion C, a Donnan equilibrium between solution and membrane will establish as well. Schematically, this is shown in Figure 2.9.

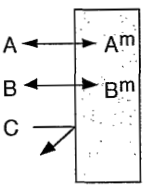

Figure 2.9: *Schematic drawing of the distribution of ions A and B between a salt mixture, containing the impermeable ion C, and a membrane*

Again, the chemical potentials of the ions A and B in both phases should be equal. Therefore, equation {2.11} holds. The conditions of electroneutrality in the solution and in the membrane can be written as:

$$|z_A|c_A = |z_B|c_B + |z_C|c_C \qquad \{2.20\}$$

$$|z_A|c_A^m = |z_B|c_B^m \qquad \{2.21\}$$

When these relations are combined with equation {2.11}, the following expression for the Donnan equilibrium can be derived:

$$\frac{c_B^m}{c_B} = \left(\frac{|z_B|c_B + |z_C|c_C}{|z_B|c_B^m} \right)^{(|z_B|/|z_A|)} \qquad \{2.22\}$$

It can be derived from equation {2.22} that the higher the concentration of the impermeable C^- ion in the solution, the higher will be that of B in the membrane. The impermeable anion will 'pump' the B ions in the membrane. This effect could be deduced as well from Figure 2.7.

2.3 PHENOMENOLOGICAL TRANSPORT MODELS

2.3.1 Phenomenological model for a system with one solvent and one solute

Transport of solvent and solute molecules through a membrane can be described in a phenomenological way. In phenomenological models, only forces and their resulting fluxes are considered, whereas the structure of the membrane is not a parameter in this model: the membrane is treated as a black box.

The following relations for the fluxes of a solvent, J_v, and a solute, J_s, through a membrane, were derived by Kedem, Katchalsky and Spiegler [4-6]:

$$J_v = -L_v \left(\frac{dP}{dx} - \sigma \frac{d\pi}{dx} \right) \qquad \{2.23\}$$

with L_v representing the permeability of the solvent, P the pressure applied, x the coordinate in the flow direction, π the osmotic pressure and σ the reflection coefficient, with $0 \leq \sigma \leq 1$,

and

$$J_s = - L_s \frac{dc_s}{dx} + (1 - \sigma) J_v \overline{c_s} \qquad \{2.24\}$$

with L_s being the solute permeability coefficient and $\overline{c_s}$ the mean solute concentration of feed and permeate.
The membrane performance is now characterized by three parameters, i.e., the solvent and the solute permeability and the reflection coefficient.

In this phenomenological model the fluxes of solvent and solute are coupled by the second term on the right hand side of equations {2.23} and {2.24}, which contain the reflection coefficient σ.

A parameter to characterize the selectivity of a membrane is the retention for a solute, R, which equals:

$$R = 1 - \frac{c_p}{c_f} \qquad \{2.25\}$$

with c_f the feed concentration and c_p the permeate concentration.
The retention can be related to the solvent flux, the solute permeability coefficient and the reflection coefficient, by integration of equation {2.24}, followed by substitution of equation {2.25} with $c_p = \frac{J_s}{J_v}$ [6]:

$$R = \frac{\sigma (1 - e^{Pe})}{1 - \sigma e^{Pe}} \qquad \{2.26\}$$

with Pe being the Péclet number which equals:

$$Pe = - J_v \frac{(1 - \sigma)}{L} \qquad \{2.27\}$$

and $L = \frac{L_s}{\Delta x}$, with Δx being the membrane thickness.

As can be calculated from equations {2.26} and {2.27}, at high solvent fluxes through the membrane, $J_v \rightarrow \infty$, the retention becomes equal to σ. This retention is called the limiting retention. For nanofiltration membranes, this limiting behavior of the retention at high fluxes has been observed experimentally [7-11]. Contrarily, for models describing the solvent and solute flux independently, the limiting retention equals unity [10, 12,13].

For $\sigma = 1$, the retention becomes independent of the flux and it will for all cases be equal to the reflection coefficient, $R = \sigma$.

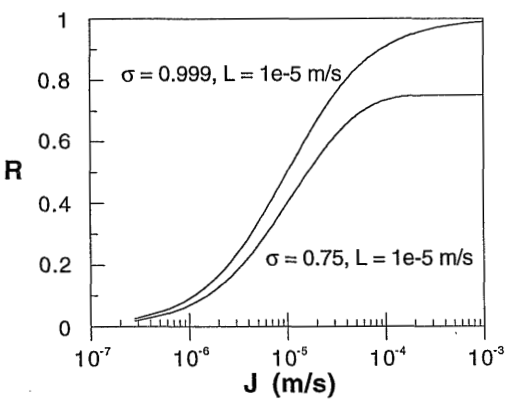

Figure 2.10: *Retention as a function of the solvent flux and of the reflection coefficient according to equation {2.26} for two membranes, one with the characteristics: $\sigma = 0.999$, $L = 1*10^{-5}$ m/s and one with: $\sigma = 0.75$, $L = 1*10^{-5}$ m/s*

Figure 2.10 shows a schematic drawing of the retention of a given solute as a function of the flux according to equation {2.26} for two different reflection coefficients.

The solute permeability coefficient is equal for both cases, whereas the reflection coefficients are $\sigma = 0.999$ and $\sigma = 0.75$, respectively. As can be seen from the figure, the retention approaches 1 for large fluxes for the case of $\sigma = 0.999$. In the other case, the retention as a function of the flux approaches asymptotically to $\sigma = 0.75$.

The phenomenological parameters σ and L can be related to the steric hindrance factors, S_F and S_D and to the wall correction factors $f(\lambda)$ and $g(\lambda)$ which were presented in the corresponding

section in this chapter. According to Nakao, the relation between the two models can be written as [2]:

$$\sigma = 1 - g(\lambda) S_F \qquad \{2.28\}$$

$$L = D f(\lambda) S_D \frac{p}{\Delta x} \qquad \{2.29\}$$

with D being the diffusion coefficient and $p / \Delta x$ the ratio of the porosity and the membrane thickness.

2.3.2 Extended Nernst-Planck model: phenomenological model for a multi-component system

The above described model can be applied for a system containing a solvent and a solute. Even if more solutes are present that do not interact, this model can be used. But in case of a system containing a solvent and more than two interacting solutes, it cannot be used anymore.
The extended Nernst-Planck equation is a phenomenological equation to describe transport of multicomponent systems. Whereas in case of the phenomenological model for a two-component system the two fluxes are the result of two driving forces, i.e., the pressure applied and the concentration difference over the membrane, in case of the extended Nernst-Planck relations, an electrical gradient is added as driving force. Therefore, three fluxes can be described, i.e., that of the solvent, that of the solute and of the electric current. Here, only the extended Nernst-Planck equation for the solute flux will be used, which is obtained by adding the three partial fluxes [14]:

$$J_i = -D_i^m \left(\frac{d c_i^m}{d x} + c_i^m \frac{z_i F}{R T} \frac{d \psi^m}{d x} \right) + K_{i,c} J_v c_i^m \qquad \{2.30\}$$

with J_i being the solute flux, D_i the chemical diffusion coefficient of i, c_i the mean solute concentration, x the coordinate in the flow direction, z_i the valency, F the Faraday constant, ψ the electric potential, R the gas constant, T the temperature, J_v the solvent flux and $K_{i,c}$ the convective coupling coefficient. This latter parameter can be considered as the product of the steric hindrance factor and the wall correction coefficient for convective transport, $K_{i,c} = S_F g(\lambda)$. The superscript m refers to the membrane phase.
The diffusion coefficient D_i^m equals the bulk diffusion coefficient corrected for the diffusion hindrance coefficient and the wall correction factor.
The first term at the right hand side of equation {2.30} represents the diffusive contribution to the solute flux, the second term the electric and the third term the convective contribution.
From equation {2.30} it follows that the concentration gradient of component i can be written as:

$$\frac{d\,c_i^m}{d\,x} = \frac{J_v}{D_i^m}\left(K_{i,c}\,c_i^m - c_{i,p} \right) - \frac{z_i\,F}{R\,T}\,c_i^m\,\frac{d\,\psi^m}{d\,x} \qquad \{2.31\}$$

with $c_{i,p} = J_i / J_v$.

The electrical potential gradient in the extended Nernst-Planck equation is induced by differences in the valencies and in the convective coupling and diffusion coefficients of the various ions permeating through the membrane. To describe this potential the description given by Bowen and Mukthar will be followed [15], [16].

To calculate the electrical potential gradient, it is considered that there is electroneutrality in the feed and permeate solution:

$$\sum_i z_i\,c_i = 0 \qquad \{2.32\}$$

and in the membrane:

$$\sum_i \left(z_i\,c_i^m \right) + z_X\,c_X^m = 0 \qquad \{2.33\}$$

with c_X^m being the fixed membrane charge concentration, and that no electric current is passing the membrane:

$$\sum_i F\,z_i\,J_i = 0 \qquad \{2.34\}$$

By multiplying equation {2.31} with the factor $z_i\,c_i^m$, combined with the condition for electroneutrality in the membrane, the electrical potential gradient over the membrane can be written as:

$$\frac{F}{R\,T}\,\frac{d\,\psi^m}{d\,x} = \frac{\dfrac{J_v}{D_i^m}\displaystyle\sum_{i=1}^{n} z_i\left(K_{i,c}\,c_i^m - c_{i,p} \right)}{\displaystyle\sum_{i=1}^{n} z_i^2\,c_i} \qquad \{2.35\}$$

The electrical field in the membrane should be constant throughout the membrane, as can be derived from the Poisson-Boltzmann equation. In its one dimensional form the Poisson-Boltzmann equation is given by:

$$\frac{d^2\,\psi^m}{d\,x^2} = -\frac{\rho}{\varepsilon} \qquad \{2.36\}$$

with ρ being the space charge and ε the dielectric constant. Because of electroneutrality in the

membrane, the space charge in the membrane is zero indicating that the first derivative of the potential to the distance is a constant.

Combining this set of equations, {2.30} to {2.35}, with the Donnan distribution given in equation {2.37}, which is equal to equation {2.10} under ideal conditions:

$$\frac{c_i^m}{c_i} = \exp\left(-\frac{z_i F \psi_{Don}}{R T}\right) \qquad \{2.37\}$$

the extended Nernst-Planck equation can be solved.
When the potential gradient over the membrane has to be calculated according to equation {2.35}, the permeate concentrations of components i should be known. Therefore, all calculations were carried out by choosing a permeate concentration which is used to calculate the concentration within the membrane at the permeate side. This concentration is then used as starting value for the numerical solution of the differential equation {2.31} by means of a fourth order Runge Kutta procedure.

With this calculation procedure, a two component system (A and B) and a three component system (A, B and C, respectively) were investigated. Components B and C are both negatively charged, while component A is positively charged. Component B has a lower negative valence and a higher diffusion coefficient than component C. The values of the various parameters within the model, i.e., D_A to D_C, $K_{A,c}$ to $K_{C,c}$ and z_A to z_C were taken from reference [15], in which these values were determined for a mixture of Na^+ (component A), Cl^- (component B) and SO_4^{2-} (component C) and are given in Table 2.1. The diffusion coefficient is calculated by assuming a hindrance factor for diffusion which equals that for a pore with a radius of 1 nm. The membrane was assumed to be negatively charged.

Table 2.1: Diffusion and convective hindrance coefficients and valencies of components A, B and C, used in the numerical calculations

	D_i (10^{-9} m^2/s)	$K_{i,c}$ (-)	z_i (-)
component A	0.84	0.967	1
component B	1.503	0.986	-1
component C	0.587	0.953	-2

It should be realized that because of the calculation procedure, the permeate concentrations of the components were kept constant, implying a small increase of the feed concentrations at each solvent flux.
Figure 2.11 shows the effect of the concentration of negative charges at the membrane on the retention of a single salt solution. From this figure it can be seen that the higher the membrane charge, the higher the retention will be, as expected from the Donnan equilibrium. Because of a higher membrane charge the concentration of co-ions within the membrane will be low, which

causes a higher retention. The membrane thickness was chosen to be 10^{-5} m and the membrane permeate concentration 0.005 mol/l. The solvent flux through the membrane was set constant at $J_v = 10^{-5}$ m/s.

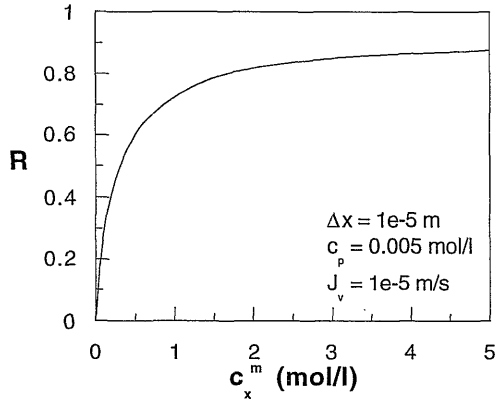

Figure 2.11: *Numerically determined retention for a single salt solution as a function of the concentration of negative charges at the membrane. $\Delta x = 10^{-5}$ m, $c_p = 0.005$ mol/l, $J_v = 10^{-5}$ m/s.*

The retention also increases by an increase in the membrane thickness, as can be seen from Figure 2.12. The curve in Figure 2.12 represents the retention of an electrolyte solution for a negative membrane charge density of 0.1 mol/l, a permeate concentration of 0.005 mol/l and a solvent flux $J_v = 10^{-5}$ m/s. At a small membrane thicknesses the solute flux through the membrane has a diffusive, electric and convective component. However, the higher the membrane thickness, the lower the diffusive and electric contribution. At very high membrane thickness, the solute flux is only dependent on the convective flow.

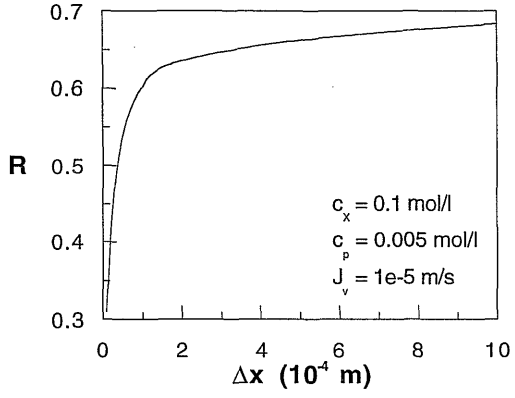

Figure 2.12: *Numerically determined retention for a single salt solution as a function of the membrane thickness. $c_X^m = 0.1$ mol/l, $c_p = 0.005$ mol/l, $J_v = 10^{-5}$ m/s.*

Figure 2.13 shows the retentions of components A, B and C within a mixture for a negatively charged membrane. The permeate concentration of A is 0.0051 mol/l, whereas that of B is 0.0011 mol/l. As can be seen from the figure, all retentions increase with increasing flux through the membrane. It can be seen from this figure, that the retention of component B which is the most permeable co-ion with the lowest valence has a negative value at all solvent fluxes. The presence of component C in the solution causes a considerable increase of the transport of B, because ion B will preferentially permeate through the membrane in combination with counter-ion A.

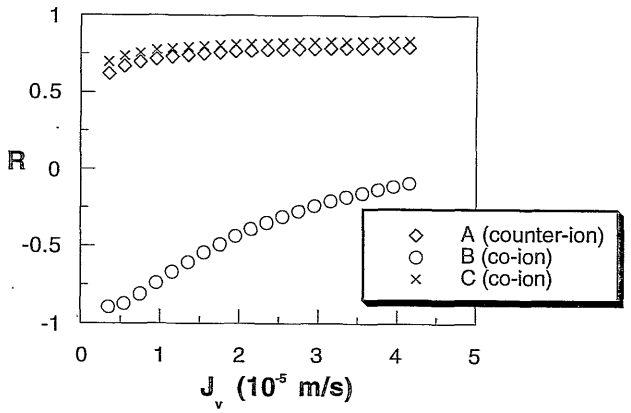

Figure 2.13: Numerically determined retention curves for ions A, B and C within a mixture as a function of the solvent flux. The membrane charge is 0.1 mol/l, $\Delta x = 10^{-5}$ m.

The influence of a third ion and its diffusion coefficient on the retention of component B is illustrated in Figure 2.14.

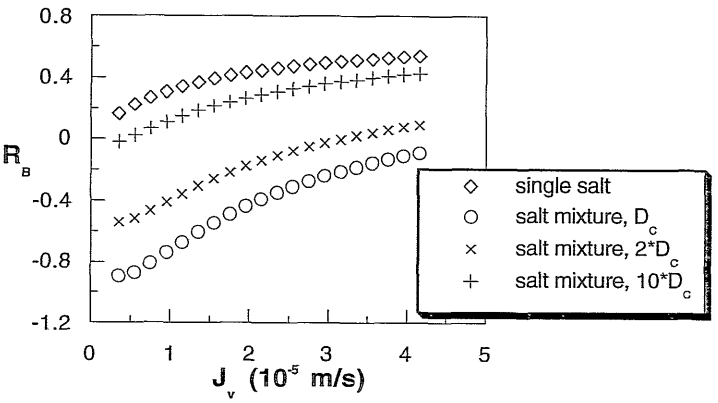

Figure 2.14: Retention of component B as a function of the diffusion coefficient coefficient of component C

The retention of component B is the highest for the single salt solution containing only components A and B. By adding a second co-ion with a lower diffusion coefficient and valency than component B, the retention of B decreases, as can be seen from this figure. By variation of the diffusion coefficient of component C from D_C to $10*D_C$ and keeping all other parameters constant, the retention of component B increased, but it remains always lower compared to the single salt solution.
From this figure it can be clearly seen that the changes in retention between a co-ion in a single salt solution and a salt mixture are dependent on the kind of second co-ion which has been added to the mixture. Both its valence and diffusion coefficient will influence the retention. With increasing negative valence and lower diffusion coefficient of the second co-ion, the transport of the first co-ion will be more favored.
The influence of the diffusion coefficient of the different components, D_i, and that of the convective coupling coefficients, $K_{i,c}$, on the retention of components B and C was calculated, by varying one parameter while keeping the others constant. The diffusion coefficient was varied between D_i and $10*D_i$, whereas the convective coupling coefficient was varied between 0 and 1. The results of these calculations are shown in Table 2.2. The retention was calculated for solvent fluxes to a maximal value of $5*10^{-5}$ m/s, which are reasonable fluxes for nanofiltration membranes.

Table 2.2: *Influence of the diffusion coefficients, D_i, and the convective hindrance coefficients, $K_{i,c}$, of components A, B and C, on the retention of B and C.*

parameter	R_B	R_C
$D_A \uparrow$	↑	↑
$D_B \uparrow$	↓	c
$D_C \uparrow$	↑	↓
$K_{A,c} \uparrow$	↑	↑
$K_{B,c} \uparrow$	↑	↓
$K_{C,c} \uparrow$	↓	↑

↑: increase, ↓: decrease, c: constant

The increase of the diffusion coefficient of a certain component caused a decrease in retention for the same component, due to the fact that the solute flux becomes higher in case of a higher diffusion coefficient. A higher diffusion coefficient of component A results in lower fluxes of the co-ions B and C. In case of a higher diffusion coefficient of component C, the retention of B increases as shown in Figure 2.14 because the transport of B becomes less favored compared to that of C.
It is still not clear why the increase of the convective coupling coefficient of a certain component resulted in higher retentions for that component, because it can be seen from equation {2.30} that a higher coupling coefficient results in a higher solute flux of that specific component.

It was concluded from these numerical calculations that the influence of the diffusion coefficients on the retention was much higher than that of the convective hindrance factors. Variation of the latter parameter from 0 to 1, hardly showed any change in retention. The retention is much more strongly dependent on the diffusion coefficient, as, for instance, could be seen from Figure 2.14.
Because the effective diffusion coefficient is the product of the bulk diffusion coefficient times a diffusive hindrance factor, it can be concluded from this that the influence of hindrance factors on diffusive transport is much higher than that on convective transport. Variation of the convective part of the extended Nernst-Plack equation does not show a very distinct influence on the salt flux in the low solvent flux range, whereas that of the convective and electric part does.

Figures 2.15 and 2.16 represent the influence of two membrane parameters, i.e., the membrane thickness and the membrane fixed charge concentration, on the calculated retention of components B and C. In Figure 2.15, the membrane charge was - 0.1 mol/l, the permeate concentration of A was 0.0051 mol/l and that of B 0.0011 mol/l. The figure shows that the membrane thickness does not have a large influence on the retention of component C. However, the rejection of component B shows a large increase when the membrane thickness becomes larger. This is caused by a decrease in the solute flux for component B at a larger membrane thickness, which is comparable to that for a single salt solution (see Figure 2.12).

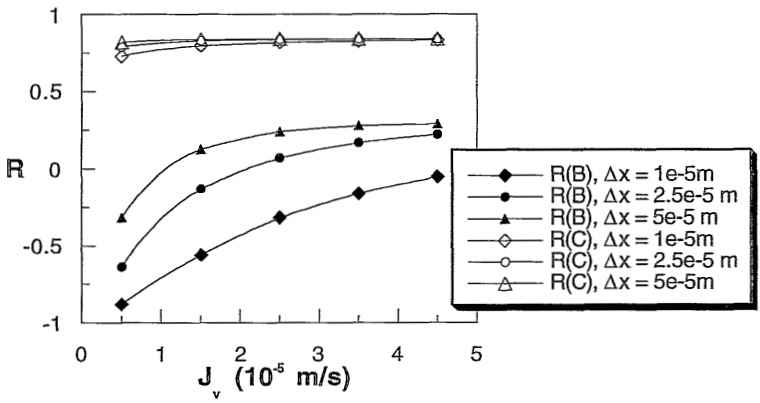

Figure 2.15: Retention as a function of the solvent flux for various membrane thicknesses

At higher solvent fluxes, the retention of components B and C increased with higher membrane charges as shown in Figure 2.16. The retention of component B showed a minimum as a function of the solvent flux, which is caused by different extents of the diffusive, electric and convective contributions to the overall solute flux as described by the extended Nernst-Planck equation. The minimum indicates that the overall concentration gradient in the membrane changes from positive to negative when going from low to high solvent fluxes. In case of low solvent fluxes, the concentration gradient will be dominated by

the electric gradient over the membrane. At higher solvent flux, the convective contribution will dominate the solute transport.
The calculations were carried out with a permeate concentration of A of 0.0051 mol/l, a permeate concentration of B of 0.0011 mol/l and a membrane thickness of $1*10^{-5}$ m.

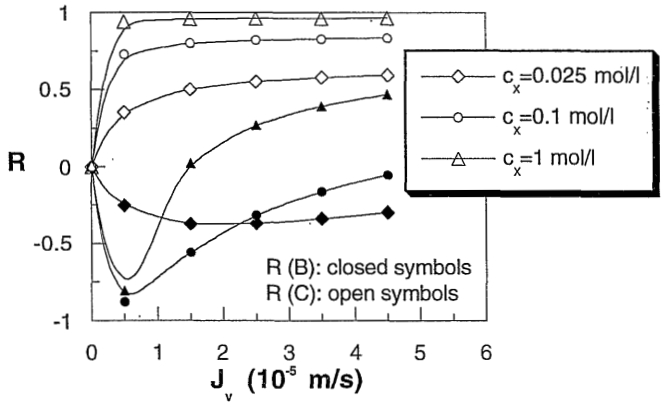

Figure 2.16: Influence of the membrane charge on the retention of components B and C.

2.4 CONCLUSIONS

The distribution of solutes between membrane and solution can be caused both by steric and by electric interaction effects. The steric effects are caused by a decreased pore area available for solute transport, because of the solute size. Furthermore, the presence of pore walls retards the transport of solutes through the membrane. These two factors contribute in case of both convective and diffusive flow, although not in the same way.
The Donnan equilibrium describes the distribution of ions between solution and membrane due to electric interactions. In this chapter the influence on the ionic distribution of the valence of co-and counter-ions, the amount of fixed membrane charge and the salt concentration in the feed has been described.
Phenomenological transport theories consider transport as the result of several driving forces. In the phenomenological model of Kedem, Katchalsky and Spiegler, the transport of solvent and solute has been described as a function of the concentration difference and the hydrodynamic pressure difference over the membrane. To determine the fluxes of the several components in a multi-component system, the extended Nernst-Planck equation can be used, which contains an electrical potential difference as an additional driving force. Some calculations with the extended Nernst-Planck model showed an increase in salt retention by both an increase in membrane charge and in membrane thickness. Furthermore, it was shown numerically that the retention of one of the co-ions in a salt mixture could achieve a negative value. At moderate membrane fluxes ($J_v < 5*10^{-5}$ m/s) the convective contribution to the solute

flux is only small compared to the diffusive and electric contribution. The retention of ions in case of a feed salt mixture showed an increase with increasing membrane thickness. The retention of the co-ion with the highest diffusion coefficient showed a minimum as a function of the solvent flux. At high solvent fluxes the retention of the ions increased with increasing membrane charge.

ACKNOWLEDGEMENTS

Jeroen Boom is kindly acknowledged for the programming of the numerical procedure to calculate the Nernst-Planck equation and for the discussions on this topic.

SYMBOLS

a:	activity	(-)
A:	area	(m^2)
c:	concentration	(mol/l)
D:	diffusion coefficient	(m^2/s)
F:	Faraday constant	(A.s/mol)
f (λ):	wall correction factor for diffusive transport	(-)
g (λ):	wall correction factor for convective transport	(-)
J_s:	solute flux	($mol/m^2.s$)
J_v:	solvent flux	(m/s)
$K_{i,c}$:	convective coupling coefficient	(-)
L:	$= L_s/\Delta x$, solute permeability coefficient corrected for the membrane thickness	(m/s)
L_s:	solute permeability coefficient in two component system	(m^2/s)
L_v:	solvent permeability coefficient in two component system	(s/m)
p	porosity	(-)
P:	pressure	(bar, N/m^2)
Pe:	Péclet-number	(-)
r:	radius	(m)
R:	gas constant	(J/mol.K)
R:	retention	(-)
S:	hindrance factor	(-)
T:	temperature	(K)
v_0:	velocity at pore center	(m/s)
x:	coordinate in flow direction	(m)
Δx:	membrane thickness	(m)
z:	valence	(-)
ε:	dielectric constant	(A.s/V.m)
η:	electro-chemical potential	(J/mol)
λ:	ratio of solute size and pore size	(-)

μ:	chemical potential	(J/mol)
ν:	stoichiometric number	(-)
π:	osmotic pressure	(bar, N/m^2)
ρ:	space charge density	(C/m^3)
σ:	reflection coefficient	(-)
ϕ:	flow rate	(m^3/s)
ψ:	electrical potential	(V)

subscripts:

D:	diffusive
Don:	Donnan
eff:	effective
f:	feed
F:	convective
i:	species i
p:	pore
p:	permeate
s:	solute
v:	solvent
X:	fixed membrane charges
+:	cationic
-:	anionic

superscript:

m:	membrane (phase)

REFERENCES

[1] Haberman, W., Sayre, R.M., "Motion of rigid and fluid spheres in stationary and moving liquids inside cylindrical tubes", David Taylor Model Basin Report no. 1143, US Navy Department, 1958

[2] Nakao, S., *Membrane transport phenomena and ultrafiltration*, in: Encyclopedia of Fluid Mechanics; Vol. 2,4,5, ed. by N.K. Cheremisinoff, Gulf Publ. Comp., Houston, 1986, p. 987

[3] Lakshminarayanaiah, Transport phenomena in membranes, Academic Press, New York, 1969

[4] Kedem, O., Katchalsky, A., *Thermodynamic analysis of the permeability of biological membranes to non-electrolytes*, Biochimica et Biophysica Acta, 27 (1958) 229

[5] Kedem, O., Katchalsky, A., *A physical interpretation of the phenomenological coefficients of membrane permeability*, J. Gen. Phys., 45 (1961) 143

[6] Spiegler, K. S., Kedem, O., *Thermodynamics of hyperfiltration (reverse osmosis): criteria for efficient membranes*, Desalination, 1 (1966) 311

[7] Jitsuhara, I., Kimura, S., *Structure and properties of charged ultrafiltration membranes made of sulfonated polysulfone*, J. Chem. Eng. Jap., 16 (1983) 389

[8] Jitsuhara, I., Kimura, S., *Rejection of inorganic salts by charged ultrafiltration membranes made of sulfonated polysulfone*, J. Chem. Eng. Jap., 16 (1983) 394

[9] Perry, M., Linder, C., *Intermediate reverse osmosis ultrafiltration (RO UF) membranes for concentration and desalting of low molecular weight organic solutes*, Desalination, 71 (1989) 233

[10] Schirg, P., Widmer, F., *Characterization of nanofiltration membranes for the separation of aqueous dye-salt solutions*, Desalination, 89 (1992) 89-107

[11] Tsuru, T., Urairi, M., Nakao, S.I., Kimura, S., *Reverse osmosis of single and mixed electrolytes with charged membranes: experiment and analysis*, J. Chem. Eng. Jap., 24 (1991) 518

[12] Mason, E. A., Lonsdale, H.K., *Statistical-mechanical theory of membrane transport*, J. Membrane Sci., 51 (1990) 1

[13] Soltanieh, M., Gill, W.N., *Review of reverse osmosis membranes and transport models*, Chem. Eng. Comm., 12 (1981) 279

[14] Schlögl, R., *Membrane permeation in systems far from equilibrium*, Ber. Bunsenges. Phys. Chem., 70 (1966) 400

[15] Bowen, W. R., Mukthar, H., *Characterisation and prediction of separation performance of nanofiltration membranes*, J. Membrane Sci., 112 (1996) 263-274

[16] Dresner, L., *Stability of the extended Nernst-Planck equations in the description of hyperfiltration through ion-exchange membranes*, J. Phys. Chem., 76 (1972) 2256-2267

CHAPTER 3

Retention measurements with electrolyte solutions

ABSTRACT

Retention measurements with single salt solutions of $CaCl_2$, NaCl and Na_2SO_4 revealed that the rejection mechanism of commercial polymeric nanofiltration membranes investigated in this study may be divided into two categories:
i) membranes for which Donnan exclusion seems to play an important role
ii) membranes for which retention is determined by both Donnan exclusion and by size effects.
In category i) both positively and negatively charged membranes were found.

Ceramic γ-Al_2O_3 ultrafiltration membranes showed similar salt retention behavior as the positively charged polymeric membranes. After modification of the γ-Al_2O_3 membrane with sodiumsilicate, the sign of the surface charge of the membrane reversed from positive to negative at a pH of 6. The retention behavior of this modified membrane was completely opposite to that of an unmodified γ-Al_2O_3 membrane.

The increase in retention with increasing pressure difference was in accordance with the Kedem-Katchalsky-Spiegler relations.

Retention measurements with salt mixtures of mono- and bivalent ions showed a decrease in retention of the monovalent ion to even negative values, whereas the bivalent ion showed a constant or slightly increasing retention when increasing the ratio bi/monovalent ion. The selectivity of the ion separation was investigated as well. It increased with increasing ion concentration and with a larger fraction of the bivalent ion within the mixture.

3.1 INTRODUCTION

One of the most important features of nanofiltration membranes is their ability to fractionate ionic mixtures. A high retention for multivalent ions is frequently combined with a moderate retention for monovalent ions. The separation of ions is determined by several factors, i.e., i) the charge density of the co-ions, which is dependent on their effective size and valency, ii) the interaction between the membrane charge sites with the counter-ions, iii) the swelling of the membrane, iv) the salt concentration and v) the membrane fixed charge density [1].
The most direct method to characterize nanofiltration membranes is the determination of the separation capability of the membranes. This is very well comparable to the actual separation process.
Retention measurements can be carried out with model salt solutions of various composition, which give a general indication of the membrane characteristics. Retention measurements with solutions of salt mixtures give more insight in differences between nanofiltration membranes than experiments with single salts.
Both experiments with single and mixed electrolyte solutions will be carried out with various commercially available nanofiltration membranes and with some lab-made ceramic membranes. Positively and negatively charged ceramic membranes will be tested in order to investigate the influence of the sign of the membrane surface charge.

3.2 THEORY

In case of single salt solutions the retention is determined by the distribution of the co-ions between membrane and solution according to the Donnan equilibrium. When dealing with salt mixtures, the diffusion coefficients and the (diffusive and convective) hindrance factors will influence the separation as well. In this section, the main mechanisms of ion separation by membranes will be summarized.

3.2.1 Donnan exclusion

If a charged membrane is in contact with an ionic solution, a Donnan equilibrium will be established. These aspects were described in more detail in Chapter 2. This section summarizes the main aspects of this theory [2-4].

Single salt solution
In case of a charged membrane in contact with an electrolyte solution, the distribution of ions between membrane and solution will be unequal because of the presence of fixed charges within the membrane. To compensate this unequal ionic distribution, a Donnan equilibrium will establish between the solution and the membrane. In case of a diluted NaCl feed solution, under ideal conditions, the distribution of the chloride ions between the feed solution and the, for instance, negatively charged membrane (superscript m) at equilibrium is given by (see

equation {2.16}):

$$c^m_{Cl^-} (c^m_{Cl^-} + c^m_{X^-}) = c^2_{Cl^-} \qquad \{3.1\}$$

With increasing salt concentration and a decreasing number of fixed membrane charges, the concentration of the co-ions in the membrane phase increases as shown in equation {3.1}. This decrease of co-ion exclusion leads to a lower salt rejection, because the exclusion of the co-ion determines the rejection of the salt. As shown in Chapter 2, the higher the valence of the co-ion, the higher the Donnan potential will be and, therefore, the lower the concentration of co-ions in the membrane will be. A higher valence of the counter-ion has a reversed effect.

Salt mixture

If a second co-ion is added to the salt solution, the Donnan equilibrium will change. For instance, by adding Na_2SO_4 to the NaCl solution, the system will contain more counter-ions Na^+, whereas the concentration of the chloride ions in the feed solution remains constant.
For the distribution of chloride ions between solution and membrane, it can be derived that (see equation {2.19}), assuming that no sulfate ions can enter the membrane:

$$\frac{c^m_{Cl^-}}{c_{Cl^-}} = \frac{c_{Na^+}}{c^m_{Cl^-} + c^m_{X^-}} \qquad \{3.2\}$$

It can be seen that an increase in the sodium ion feed concentration at constant chloride ion feed concentration and constant membrane fixed charges, results in an increase of the concentration of the chloride ions in the membrane. It is even possible that the chloride ion concentration in the membrane becomes higher than that in the solution.
When the sulfate ions can enter the membrane to some extent, then the distribution coefficient of Cl^- between membrane and solution will become smaller.
When an uncharged membrane is in contact with a solution containing ions that are able to pass the membrane, for instance Na^+ and Cl^-, and others that are not, like for instance SO_4^{2-}, an equilibrium will be established between the solution and the membrane.
Under ideal conditions, in which the activity coefficients are assumed to be unity and the concentration of the sulfate ions in the membrane equals zero, the following relation can be derived, see equation {2.22}:

$$c_{Cl^-} (c_{Cl^-} + 2\, c_{SO_4^{2-}}) = (c^m_{Cl^-})^2 \qquad \{3.3\}$$

From this equation, it can be seen that an increase in the SO_4^{2-} concentration, without changing the Cl^- concentration in the solution, leads to a higher Cl^- concentration in the membrane phase. Furthermore, a higher Cl^- concentration in the solution will cause a higher Cl^- concentration in the membrane phase as well.
When retention measurements are carried out with a mixture of SO_4^{2-} and Cl^-, this means that a higher concentration of SO_4^{2-} in the feed solution will often cause a lower chloride ion retention. In case of high concentrations of the (more) impermeable SO_4^{2-} ion, the chloride

ions may even be transported against their own concentration gradient. Then, negative retentions can be observed.

A similar theoretical derivation can be given if instead of a mixture with an impermeable anion, an impermeable cation is used, for instance Ca^{2+}. If it is assumed again that Na^+ and Cl^- are able to pass the membrane then the distribution of ions between the solution and the membrane can be given as:

$$c_{Na^+}\,(\,c_{Na^+} + 2\,c_{Ca^{2+}}\,) = (\,c^{m}_{Na^+}\,)^2 \qquad \{3.4\}$$

In this case a higher Ca^{2+} concentration will 'push' the Na^+-ions through the membrane.
For the derivation of equation {3.4} it was assumed that Ca^{2+} cannot enter the membrane. When a low concentration of these ions is present in the membrane, the amount of Na^+ in the membrane will decrease consequently.

Although the Donnan equilibrium may affect the ionic retention in case of salt mixtures, it is not the only determining factor, like it is in single salt solutions [5]. As shown in Chapter 2, differences in diffusion coefficients add to the final retention as well. Generally, it can be stated that for both co and counter-ions, the multiple charged ions are retained better within a mixture than in a single salt solution, whereas the monovalent ions will be retained less.

The diffusion coefficients of the ions have an influence on both the diffusive and the electrical contribution of the ion flux as shown by the extended Nernst-Planck equation. As an example the relation between the diffusion coefficient and the electrical potential gradient will be qualitatively illustrated for a mixture containing sulfate, chloride and sodium ions. The diffusion coefficients of these ions have the following sequence: $D_{SO_4} < D_{Na} < D_{Cl}$. In a solution with only sodium chloride, the electrical potential will be negative, because the transport of sodium ions has to be accelerated, whereas that of chloride ions should be slowed down to achieve identical ion fluxes to maintain electroneutrality. Contrarily, in a solution with sodium sulfate, the electrical potential will be positive, because the transport of the sulfate ions should increase and that of the sodium ions decrease. In case of a mixture of sodium chloride and sodium sulfate, the potential will be in between that of the single salt solutions. Therefore, in a mixture with sulfate, chloride and sodium ions, the contribution of the electric potential to the transport of chloride ions will be always higher than that in case of a single salt solution and its transport through the membrane will, as a result, be higher. In case of sulfate ions, the electrical component of the transport will be lower than in case of a single salt solution, causing a diminished transport of sulfate ions.

3.2.2 Transport through a membrane

Phenomenological model for single salt solutions

For the description of transport of the components of a single salt solution, the phenomenological relations derived by Spiegler, Kedem and Katchalsky can be used as described in Chapter 2 [6].
The solvent flux, J_V, is given by:

$$J_V = -L_V \left(\frac{dP}{dx} - \sigma \frac{d\pi}{dx} \right) \qquad \{3.5\}$$

with L_V being the permeability constant of the solvent, dP the pressure gradient applied across the membrane, x the coordinate in flow direction, $d\pi$ the osmotic pressure gradient across the membrane and σ the reflection coefficient.
The solute flux, J_S, equals:

$$J_s = - L_s \frac{dc_s}{dx} + (1 - \sigma) J_v \overline{c_s} \qquad \{3.6\}$$

with dc_S being the solute concentration gradient over the membrane, L_S the permeability constant of the solute and $\overline{c_s}$ the average concentration.
The retention of the membrane, R, is defined as:

$$R = \frac{c_f - c_p}{c_f} \qquad \{3.7\}$$

with c_f the concentration of the feed and c_p that of the permeate.
The relation between the solvent flux and the retention can be written as:

$$R = \frac{\sigma (1 - e^{Pe})}{1 - \sigma e^{Pe}} \qquad \{3.8\}$$

with $Pe = - J_v \frac{(1 - \sigma)}{L}$ and $L = \frac{L_s}{\Delta x}$, Δx being the membrane thickness.

Phenomenological model for salt mixtures

In case of a salt mixture the flux of each of the solutes, i, can be described by the extended Nernst-Planck equation:

$$J_i = -D_i^m \left(\frac{d\, c_i^m}{d\, x} + c_i^m \frac{z_i F}{R T} \frac{d\, \psi^m}{d\, x} \right) + K_{i,c} J_v c_i^m \qquad \{3.9\}$$

with J_i being the solute flux, D_i the chemical diffusion coefficient of i, c_i its concentration, x

the coordinate in the flow direction, z_i the valency, F the Faraday constant, ψ the electric potential, R the gas constant, T the temperature, J_v the solvent flux and $K_{i,c}$ the convective coupling coefficient. The superscript m refers to the membrane phase.
In this chapter the results of the retention measurements will be described qualitatively. In Chapter 6, a quantitative description will be given, when the experimental results are compared with the calculated data.

3.3 EXPERIMENTAL

3.3.1 Retention measurements

Single salt solutions

All polymeric and ceramic nanofiltration membranes available were preliminary characterized with single salt retention measurements. These retention measurements were carried out with three salts, $CaCl_2$, NaCl and Na_2SO_4, (Merck, p.a.) respectively, at three different initial concentrations, 0.001, 0.005, 0.01 M, respectively, at a constant feed pressure difference of 5 bar.
The water was demineralized by a Milli-Q-Plus unit. The pH value of the water varied between 5.6 and 6.2.
These retention measurements were carried out in a stirred dead-end filtration set-up, by which the membrane flux was recorded automatically. The area of the membranes in the cells used for the retention measurements is 38.5 cm^2. The stirred permeation cell was pressurized by nitrogen. The permeate is collected in a vessel which was placed on a balance. The mass increase of the permeate on the balance was recorded in time by a computer.

Firstly, all membranes were permeated with water for four hours. Then, the feed solution was changed from pure water to a salt solution. After a stabilization time of two hours the concentration of the feed was measured and subsequently permeation samples were taken. Salt retention measurements were started with the lowest concentration. The sequence of the salts was $CaCl_2$, NaCl and Na_2SO_4, respectively. When electrolyte solutions were changed, the membrane was flushed for at least two hours with pure water.

More extended retention measurements with single salt solutions were performed with some of the membranes. In this latter case the experiments were carried out at four or five different pressure differences and at different electrolyte concentrations. The pressure differences used were in the range of 3 to 7 bars and the concentrations were 0.001, 0.005 and 0.01 M, respectively. Five polymeric membranes were chosen for the extended measurements, ASP35, NF45, UTC70, UTC90 and CTA-LP membranes and a ceramic γ-Al_2O_3 membrane.

The concentrations of the single salt solutions were determined by conductivity measurements.

Salt mixtures

For several membranes pressure-dependent retention measurements were carried out with salt mixtures. The mixtures had either the same anion ($CaCl_2$/NaCl) or the same cation (NaCl/Na_2SO_4). For both types of mixtures three different concentrations were used, based on either the cations or the anions, 0.001, 0.005 or 0.01M, respectively. Also the ratio of the cations Ca^{2+}/Na^+ and that of the anions Cl^-/SO_4^{2-}, was varied; 1/9, 1/1, 9/1, respectively. The pressure differences applied were in the range of 3 to 7 bar.
The concentrations of sodium and calcium ions in the cation mixtures were determined by atomic absorption spectroscopy (Spectra 10, Varian). The wavelength at which Ca^{2+} was determined was 422.7 nm. The burning gas was a mixture of N_2O and acetylene within a reducing flame. To determine the sodium ion concentration, a wavelength of 589.0 nm was used. Air and acetylene were the burning gases within an oxidizing flame. To suppress ionization of the sodium ions in the air-acetylene flame, 2000 ppm cesiumchloride was added to all samples.
HPLC was used to determine the concentrations of the individual anions (pump: Waters, Millipore 510; autosampler: Waters 717 plus; column: Waters IC-Pack anion; detector: Waters conductivity meter 430). The eluens used was a mixture of 20 ml gluconate/borate buffer solution, 20 ml n-butanol and 120 ml acetonitril in 1 liter of demineralized water.

3.3.2 Membranes

Both polymeric and ceramic membranes were used.

The following polymeric *membranes* were used:
* ASP35 [a,b,c] (Advanced Membrane Technology)
* MPF21; MPF32 (Kiryat Weizmann)
* UTC20; UTC60; UTC70 [a]; UTC90 [a,b] (Toray)
* CTA-LP [a,b,c]; TFCS (Fluid Systems)
* NF45 [a,c]; NF70 (FilmTec)
* BQ01; MX07; HG01; HG19; SX01; SX10 (Osmonics)
* 8040-LSY-PVD1 (Hydranautics)
* NF CA30; NF PES10 (Hoechst)
* WFN0505 (Stork Friesland).

The ASP35, UTC20, UTC60, UTC70, UTC90, CTA-LP, TFCS, NF45, NF70, BQ01, MX07, HG01, HG19, SX01, SX10, 8040-LSY-PVD1, NF CA30, NF PES10 and the WFN0505 membrane were all kindly supplied by the manufacturers.

With all above mentioned membranes preliminary salt retention measurements were carried out. The membranes marked with [a] were used for pressure-dependent retention measurements with single salt solutions, membranes with [b] for retention measurements with anion mixtures

and membranes with ^{c} for retention measurements with cation mixtures.

Ceramic membranes used were γ-Al_2O_3 membranes and modified γ-Al_2O_3 membranes.
The synthesis of the γ-Al_2O_3 membrane was described by Uhlhorn et al. [7]. The supported γ-Al_2O_3 membrane was made by a sol-gel method and was sintered at a temperature of 600°C.
Modifications of the γ-Al_2O_3 membrane were carried out to achieve both positively and negatively charged membranes. Since γ-Al_2O_3 membranes have an isoelectric point of 7-9, they are positively charged when they are immersed in water with a pH of 6 [8]. To obtain negative charges, the γ-Al_2O_3 membranes were modified with sodiumsilicate. By adsorption of the sodiumsilicate at the membrane surface, followed by calcination, it was tried to apply a silica layer on top of the membrane. Since the isoelectric point of SiO_2 is around pH = 2-3, the membrane surface charge should be negative when immersed in water [8].
The modification with sodiumsilicate was carried out by impregnation of the membranes for 16 hours in a solution of 1 w% sodiumsilicate in ultrapure water. Then, the membranes were dried and heated to 400 °C for 3 hours (heating rate: 25 °C/hour). In some cases this treatment was repeated. X-ray Photon Spectroscopy (Kratos XSAM 800 XPS) was used to characterize the modifications of the γ-Al_2O_3 membranes.

3.4 RESULTS

3.4.1 Salt retention measurements

Salt retention measurements with $CaCl_2$, NaCl and Na_2SO_4 at a pressure difference of 5 bar were carried out with all membranes mentioned in the Experimental Section. For the UTC60 membrane $MgSO_4$ was used instead of Na_2SO_4. For the PES10 and PVDI membranes only $CaCl_2$ and NaCl were used. In addition, the pure water permeability was determined for all the membranes.
An overview of the results of these salt retention measurements is given in Appendix I and the water permeabilities are shown in Appendix II. The water permeabilities of all membranes were in the range of 1.0 - 6.6 l/m^2.h.bar.
The salt retention measurements showed that the behavior of most of the membranes could be classified into two main categories:
i) membranes for which Donnan exclusion seemed to play an important role
ii) membranes for which retention was neither completely determined by Donnan exclusion nor by size effects.

The former category of membranes, for which Donnan exclusion determined the separation, could be subdivided into two membrane types. The first type showed the following salt retention sequence: R (Na_2SO_4) > R (NaCl) > R ($CaCl_2$), which is typically for a negatively charged membrane. In general, the retention of these membranes decreased with increasing concentration.

The ASP35 membrane was an example of this category, as shown in Figure 3.1.
Other membranes of this type were: UTC70, HG01, HG19, BQ01 and WFN0505. For PVD1 and PES10 the NaCl retention was higher than the $CaCl_2$ retention, whereas for these membranes no experiments with Na_2SO_4 were carried out. Both membranes could also be classified within this type.

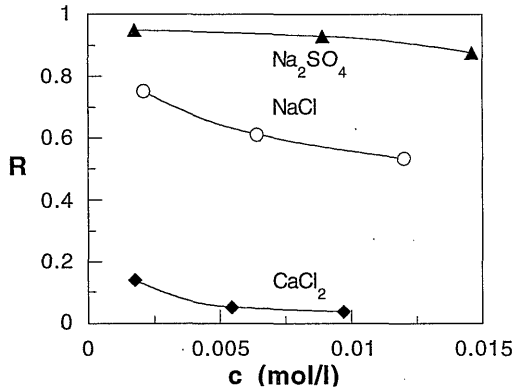

***Figure 3.1**: Retention of different salts as a function of the feed concentration for a ASP35 membrane. Pressure: 5 bar*

The second type of membranes of category i) showed a salt retention sequence: R ($CaCl_2$) > R (NaCl) > R (Na_2SO_4), which was reversed compared to that of the first membrane type (See Figure 3.2). This sequence is typical for positively charged membranes.

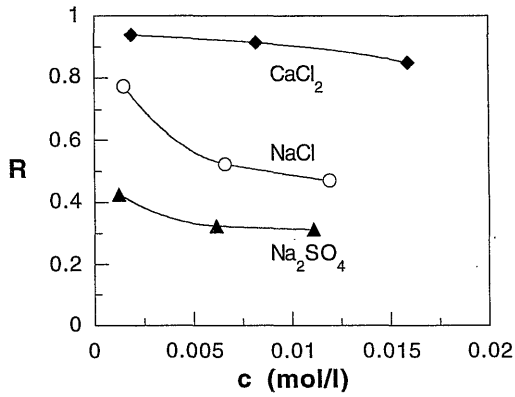

***Figure 3.2:** Retention of different salts as a function of the feed concentration for a MPF21 membrane. Pressure: 5 bar*

The retention of this membrane type also decreased with increasing salt concentration.
The membranes of this type were MPF21 and MPF32. For a γ–Al_2O_3 ultrafiltration membrane salt retention measurements were carried out at only one concentration, i.e., at c = 0.005 M, but the observed salt retention sequence R ($CaCl_2$) > R (NaCl) > R (Na_2SO_4) was similar to

that of the above mentioned positively charged polymeric membranes. The retention of $CaCl_2$ was 0.90, whereas the membrane did not show any retention at all for Na_2SO_4. The retention of NaCl was in between, 0.57.

The last category of polymeric membranes was classified according to the salt retention sequence of R (Na_2SO_4) > R ($CaCl_2$) > R (NaCl).

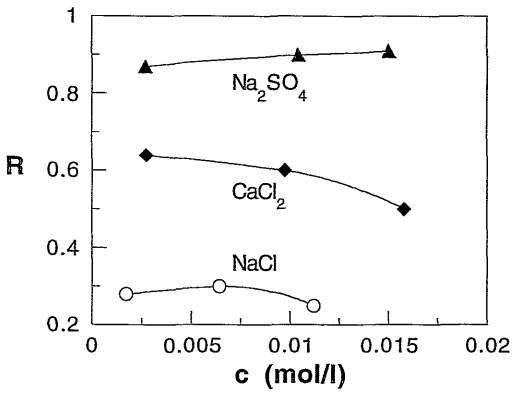

Figure 3.3: *Retention of different salts as a function of the feed concentration for a NF45 membrane. Pressure: 5 bar*

Figure 3.3 with NF45 as membrane represents an example of this category. Other membranes of this category were TFCS, CTA-LP, UTC90, SX10, MX07 and CA30.

The results of the first two membrane types could be explained by the Donnan exclusion theory. Both the high retention for sulfate ions and the low retention for the calcium ions for the first class of membranes (negatively charged) and the high retention for the calcium ions and the low retention for the sulfate ions for the second class of membranes (positively charged) could be explained by the Donnan theory.
In case of the retention sequence R (Na_2SO_4) > R (NaCl) > R ($CaCl_2$), the retention for the bivalent anion was the highest, whereas that of the bivalent cation was the lowest. The retention of the salt with a mono-mono-valent ion pair was in between the other two. If it is assumed now, that the membranes of the first type are negatively charged, the high retention for the sodium sulfate (bivalent co-ion, monovalent counter-ion) and the low(er) retention for calcium chloride (bivalent counter-ion, monovalent co-ion) are in accordance to the Donnan exclusion model. The decrease of the retention with increasing concentration is also in agreement with this model, because the Donnan exclusion diminishes at high feed electrolyte concentrations, like was shown in Chapter 2 [5]. In case of a higher ionic strength, the membrane charge will be shielded to a large extent, resulting in a lower effective charge and consequently a lower retention is obtained [9]. This type of retention sequence was observed by several other authors as well and attributed to the negative charge of the nanofiltration

membranes used [1,10,11].
The behavior of the second type of membrane could be explained in the same way, assuming that the membranes are now positively charged. For the γ-Al_2O_3 membrane this was also the case, since the isoelectric point of Al_2O_3 is in the range of pH = 7-9. For positively charged membranes the retention of the bivalent cation, Ca^{2+}, was the highest, whereas that of the bivalent counter-ion (sulfate) was the lowest.

The results of the third class of membranes cannot be explained by Donnan exclusion, because both the retention for the bivalent cation and that of the bivalent anion were high. Neither could the retention sequence be explained by differences in size of the different ions. Although the sizes of the hydrated sulfate and calcium ions are larger than those of the sodium and chloride ions, the calcium ion is on its turn larger than the sulfate ion which is shown in Table 3.1. The sizes of the ions are calculated from their diffusion coefficients by the Stokes-Einstein equation [12]. So, in case of separation on base of size exclusion, the calcium ions would have shown the highest retention. Not only size effects seemed to determine separation in this case.

Table 3.1: *Diffusion coefficients in water and hydrodynamic radii for several ions*

ion	D (10^{-9} m^2/s)	r (Å)
Na^+	1.33	1.64
Cl^-	2.03	1.07
Ca^{2+}	0.92	2.37
SO_4^{2-}	1.06	2.05

Possibly, the retention behavior of the membranes of this category was determined by a combination of both charge and size exclusion.It may also be possible, that both negative and positive charges are present at the surface of the membranes of this class. The experiments performed did not clarify any of these hypotheses. Nyström et al. reported for a NF40 membrane (which was the predecessor of the NF45 membrane) a higher retention for $MgCl_2$ than for NaCl [13]. They suggested that this was affected by the difference in size between the magnesium and sodium ions.

Finally, there are some membranes that did not seem to fit in one of the categories. The SX01 membrane had equal retentions for Na_2SO_4 and for $CaCl_2$, whereas the NaCl retention was lower. The NF70 membrane had about the same retention for $CaCl_2$ and NaCl, while the Na_2SO_4 retention was slightly higher. The same was found for the UTC60 membrane, although in this case $MgSO_4$ was used instead of Na_2SO_4.

To investigate the influence of the membrane charge on the separation of the salts, two different additional experiments were carried out with ceramic membranes. Firstly, the pH of the sodium sulfate solution was changed from 6 to 10, passing the isoelectric point of the Al_2O_3 and therefore, changing the membrane surface charge from positive to negative.

Secondly, γ- Al_2O_3 membranes were modified with silicate to achieve a negatively charged surface.

When the pH was changed from 6 to 10, the retention of Na_2SO_4 increased from 0 to 0.50. This was achieved by the inversion of the surface charge from positive to negative, which on its turn made Donnan exclusion more effective.

Whereas the unmodified γ-Al_2O_3 membranes did not show any retention for Na_2SO_4 at all at pH=5.5, a γ-Al_2O_3 membrane modified with sodiumsilicate showed, initially, a retention of 0.75 for a 0.001M Na_2SO_4 solution. Then, the retention started to decrease and reached a value of 0.64 after 4 hours of operation. After a total operation time of 13 hours, no retention for Na_2SO_4 was observed anymore. Measuring the retention for $CaCl_2$ of this membrane afterwards showed that it was identical to that of an unmodified γ-Al_2O_3 membrane.
Using a membrane which was modified twice with sodiumsilicate, the retention of a 0.005M Na_2SO_4 solution was above 0.78 during 5.5 hours of operation. A retention measurement with $CaCl_2$ confirmed again that the surface charge of the membrane had changed from positive to negative, because no retention for $CaCl_2$ was found anymore, whereas the unmodified ceramic membrane showed a retention higher than 0.90.
A 0.005M solution of NaCl showed retentions between 0.07 and 0.24, but in contrast to the stable retention values in case of the unmodified membranes, the extent of the retention decreased in time.
A final experiment with these sodiumsilicate modified membrane showed a continuous decreasing retention for Na_2SO_4 going from 0.40 to only 0.20.
It has been clearly shown that the modification with sodiumsilicate causes a reversal of the membrane surface charge from positive to negative, although the membrane formed was not stable in the solutions used in the above described experiments.

3.4.2 Flux dependent retention measurements

Single salt solutions

Figure 3.4 shows the Na_2SO_4 retention as a function of the solvent flux for a UTC70 membrane. This figure illustrates the behaviour of all membranes for all electrolytes: the higher the solvent flux, the higher the retention. This is a general phenomenon, because an increase in pressure difference causes a higher water flux, whereas the salt flux through the membrane is mainly diffusion-driven and, therefore, does not change that much, as can be seen from equations {3.5} and {3.6}. Since the salt concentration in the permeate equals the ratio of the salt flux and the water flux, it can be seen that the resulting retention will increase. Furthermore, the figure shows again that the lower the salt concentration, the higher the retention.
The curves in the figure are drawn according to equation {3.8}, with a fixed value for the

membrane thickness normalized permeability and fitted values for the reflection coefficient σ. Firstly, both the permeability and the reflection coefficient were fitted for each of the lines. Secondly, the mean value of the permeability coefficient was calculated and the reflection coefficient was fitted again. The value of the membrane thickness normalized permeability coefficient determined was $1.01*10^{-7}$ m/s. The values of the reflection coefficient decreased from a value of 1 in case of the 0.001M solution, to 0.87 in case of the 0.005M solution to 0.82 in case of the highest salt concentration.

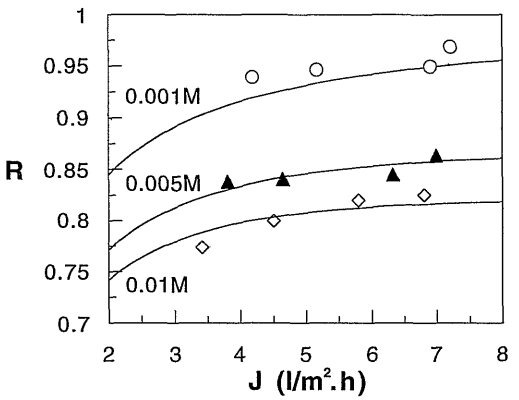

Figure 3.4: *Na_2SO_4 retention as a function of the solvent flux at several feed concentrations. UTC70 membrane*

Salt mixtures

Retention measurements with salt mixtures were carried out with various membranes: UTC90, ASP35, CTA-LP and NF45.
For the UTC90, ASP35 and CTA-LP membranes the retention measurements were carried out with a mixture of NaCl and Na_2SO_4. From the single salt retention measurements, the ASP35 membrane was characterized as negatively charged, whereas the CTA-LP and UTC90 membranes were from the second class of nanofiltration membranes for which both charge and size seemed to play a role in separation.
For the ASP35, CTA-LP and NF45 membranes retention measurements were carried out with a mixture of $CaCl_2$ and NaCl. The NF45 membrane was categorized as a membrane for which charge was not the only determining factor concerning ion separation.

Experiments with NaCl/Na_2SO_4
The retentions of Cl^- and SO_4^{2-} are plotted in Figures 3.5 and 3.6 as a function of the solvent flux for a UTC90 membrane, for various molar fractions of Cl^- and SO_4^{2-}. The total concentration of anions was 0.01M.
Figure 3.7 shows the chloride and sulfate ion retention as a function of the chloride fraction for a CTA-LP membrane.
It can be seen from Figures 3.5 and 3.7 that the retention for Cl^- drastically decreased by the

addition of Na_2SO_4 to the NaCl solution for both the UTC90 and the CTA-LP membrane. In case of UTC90, the retention decreased from around 0.80 for the chloride ions in a single salt solution to a negative retention in the mixture with a ratio of chloride/sulfate of 1/9. In case of the CTA-LP membrane the retention decreased even more drastically. For both membranes the chloride ion retention became negative, which meant that the chloride ions were transported against their own concentration gradient. The increased transport of chloride ions and the decrease of that of the sulfate ions can be explained by the electrical potential gradient that will occur because of the different diffusion coefficients of the ions.

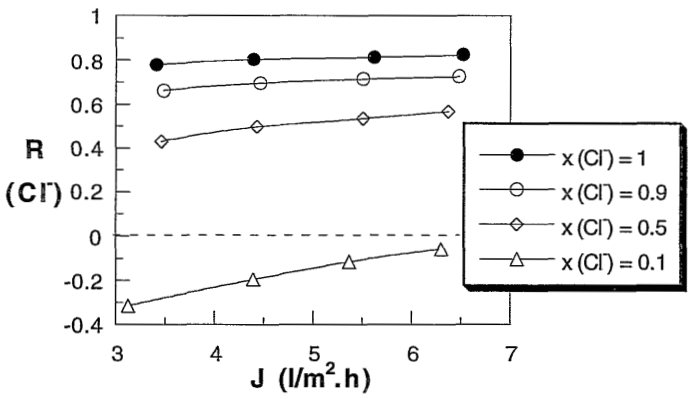

***Figure 3.5**: Retention of chloride ions using a feed mixture of Cl^- and SO_4^{2-} as a function of the solvent flux for various ionic compositions. Membrane: UTC90. Overall anion concentration = 0.01M*

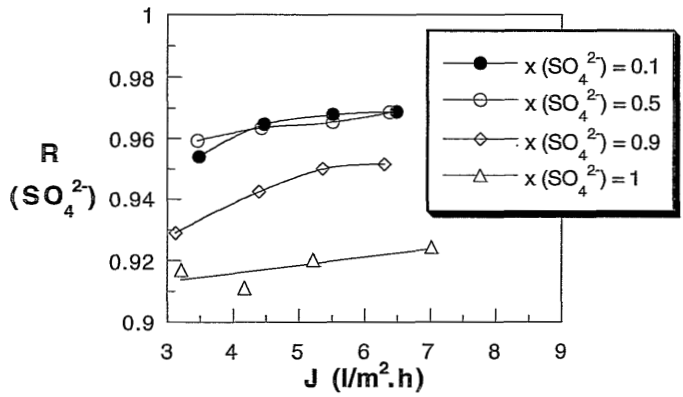

***Figure 3.6:** Retention of sulfate ions using a feed mixture of Cl^- and SO_4^{2-} as a function of the solvent flux for various ionic compositions. Membrane: UTC90. Overall anion concentration = 0.01M*

As shown in the theoretical section of this chapter, the electrical potential will diminish the transport of the sulfate ions within a mixture containing chloride ions, whereas the chloride ion

transport will be higher, both compared to the transport in case of a single salt solution.
The Donnan equilibrium may contribute as well to the decreasing chloride ion retention by the addition of Na_2SO_4. Since the concentration of the sulfate ions in the membrane is very small, an increase of the Na^+ concentration in the feed will cause a higher Cl^- concentration in the membrane as shown in equation {3.3}. In case of merely convective transport, this will cause a higher chloride ion flux and, therefore, a decreasing rejection of the chloride ions could be expected.

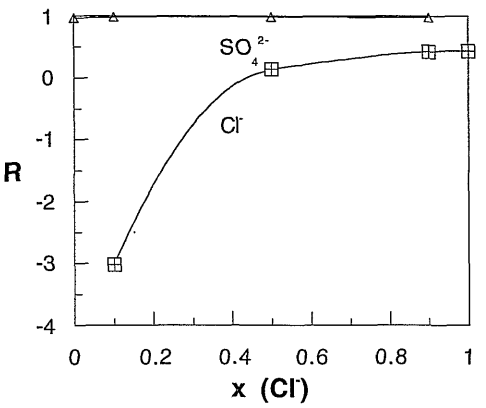

Figure 3.7: *Retention of chloride (⊞) and sulfate (Δ) ions using a feed mixture of Cl^- and SO_4^{2-} as a function of the fraction, x, of chloride ions in the feed solution. Membrane: CTA-LP. Overall anion concentration = 0.01M, P = 5 bar*

By increasing the solvent flux through the membrane, the chloride ion retention for all fractions increased.
For the sulfate ions (see Figures 3.6 and 3.7), the retention increased when the sulfate fraction in the feed solution was decreased, but this effect was only small. Furthermore, it could be seen that the retention for the sulfate ion increased with increasing solvent flux through the membrane, as was expected.

Summarizing the results, in a mixture the retention of the co-ion having the highest valency and the lowest diffusion coefficient remained constant or increased a little compared to that in a single salt solution, whereas the retention of the other co-ion with a low valency and a higher diffusion coefficient decreased drastically. This behavior of co-ions in a mixture has been observed before [14-20].
Although the retention data for the ASP35 membrane were somewhat different from those of the UTC90 and CTA-LP membrane, the observed dependence of the retention of the chloride and sulfate ions on their fractions in the feed solution was similar. The retention and selectivity data of these three membranes are presented in [21].

The selectivity of the separation process can be calculated from the data shown in Figures 3.5 and 3.6. The selectivity for separation of compounds 1 and 2, $S_{1,2}$, can be defined as the ratio

of components 1 and 2 in the permeate compared to that in the feed:

$$S_{1,2} = \frac{\left(\frac{c_{p,1}}{c_{p,2}}\right)}{\left(\frac{c_{f,1}}{c_{f,2}}\right)}$$

with c_p and c_f being the concentration in the feed and permeate, respectively,
or:

$$S_{1,2} = \frac{1 - R_1}{1 - R_2}$$

with R being the retention of each of the compounds. The selectivity, S, is always larger than or equal to one. At a selectivity of one, no separation of the compounds has been achieved.

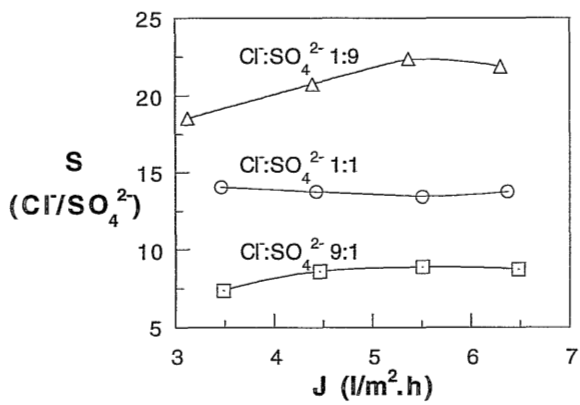

Figure 3.8: *Selectivity between Cl^- and SO_4^{2-} as a function of solvent flux for different ratios Cl^-/SO_4^{2-}. Membrane: UTC90. Overall anion concentration = 0.01M*

Figure 3.8 shows the selectivity as a function of the solvent flux through the membrane for different ratios of Cl^-/SO_4^{2-}, whereas the total anion concentration remained constant at 0.01M. For the ion ratio Cl^-/SO_4^{2-} of 1/9 the selectivity increased with increasing solvent flux, whereas for the other two ratios the selectivity remained constant. It appeared that the selectivity of the Cl^-/SO_4^{2-} increased when the ratio chloride/sulfate decreased. The improvement of the selectivity with increasing sulfate fraction is caused by the decrease in chloride ion retention when sulfate ions are added to the NaCl solution. The slight increase of the sulfate ion retention at higher sulfate fractions contributed as well to the increasing selectivity.
Figure 3.9 shows the selectivity of Cl^-/SO_4^{2-} of UTC90 as a function of the solvent flux for different total anion concentrations, keeping the ratio Cl^-/SO_4^{2-} constant. By increasing the concentration of anions, the selectivity increased as well, which was caused by the fact that the

increase of the concentration had a stronger effect on the chloride ion retention than it had on the retention of the sulfate ions.

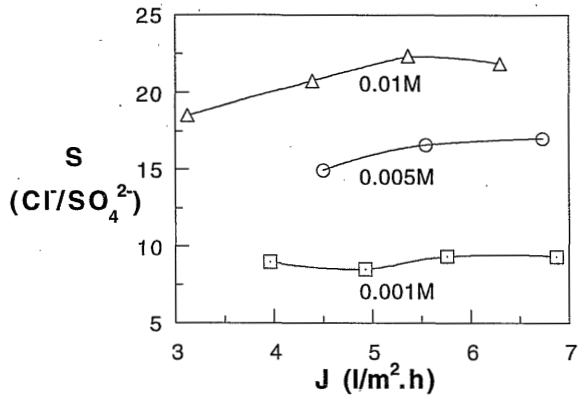

Figure 3.9: *Selectivity between Cl^- and SO_4^{2-} as a function of solvent flux for different concentrations anions. Membrane: UTC90. Ratio Cl^-/SO_4^{2-}: 1/9*

Figure 3.10 shows the selectivity of the three membranes investigated as a function of the solvent flux through the membrane. The ratio chloride/sulfate was 1/9 and the total anion concentration 0.005M. The selectivity of the CTA-LP membrane was by far the highest, whereas that of the ASP35 membrane was the lowest. When the selectivity for the chloride-sulfate ion mixture was compared to the retention of the membranes for the single salt solutions of sodium chloride and sodium sulfate, it could be stated that the CTA-LP membrane combined a high retention for sodium sulfate with a low retention for sodium chloride, which resulted in very high selectivities for the chloride/sulfate separation.

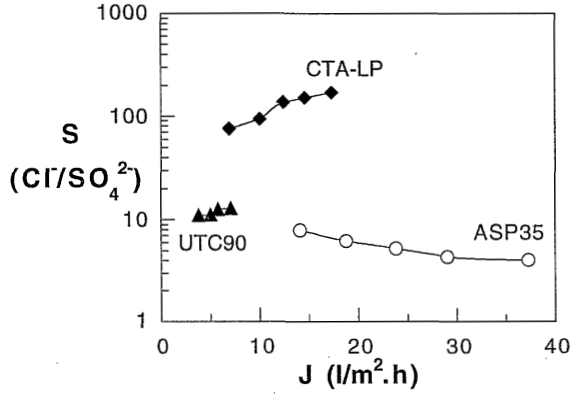

Figure 3.10: *Selectivity between Cl^- and SO_4^{2-} as a function of solvent flux for different nanofiltration membranes. Ratio Cl^-/SO_4^{2-}: 1/9. Anion concentration = 0.005M*

Comparison of the retentions for the single salt solutions of the UTC90 membrane with those of the CTA-LP membrane, revealed that the main difference was a higher sodium chloride retention for the UTC90 membrane. Therefore, the difference in selectivity between these two membranes might be estimated from the differences in retentions between the sulfate and the chloride ions in the single salt solutions. The higher this difference is, the higher the selectivity that may be expected.
The retentions for sodium chloride in the single salt solution with the ASP35 and the CTA-LP membrane were more or less comparable. Since the selectivity of the ASP35 membrane was much lower than that of the UTC90 membrane, the difference in selectivity seems to be mainly caused by the much higher retention for sodium sulfate in case of the UTC90 membrane.

Although the extent of the retention and selectivity was different for the three membranes investigated, their qualitative behavior was the same. So, no qualitative difference was found between the charged membrane ASP35 and the uncharged CTA-LP and UTC90 membranes. The anion with the highest retention in the case of single salt solutions stays more or less constant in a salt mixture. For all membranes tested sulfate was the best retained anion. The retention of the other anion, in this case the chloride ion, decreased for the membranes tested. The more sulfate ions the solution contained, the more the chloride ion retention was decreased compared to the retention in the binary salt solution.

Experiments with $NaCl/CaCl_2$
In case of the cation mixtures, the calcium ion retentions increased or remained stable compared to the single salt solution. The sodium ion retention in the mixture decreased as the fraction of calcium increased. This was the case for the CTA-LP and NF45 membrane, that were characterized as membranes for which the charge was not the only determining factor in separation, but for the negatively charged ASP35 membrane as well. For the CTA-LP and NF45 membrane, the sodium ion retention became negative for low sodium fractions in the feed. For these two membranes the separation behavior for the cation mixture resembled that for the membranes investigated for the anion mixture. In case of retention measurements with single salt solutions, the CTA-LP and NF45 membrane showed a higher retention for calcium than for sodium chloride. In case of a mixture of these two cations, the retention of the ion with the lowest diffusion coefficient remained constant, whereas that of the other ion decreased. Therefore, the sodium ions were preferentially transported through the membrane over the calcium ions, together with permeating chloride ions. This is shown in Figures 3.11 and 3.12.
Considering the electrical potential gradient that influences the ionic transport, in case of a single salt sodium chloride solution, the electric field will be negative because the permeability of the chloride ions is higher than that of the sodium ions. The transport of the sodium ions will be accelerated and that of the chloride ions slowed down, until both are equal. In case of a calcium chloride solution, the electrical potential will be even more negative. For a mixture of sodium and calcium chloride, the electrical gradient will be in between, so the transport of the sodium ions will be accelerated even more than it is in case of a single salt solution. This

explains the decreased retentions for the sodium ions.
The retention of the calcium ions increased when the fraction of calcium in the feed solution decreased. Only in case of the calcium fraction of 0.5 the retention was higher than that for the fraction of 0.1. This might be caused by a measurement error.

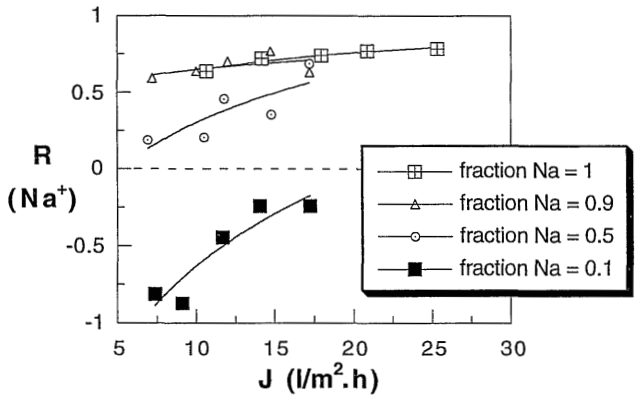

Figure 3.11: *Retention of sodium ions using a feed mixture of Na^+ and Ca^{2+} as a function of solvent flux for different ionic compositions. Membrane: CTA-LP. Overall cation concentration = 0.001M*

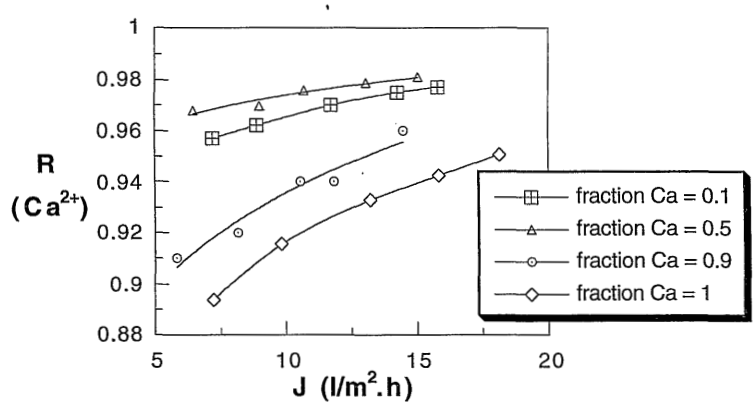

Figure 3.12: *Retention of calcium ions using a feed mixture of Na^+ and Ca^{2+} as a function of solvent flux for different ionic compositions. Membrane: CTA-LP. Overall cation concentration = 0.01M*

Although the negatively charged ASP35 membrane showed a higher retention for calcium chloride within the single salt solution than for sodium chloride, the retention of calcium ions within the cation mixture increased and that of sodium ions decreased. The decreasing sodium ion retention and the increasing retention of the calcium ions as a function of the calcium fraction are shown in the Figures 3.13 and 3.14, despite of some scattering in the data. The high calcium ion retention for the ASP35 membrane in case of a cation mixture is partially

caused by the Donnan potential at the membrane-permeate interface. Since the Donnan potential is equal for all ions, it will cause a larger concentration decrease for calcium ions than for sodium ions, because of the higher valency of the former. This effect is illustrated by equation {2.37}. Furthermore, the higher diffusion coefficient of sodium compared to calcium favored the sodium transport.

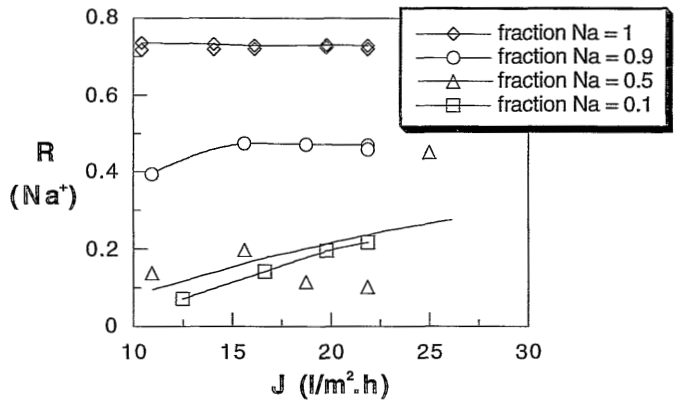

Figure 3.13: Retention of sodium ions using a feed mixture of Na^+ and Ca^{2+} as a function of solvent flux for different ionic compositions. Membrane: ASP35. Overall cation concentration = 0.001M

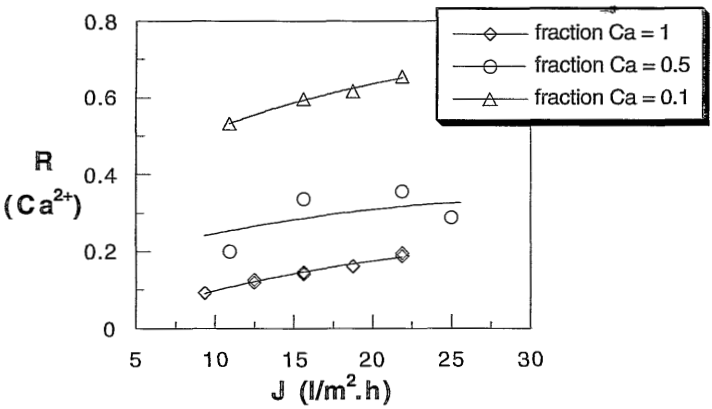

Figure 3.14: Retention of calcium ions using a feed mixture of Na^+ and Ca^{2+} as a function of solvent flux for different ionic compositions. Membrane: ASP35. Overall cation concentration = 0.001M

The selectivity for the sodium/calcium separation of the CTA-LP membrane is shown in Figure 3.15. As can be seen, the selectivity was the highest when the ratio Na^+/Ca^{2+} was low, because in that case the sodium ions were forced against their own concentration gradient through the membrane. As distinct from the selectivity of the anion mixtures for which the selectivity remained constant or increased a little at higher solvent fluxes, the selectivity of the

Na^+/Ca^{2+} separation decreased with increasing solvent flux for a Na^+/Ca^{2+} ratio of 1/9. For the other two ratios the selectivity was not much influenced by the water flux. The selectivity of the NF45 membrane resembles that of the CTA-LP membrane.

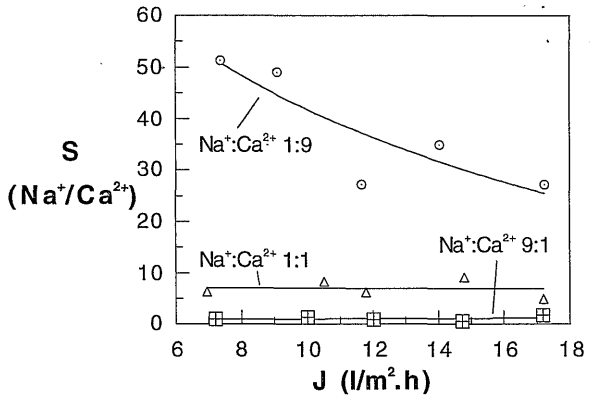

***Figure 3.15**: Selectivity of Na^+/Ca^{2+} as a function of the solvent flux for different ratios Na^+/Ca^{2+}. Membrane: CTA-LP. Total anion concentration = 0.001M*

The selectivity of the sodium/calcium separation of the ASP35 is much lower than that of the CTA-LP and the NF45 membrane as shown in Figure 3.16. In case of high sodium fractions, the selectivity becomes smaller than one, which means that calcium ions are transported preferentially through the membrane above sodium ions.

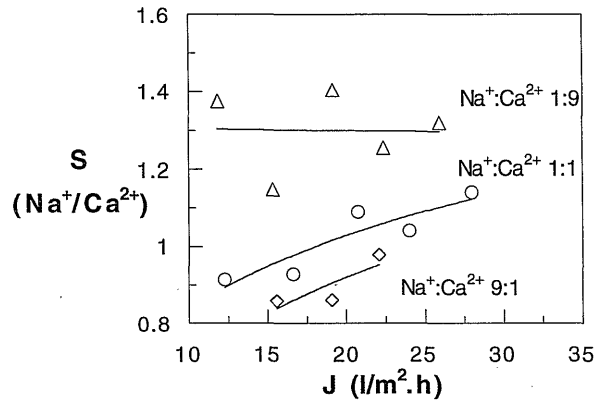

***Figure 3.16**: Selectivity of Na^+/Ca^{2+} as a function of the solvent flux for different ratios Na^+/Ca^{2+}. Membrane: ASP35. Total anion concentration = 0.005M*

An increase of the total cation concentration caused an increase of the selectivity for the CTA-LP and the NF45 membrane. The selectivity behavior of the CTA-LP membrane is shown in Figure 3.17. This increase is caused by the preferable sodium ion permeation through the membrane in case of a higher cation concentration in the feed as explained before in this

section. An indication for the improvement of selectivity at higher ionic strengths could be obtained from equation {2.22} that showed an increasing distribution coefficient of the more permeable ion between membrane and solution with increasing concentration of the less permeable ion. If the distribution of the less permeable ion is not increased to the same extent, the selectivity will be higher at higher ionic strengths. For the ASP35 membrane the scattering of the selectivity data was too high to draw conclusions concerning the influence of the concentration.

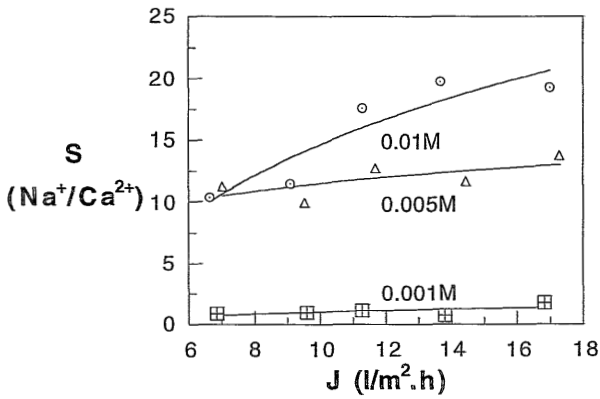

Figure 3.17: Selectivity of Na^+/Ca^{2+} as a function of the solvent flux for different total cation concentrations. Membrane: CTA-LP. Ratio Na^+/Ca^{2+}= 9/1

For the CTA-LP membrane both cation and anion mixtures were separated. The highest selectivity was found for the anion mixture, which was mainly caused by the higher retention for the sulfate ions in the anion mixture compared to calcium ions in the case of the cation mixture.

3.5 CONCLUSIONS

Salt retention measurements with nanofiltration membranes showed two different concepts with respect to the mechanism of separation. For one class of membranes Donnan exclusion seemed to be the determining mechanism. This first class could be further subdivided into two groups: negatively charged membranes, which showed a salt retention sequence R (Na_2SO_4) > R (NaCl) > R ($CaCl_2$), and positively charged membranes with a salt retention sequence: R ($CaCl_2$) > R (NaCl) > R (Na_2SO_4), both at pH = 5.5. A ceramic γ- Al_2O_3 membrane showed the same retention sequence as the positively charged polymeric membranes. For the second type of nanofiltration membranes neither surface charge nor size effects fully determined the separation. The retention sequence for these membranes was: R (Na_2SO_4) > R ($CaCl_2$) > R (NaCl).

The modification of a γ-Al_2O_3 membrane with sodiumsilicate was successful with respect to

the change of the charge from positive to negative at a pH of 6. Initially, for the modified membrane a high retention for Na_2SO_4 was found, while all $CaCl_2$ passed the membrane. However, these modified membranes appeared to be unstable in time and the retention for Na_2SO_4 decreased to zero, which was identical to the unmodified γ-Al_2O_3 membrane.

Retention measurements carried out at various pressure differences, i.e., at different solvent fluxes through the membrane, showed that the retention increased with increasing solvent flux.

Retention measurements for UTC90, ASP35 and CTA-LP membranes with salt mixtures of Na_2SO_4/NaCl showed a decrease in chloride ion retentions and an increase in sulfate ion retentions with increasing sulfate fractions in the mixture, as could be expected from both the diffusion potential and from the Donnan theory. Selectivity between chloride/sulfate increased with increasing sulfate fraction and with the total anion concentration. In case of the cation NaCl/$CaCl_2$ mixtures, the Na^+ retention decreased with the addition of Ca^{2+}-ions for membranes for which both charge and size effects determined the separation and for a negatively charged membrane. For the former membranes, a high total concentration of cations resulted in a high selectivity. In case of the negatively charged membrane, the Donnan potential in combination with the difference in diffusion coefficients caused a high retention for the bivalent cation compared to that of the monovalent cation. Therefore, although the calcium ion concentration within the membrane is much higher than that of the sodium ions, sodium was the preferentially permeating ion within the cation mixture. All membranes showed a higher selectivity between Na^+/Ca^{2+} in case of a higher the calcium fraction.

When comparing the retention data of the single salt solutions with those of the salt mixtures, the membrane which had the higher retention for the bivalent ion in case of a binary solution (for the sulfate or calcium ion), showed the highest selectivity.

ACKNOWLEDGEMENTS

Jeroen van Beckum, Edwin van der Steeg, Marieke ten Have and John Glorie are acknowledged for their experimental work on the single salt solutions, Carla Koopman, Carla Reitsma and José Nolten for their experimental work on the salt mixtures and Bert Pennings on the experimental work on the ceramic membranes. Carla Koopman is acknowledged for fruitful discussions on the topic of the salt mixtures.

SYMBOLS

c:	concentration	(mol/l)
D:	diffusion coefficient	(m^2/s)
f:	diffusive wall correction factor	(-)
g:	convective wall correction factor	(-)

J:	flux	(m/s) or (mol/m^2.s)
L:	$= L_s/\Delta x$,	
	solute permeability coefficient corrected for the membrane thickness	(m/s)
L_s:	solute permeability coefficient in two component system	(m^2/s)
L_v:	solvent permeability coefficient in two component system	(s/m)
p	porosity	(-)
P:	pressure	(bar, N/m^2)
Pe:	Péclet-number	(-)
r:	radius	(m)
R:	retention	(-)
S_D:	hindrance factor for diffusive transport	(-)
S_F:	factor for convectional transport	(-)
x:	coordinate in direction of transport	(m)
λ:	$= r_s / r_p$	(-)
π:	osmotic pressure	(N/m^2)
σ:	reflection coefficient	(-)
Δx:	membrane thickness	(m)

subscripts:

f:	feed
p:	permeate
p:	pore
s:	solute
v:	solvent

REFERENCES

[1] Bhattacharyya, D., McCarthy, J.M., Grieves, R.B., *Charged membrane ultrafiltration of inorganic ions in single and multi-salt systems*, AIChE J., 20 (1974) 1206

[2] Helfferich, F., Ionenaustaucher, Verlag Chemie, Weinheim, 1959

[3] Starzak, M. E., The Physical Chemistry of Membranes, Academic Press, Orlando, 1984

[4] Mulder, M. H. V., Basic principles of membrane technology, Kluwer, Dordrecht, 1996

[5] Bardot, C., Gaubert, E., Yaroshchuk, A., *Unusual mutual influence of electrolytes during pressure-driven transport of their mixtuires across charged porous membranes*, J. Membrane Sci., 103 (1995) 11-17

[6] Spiegler, K. S., Kedem, O., *Thermodynamics of hyperfiltration (reverse osmosis): criteria for efficient membranes*, Desalination, 1 (1966) 311

[7] Uhlhorn, R. J. R., Huis In 't Veld, M.H.B.J., Keizer, K., Burggraaf, A.J., *Synthesis of ceramic membranes. Part I Synthesis of non-supported and supported ganma-alumina membranes without defects*, J. Mats. Sci., 27 (1992) 527-537

[8] Parks, G. A., *The isoelectric points of solid oxides, solid hydroxides and aqueous hydroxo complex systems*, Chem. Rev., 65 (1965) 177

[9] Cadotte, J., Forester, R., Kim, M., Petersen, R., Stocker, T., *Nanofiltration membranes broaden*

the use of membrane separation technology, Desalination, 70 (1988) 77

[10] Ikeda, K., Nakano, T., Ito, H., Kubota, T.,Yamamoto, S., *New composite charged reverse osmosis membrane*, Desalination, 68 (1988) 109

[11] Simpson, A. E., Kerr, C.A., Buckley, C.A., *The effect of pH on the nanofiltration of the carbonate system in solution*, Desalination, 64 (1987) 305-329

[12] Atkins, P. W., Physical Chemistry, third ed., W.H. Freeman, New York, 1986

[13] Nyström, M., Kaipia, L., Luque, S., *Fouling and retention of nanofiltration membranes*, J. Membrane Sci., 98 (1995) 249-262

[14] Eriksson, P., *Nanofiltration extends the range of membrane filtration*, Environmental Progress, 7 (1988) 58

[15] Horst, H. C., van der, Timmer, J.M., Robbertsen, T., Leenders, J., *Use of nanofiltration for concentration and demineralization in the diary industry*, J. Membrane Sci., 104 (1995) 205-218

[16] Tsuru, T., Nakao, S.I., Kimura, S., *Calculation of ion rejection by extended Nernst-Planck equation with charged reversed osmosis membranes for single and mixed electrolyte solutions*, J. Chem. Eng. Jap., 24 (1991) 511

[17] Tsuru, T., Urairi, M., Nakao, S.I., Kimura, S., *Negative rejection of anions in the loose reverse osmosis separation of mono- and divalent ion mixtures*, Desalination, 81 (1991) 219

[18] Tsuru, T., Urairi, M., Nakao, S.I., Kimura, S., *Reverse osmosis of single and mixed electrolytes with charged membranes: experiment and analysis*, J. Chem. Eng. Jap., 24 (1991) 518

[19] Alami-Younssi, S., Larbot, A., Persin, M., Sarrazin, J., Cot, L., *Rejection of mineral salts on a gamma alumina nanofiltration membrane. Application to environmental process*, J. Membrane Sci., 102 (1995) 123-129

[20] Bowen, W. R., Mukthar, H., *Characterisation and prediction of separation performance of nanofiltration membranes*, J. Membrane Sci., 112 (1996) 263-274

[21] Peeters, J. M. M., "Electrolyte retentions for nanofiltration membranes", Report No. MT9611a, University of Twente, Enschede, The Netherlands, 1996

APPENDIX I

Salt retention measurements with different nanofiltration membranes

All experiments were carried out at ΔP=5 bar

CLASS I), NEGATIVELY CHARGED MEMBRANES:

UTC70

c (10^{-3} mol/l) $CaCl_2$	R (-)	c (10^{-3} mol/l) NaCl	R (-)	c (10^{-3} mol/l) Na_2SO_4	R (-)
1.08	0.91	1.53	0.943	1.10	0.966
6.31	0.897	6.36	0.936	6.1	0.953
11.0	0.886	11.0	0.919	11.5	0.929

ASP35

c (10^{-3} mol/l) $CaCl_2$	R (-)	c (10^{-3} mol/l) NaCl	R (-)	c (10^{-3} mol/l) Na_2SO_4	R (-)
1.78	0.14	2.1	0.75	1.76	0.95
5.45	0.52	6.4	0.612	8.9	0.93
9.7	0.38	12.0	0.534	14.6	0.876

HG01

c (10^{-3} mol/l) $CaCl_2$	R (-)	c (10^{-3} mol/l) NaCl	R (-)	c (10^{-3} mol/l) Na_2SO_4	R (-)
1.1	0	0.971	0.018	1.16	0.293
5.0	0.01	4.97	0.029	5.48	0.109
9.6	0.01	9.37	0.024	9.92	0.045

HG19

c (10^{-3} mol/l) $CaCl_2$	R (-)	c (10^{-3} mol/l) NaCl	R (-)	c (10^{-3} mol/l) Na_2SO_4	R (-)
1.1	0	1.0	0.313	1.01	0.805
4.9	0	5.04	0.11	5.35	0.437
9.5	0	9.37	0.082	10.0	0.269

BQ01

c (10^{-3} mol/l) $CaCl_2$	R (-)	c (10^{-3} mol/l) NaCl	R (-)	c (10^{-3} mol/l) Na_2SO_4	R (-)
1.17	0.19	-	-	3.0	0.95
5.98	0.08	8.24	0.57	12.1	0.90
11.2	0.03	15.5	0.49	22.8	0.75

WFN0505

c (10^{-3} mol/l) $CaCl_2$	R (-)	c (10^{-3} mol/l) NaCl	R (-)	c (10^{-3} mol/l) Na_2SO_4	R (-)
0.76	0.03	1.88	0.41	1	0.59
-	-	6.91	0.35	5	0.57
-	-	12.9	0.30	1	0.51

PES10

c (10^{-3} mol/l) $CaCl_2$	R (-)	c (10^{-3} mol/l) NaCl	R (-)
1	0.15	1.35	0.39
5	0.07	3.3	0.31
10	0.01	7.50	0.19

PVD1

c (10^{-3} mol/l) $CaCl_2$	R (-)	c (10^{-3} mol/l) NaCl	R (-)
1.17	0.18	0.99	0.55
6.64	0.16	5.13	0.39
13.4	0.16	9.9	0.26

CLASS I), POSITIVELY CHARGED MEMBRANES:

KW32

c (10^{-3} mol/l) $CaCl_2$	R (-)	c (10^{-3} mol/l) NaCl	R (-)	c (10^{-3} mol/l) Na_2SO_4	R (-)
1.46	0.951	1.87	0.774	1.09	0.396
6.54	0.946	9.4	0.555	5.37	0.318
14.6	0.881	12.1	0.517	10.5	0.283

KW21

c (10^{-3} mol/l) $CaCl_2$	R (-)	c (10^{-3} mol/l) NaCl	R (-)	c (10^{-3} mol/l) Na_2SO_4	R (-)
1.88	0.938	1.47	0.774	1.22	0.425
8.2	0.914	6.6	0.524	6.15	0.323
15.9	0.849	11.9	0.47	11.1	0.312

CLASS II):

TFCS

c (10^{-3} mol/l) $CaCl_2$	R (-)	c (10^{-3} mol/l) NaCl	R (-)	c (10^{-3} mol/l) Na_2SO_4	R (-)
1.40	0.804	1.41	0.696	1.37	0.94
6.64	0.827	6.43	0.72	6.98	0.928
13.4	0.83	12.2	0.705	13.1	0.914

CTA-LP

c (10^{-3} mol/l) $CaCl_2$	R (-)	c (10^{-3} mol/l) NaCl	R (-)	c (10^{-3} mol/l) Na_2SO_4	R (-)
1.3	0.668	1.41	0.592	1.26	0.975
6.7	0.789	5.61	0.43	5.9	0.958
1.29	0.804	11.2	0.443	12.3	0.917

UTC90

c (10^{-3} mol/l) $CaCl_2$	R (-)	c (10^{-3} mol/l) NaCl	R (-)	c (10^{-3} mol/l) Na_2SO_4	R (-)
1	0.963	1.14	0.868	1.11	0.985
5	0.926	5.84	0.844	5.74	0.931
10	0.924	12.1	0.804	10.4	0.911

SX10

c (10^{-3} mol/l) $CaCl_2$	R (-)	c (10^{-3} mol/l) NaCl	R (-)	c (10^{-3} mol/l) Na_2SO_4	R (-)
1.25	0.856	1.34	0.851	1.48	0.978
6.88	0.890	5.92	0.778	6.85	0.966
12.6	0.847	12.2	0.697	13.8	0.918

MX07

c (10^{-3} mol/l) $CaCl_2$	R (-)	c (10^{-3} mol/l) NaCl	R (-)	c (10^{-3} mol/l) Na_2SO_4	R (-)
2.03	0.83	1.56	0.27	2.37	0.97
8.54	0.75	6.6	0.20	9.32	0.96
14.6	0.57	12.3	0.24	18.6	0.98

NF45

c (10^{-3} mol/l) $CaCl_2$	R (-)	c (10^{-3} mol/l) NaCl	R (-)	c (10^{-3} mol/l) Na_2SO_4	R (-)
2.71	0.64	1.70	0.28	2.5	0.87
8.73	0.60	6.41	0.30	1.0	0.90
15.8	0.50	11.2	0.25	15.0	0.91

CA30

c (10^{-3} mol/l) $CaCl_2$	R (-)	c (10^{-3} mol/l) NaCl	R (-)	c (10^{-3} mol/l) Na_2SO_4	R (-)
0.716	0.291	1.50	0.29	2.32	0.91
5.0	0.304	5.27	0.132	9.2	0.704
13.9	0.353	10.2	0.129	13.9	0.643

OTHERS:

SX01

c (10^{-3} mol/l) $CaCl_2$	R (-)	c (10^{-3} mol/l) NaCl	R (-)	c (10^{-3} mol/l) Na_2SO_4	R (-)
1.15	0.854	1.19	0.714	1.37	0.926
6.47	0.926	5.26	0.537	6.23	0.956
14.5	0.866	11.0	0.484	13.0	0.88

NF70

c (10^{-3} mol/l) $CaCl_2$	R (-)	c (10^{-3} mol/l) NaCl	R (-)	c (10^{-3} mol/l) Na_2SO_4	R (-)
1.32	0.84	1.19	0.88	1.12	0.93
6.63	0.85	6.85	0.83	6.86	0.97
16.1	0.77	13.8	0.78	13.1	0.91

UTC60

c (10^{-3} mol/l) $CaCl_2$	R (-)	c (10^{-3} mol/l) NaCl	R (-)	c (10^{-3} mol/l) $MgSO_4$	R (-)
1	0.44	1.14	0.66	1	0.94
5	0.56	4.69	0.56	5	0.84
10	0.57	9.3	0.53	10	0.51

CHAPTER 4

Retention measurements with saccharide and dendrimer solutions

ABSTRACT

Saccharides and dendrimers were used as model solutes for retention measurements with different nanofiltration membranes.

Saccharides showed higher retentions than the dendrimer molecules, although the latter were larger.

The retention measurements with CN- and NH_2-terminated dendrimers having the same number of endgroups revealed that differences in size were not the only determining factor for separation. The retention of the amine-terminated dendrimers was always higher than that of the nitrile-terminated dendrimer. Measurements with fully protonated dendrimers showed a higher retention as well. The dendrimer retention measurements were difficult to interpret since their size is pH-dependent.

4.1 INTRODUCTION

The investigation of the effect of solute size on membrane retention can be carried out with a series of uncharged solutes, differing in size but with comparable interaction with the membrane. For ultrafiltration membranes, this type of experiments is often carried out with a series of polymers, varying in molecular weight. In case of nanofiltration membranes, (poly)ethyleneglycols or (poly)saccharides are often used for this purpose [1-4].
In this chapter experiments will be described with three different saccharides, glucose, sucrose and raffinose, which vary in molecular size from 3.7 to 5.8 Å, whereas their molecular masses range from 180 to 594 g/mol.
The second type of model solutes used in retention measurements were dendrimer molecules. These dendrimers were chosen because of their well-defined size, ranging from 4.5 to 13.5 Å solute radius, and their spherical shape.

4.2 THEORY

4.2.1 Solute transport

The equations used to describe the transport of saccharides and dendrimers through the membrane were already shown in Chapter 2. The main aspects of the theory will be shortly described here. The solvent and solute flux can be written as [5]:

$$J_V = -L_V \left(\frac{dP}{dx} - \sigma \frac{d\pi}{dx} \right) \qquad \{4.1\}$$

$$J_s = - L_s \frac{dc_s}{dx} + (1 - \sigma) J_v \overline{c_s} \qquad \{4.2\}$$

with J_V, the solvent flux, J_S, the solute flux, L_V the permeability constant of the solvent, L_S that of the solute, dP the pressure gradient across the membrane, x the coordinate in direction of the transport, $d\pi$ the osmotic pressure gradient, σ the reflection coefficient and $\overline{c_s}$ the mean concentration of the solute.

The retention of the membrane, R, is defined by:

$$R = \frac{c_f - c_p}{c_f} \qquad \{4.3\}$$

with c_f being the concentration of the feed and c_p that of the solute in the permeate.

The equations {4.1}, {4.2} and {4.3} can be combined to [5]:

$$R = \frac{\sigma (1 - e^{Pe})}{1 - \sigma e^{Pe}} \qquad \{4.4\}$$

with $Pe = - J_v \frac{(1 - \sigma)}{L}$, and $L = \frac{L_s}{\Delta x}$.

Equation {4.4} allows to calculate the reflection coefficient and the solute permeability coefficient at a specific feed concentration, using these two parameters to fit the relation between the retention and the solvent flux. In contrast to the reflection coefficient, the retention is dependent on the pressure difference applied.
The reflection coefficient and the permeability coefficient of the solute are material properties in the pore model as proposed by Nakao [6]. As shown in Chapter 2, it is assumed in this model that the membrane contains pores. However, the determination of an effective pore size does not imply the existence of distinct pores in nanofiltration membranes according to Bowen and co-workers. They assumed the hindrance of transport of a molecule through a membrane matrix equal to that of transport through pores with a specific pore size [7].

The reflection coefficient can be written as a function of the hindrance factor for convective transport, S_F, and the convective wall correction factor, g, as a function of λ, which is the ratio of solute size and pore size, ($\lambda = r_s / r_p$ with r_s being the radius of the solute and r_p the radius of the pore):

$$\sigma = 1 - g(\lambda) S_F \qquad \{4.5\}$$

S_F and $g(\lambda)$ were defined by equations {2.3} and {2.6}.

The permeability of the solute is related to the diffusion coefficient of the solute, D, the hindrance factor for convective transport, S_D and the diffusive wall correction factor, f, as a function of λ. It can be written as:

$$L = D f(\lambda) S_D \frac{\varepsilon}{\Delta x} \qquad \{4.6\}$$

S_D and $f(\lambda)$ were defined by equations {2.1} and {2.2}, whereas $p/\Delta x$ is the membrane porosity divided by its thickness.

Describing the transport of solvent and solute molecules by the equations shown above, it is assumed that the hindrance of transport is only caused by steric hindrance and no interaction between the molecules and the membrane is assumed.
In this chapter, the results of both saccharide and dendrimer retention measurements will be described qualitatively. In Chapter 6 of this thesis the results of the retention measurements with the saccharides will be discussed into more detail using the equations mentioned above.

4.2.2 Dendrimers

Dendrimers are a new type of molecules that have a well-defined, highly branched structure. These molecules are formed from a central core. By repetitive synthesis steps, identical building blocks react with this core, forming a spherical, three-dimensional configuration [8-10]. An example of the sequential growth of a dendrimer molecule is shown in Figure 4.1.

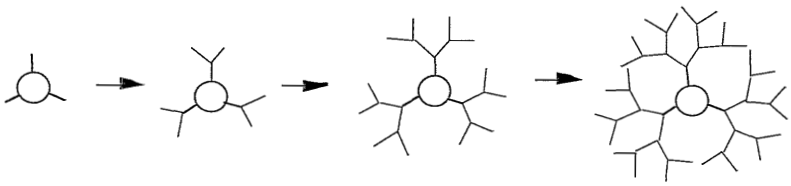

Figure 4.1: Stepwise growth of a dendrimer molecule

The stepwise formation of dendrimers can be controlled and therefore, the chemical and physical properties of the dendrimers as well as their size can be regulated.
Dendrimers are now commercially available in low quantities from DSM. This company produces dendrimers from diaminobutane as the core molecule and acrylonitrile as the building blocks [11,12]. To every primary amine group, two equivalents of acrylonitrile are added and this gives the nitrile-type of dendrimer. Hydrogenation of the nitrile group to a primary amine group leads to the amine type of dendrimer. Then again acrylonitrile can be added to form a next generation of the dendrimer. The reaction scheme to form the first generation of the nitrile and the amine-terminated dendrimer is shown in Figure 4.2.

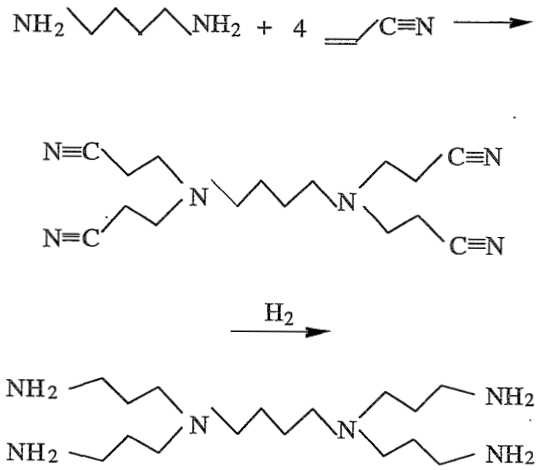

Figure 4.2: Synthesis steps of the first generation of a nitrile- and amine-terminated polypropyleneimine dendrimer used

Dendrimers seem to be a rather good model species for the characterization of nanofiltration membranes, because both their size and their shape seem to be well-defined. The dendrimer size is in the same order of magnitude as that of the (imaginary) pores in nanofiltration membranes, being one or two nanometers, whereas their shape is more or less spherical. This can be seen in Figure 4.3 that shows the chemical structure of a dendrimer with 32 amine endgroups.

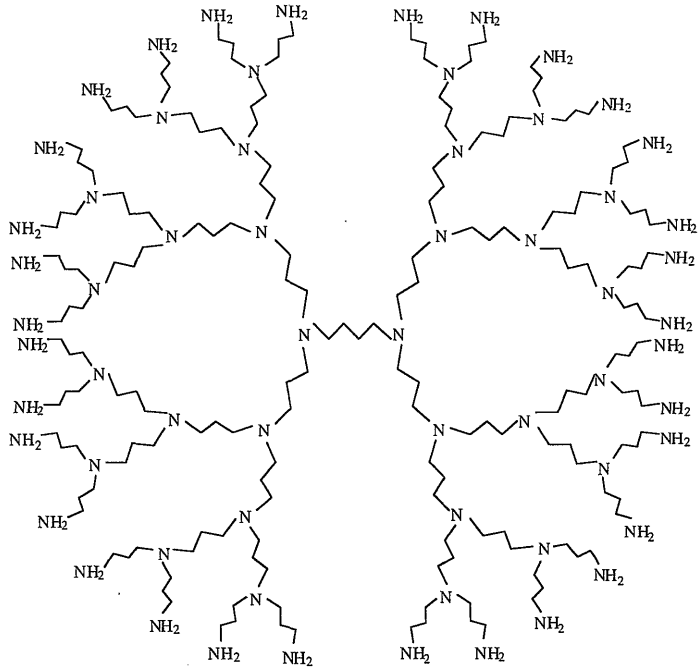

***Figure 4.3**: Chemical structure amine-terminated polypropyleneimine with 32 endgroups, DAB-dendr-$(NH_2)_{32}$*

One of the main problems in using dendrimers as a model species was the quantitative determination of the concentration. In the experimental part the procedure will be described to determine the dendrimer concentration in aqueous solutions.

4.3 EXPERIMENTAL

4.3.1 Saccharides

In the retention measurements, glucose, sucrose and raffinose (Merck, p.a.) were used. Saccharide retention measurements were performed with several nanofiltration membranes at a fixed concentration and one pressure difference. Ultrapure water was used as solvent. For some membranes, retention measurements were carried out at various pressures, i.e., solvent

fluxes as well.
The radii of the saccharides were calculated with the Stokes-Einstein relation from the diffusion coefficients of these molecules in water [13]. The molecular masses, M_w, diffusion coefficients, D, and hydrodynamic radii are given in Table 4.1.

Table 4.1: Molecular mass, diffusion coefficient and radii of saccharides used in retention measurements

saccharide	M_w (g/mol)	D ($*10^{-10}$ m^2/s) [13]	radius (Å)
glucose	180.2	6.73	3.24
sucrose	342.3	5.21	4.19
raffinose	504.5	4.34	5.03

The saccharide concentration was determined by HPLC measurements (Waters 610 Fluid Unit; column: Waters, KS801; detector: Waters 410 Differential Refractometer, T = 50°C, ϕ = 1 ml/min).

4.3.2 Dendrimers

The dendrimers used in the retention experiments are polypropyleneimine dendrimers (DSM, Fine Chemicals) with both amine and nitrile end groups. The chemical names of these dendrimers are:

1,4 diaminobutane {4}: (1-azabutylidene)$^{x-4}$: propionitrile and

1,4 diaminobutane {4}: (1-azabutylidene)$^{x-4}$: propylamine,

where x is the cascade number for each generation (x = 4, 8, 16, 32 or 64, respectively). The names of the dendrimers will be abbreviated as DAB-dendr-$(CN)_x$ and DAB-dendr-$(NH_2)_x$. The main characteristics of the dendrimers used are summarized in Table 4.2. The volumes and radii reported are determined by viscosity measurements. For DAB-dendr-$(CN)_x$ these were measured in acetone, for DAB-dendr-$(NH_2)_x$ in D_2O.
For both dendrimer types ultrapure water was used as solvent. The NH_2-terminated dendrimers were well soluble in water, whereas the CN-terminated dendrimers were only soluble to a certain extent. It should be realized that the size of the nitrile-terminated dendrimers shown in Table 4.2 was determined in acetone. The size of these molecules in water will probably be smaller, because of low interaction between water and the nitrile-terminated dendrimer.

***Table 4.2**: General features of polypropyleneimine dendrimers used in experiments (information by DSM)*

Generation	MW (g/mol)	theoretical endgroups	volume (Å^3)[a)]	radius (Å)
0.5	300	4 CN	478	4.9
1	317	4 NH_2	948	6.1
1.5	741	8 CN	1477	7.1
2	773	8 NH_2	2824	8.8
2.5	1622	16 CN	3663	9.6
3	1687	16 NH_2	6947	11.8
3.5	3385	32 CN	7869	12.3
4	3514	32 NH_2	15872	15.6
4.5	6910	64 CN	16523	15.8
5	7166	64 NH_2	32367	19.8

a): Determined by viscosity measurements, for DAB-dendr-$(CN)_x$ in acetone, for DAB-dendr-$(NH_2)_x$ in D_2O. Information by DSM.

The concentration of DAB-dendr-$(NH_2)_x$ used was approximately 1 g/l and for the DAB-dendr-$(CN)_x$ 0.2 to 0.5 g/l. In water both dendrimer types will behave as a base. In case of an amine-terminated dendrimer both its amine (primary) endgroups and the tertiary amine groups in the interior of the molecule will be possibly charged, whereas in case of the nitrile-terminated dendrimer the tertiary amine groups inside the molecule will be charged.
To analyze the dendrimers qualitatively, UV absorption appeared to be the most appropriate technique. The measurements were carried out with a Philips PU 8720 UV/Vis Scanning Spectrophotometer with a deuterium lamp as radiation source. The temperature in the instrument was thermostated at 21°C.
UV absorption measurements showed that all dendrimers had one single absorption peak with the base in the wavelength range of 190 to 250 nm and with the top at about 210 nm. One of the main problems was the shift in the maximum of the absorption peak with changing dendrimer concentration. This shift was always larger than 15 nm in the concentration range of 0.02-0.4 g/l. The change in the maximum of the absorption peak (lower concentrations resulted in lower wavelengths) sometimes caused a maximum absorption at a wavelength lower than 190 nm. In that case the extent of absorption could not be determined, as a wavelength of 190 nm is the minimum wavelength at which UV absorption can be detected.
Since it was assumed that the wavelength shift was caused by a variation in pH, the dendrimer solutions were buffered with a tris-hydroxymetyl-aminobutane / HCl buffer (tris-buffer) with pH=8 to prevent the shift. The buffer does not absorb UV light in the wavelength range investigated. For the buffered dendrimer solution the decrease of the absorption maximum was

only 5 nm. The influence of the buffer on the wavelength of the maximum absorption is given in Figure 4.4. The concentration of buffer which was added to the samples after the retention measurement was 20 mM.

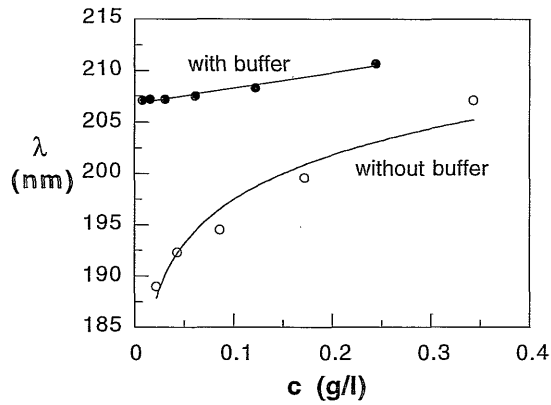

Figure 4.4: Wavelength (λ) of the UV absorption peak at different concentrations of DAB-dendr (CN)$_8$ without and with tris-buffer (pH=8)

The dendrimer samples purchased from DSM contain between 0.2 and 30 weight percent water, some methanol (less than 0.1 w%) and cobalt (9-258 ppm) which is used as a catalyst in the synthesis.

4.3.3 Membranes

The polymeric membranes which were used for saccharide and dendrimer retention measurements are:

* ASP35 [a](Advanced Membrane Technology)
* MPF21; MPF32 (Kiryat Weizmann)
* UTC60; UTC70, UTC90[a] (Toray)
* CTA-LP[a]; TFCS (Fluid Systems)
* NF45[a] (FilmTec)
* BQ01, MX07 (Osmonics)
* CA30, PES10 (Hoechst)

Advanced Membrane Technology, Toray, Fluid Systems, FilmTec, Osmonics and Hoechst kindly supplied the membranes.

With these membranes saccharide retention measurements were carried out at one pressure difference (5 bar). The ceramic membrane used was a γ-Al_2O_3 ultrafiltration membrane, which was made at our laboratory. The procedure of the formation of this membrane was given in Chapter 3.

With the membranes marked with [a], solvent flux dependent retention measurements were performed as well.

The dendrimer retention measurements were carried out with PES10, CA30, UTC20 (Toray),

ASP35 and NF45 membranes and a ceramic γ-Al_2O_3 membrane.

4.3.4 Retention measurements

The retention measurements were carried out using stirred dead-end cells as described in Chapter 3. The pressure differences applied were in the range of 3 to 7 bar.
The area of the membranes in the cells used for the retention measurements is 38.5 cm^2. The solvent was demineralized water filtered by a Milli-Q-Plus unit.
Firstly, all membranes were equilibrated by filtering pure water for two hours at a hydrostatic pressure difference of 7 bar. Then, the feed solution was changed from pure water to a saccharide or dendrimer solution. After a stabilization time of two hours the concentration of the feed was measured and subsequently permeation samples were taken. Thereafter, the pressure difference was increased and stabilization times of one hour were used.
In between retention measurements with different saccharides or dendrimers, the membrane was flushed for at least two hours with pure water.

Saccharide solutions

Preliminary retention measurements as well as solvent flux-dependent retention measurements were carried out with saccharide solutions. In case of the preliminary retention measurements the saccharide concentration used was 1 g/l, whereas the pressure difference applied was 5 bars. For some membranes flux-dependent retention measurements were carried out as well, applying pressure differences in the range of 3 to 7 bars. In this case the concentration was 2 g/l.
Firstly, the retention of glucose was determined, followed by sucrose and raffinose.

Dendrimer solutions

Dendrimer retention measurements were started with the smallest available dendrimers (x = 4) in the pressure difference range of 3 to 7 bar. These were followed by retention measurements with a dendrimer with a higher molecular weight. Firstly, different generations of dendrimers with CN-endgroups were measured, then different generations of dendrimers with NH_2-endgroups. When the retention for a dendrimer of a certain generation (i.e., generation = X) was higher than 0.97, the retention of the dendrimer with a generation of X+1 was not determined anymore, because the absolute error in the determination of the dendrimer concentration was 0.04.

Some experiments were carried out to investigate the influence of the dendrimer concentration on the retention. The concentrations used were 0.4, 1.2 and 2.0 g/l DAB-dendr-$(CN)_8$.
Since the pH of the solution might influence the charge of the dendrimers, their size and the charge of the membrane, retention experiments were carried out at different pH values. Experiments were carried out with buffered solutions, having pH values of 6 and 8,

respectively. To obtain a value of pH=6 a phosphate buffer was used and for pH = 8 a trisbuffer (tris(hydroxymetyl)aminomethane/HCl). The phosphate buffer was used to investigate the retention of the dendrimers at their equivalence points that were determined by titration. The pH of the equivalence point was 5.8 for the nitrile-terminated dendrimers (X=64) and 6.0 for the amine-terminated ones (X=64).
Furthermore, experiments were carried out at a pH value of 3 to investigate the protonated dendrimers. This pH was obtained by addition of HCl to the dendrimer solution.
To check the influence of the buffers and the acid on the membrane, the pure water flux through the membrane was compared with the solvent flux obtained for the buffered or acidic dendrimer solution. When the solvent flux through the membrane changed drastically using these solutions, experiments were not continued, because in that case the membrane may be modified by either buffer or acid because of adsorption or chemical destabilization.

4.4 RESULTS

4.4.1 Saccharide retention measurements

The saccharide retention measurements were carried out with different polymeric nanofiltration membranes and a ceramic γ-Al_2O_3 membrane, as mentioned in the Experimental Section. The results of all saccharide retention measurements at a pressure difference of 5 bar are shown in Appendix II.
For the membranes investigated, the saccharides showed an increasing retention with an increasing molecular weight. The larger the molecules, the more the transport through the membrane will be hindered and therefore, the retention will increase.

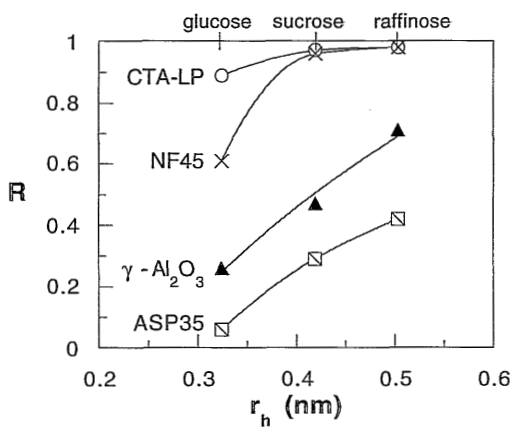

Figure 4.5: Saccharide retentions as a function of the radius of hydration for a ASP35, a γ-Al_2O_3, a UTC70 and a NF45 membrane. Concentration: 1 g/l, pressure difference: 5 bar

For some membranes the retention had already reached a high retention level for glucose (R > 0.95) and hardly any increase was observed for the larger molecules sucrose and raffinose. This is the case for the membranes: UTC60, UTC70 and TFCS. Other membranes showed a distinct improvement of retention between glucose and sucrose, e.g., the MPF21, MPF32, CTA-LP, MX07 and NF45 membranes. For some of the membranes the retention for raffinose was still less than 0.90.
Some examples of saccharide retention as a function of the hydrodynamic radius of these molecules are shown in Figure 4.5.

Figure 4.6 shows the saccharide retentions of a CTA-LP membrane at different solvent fluxes. As can be seen the retention increases with increasing solvent flux as can be expected from equation {4.4}, and approaches an asymptotic limit. The theories describing the retention of the saccharides as a function of the solvent flux have been discussed in more detail in Chapter 2. The flux-dependent saccharide retentions of the other membranes investigated showed a similar behavior.

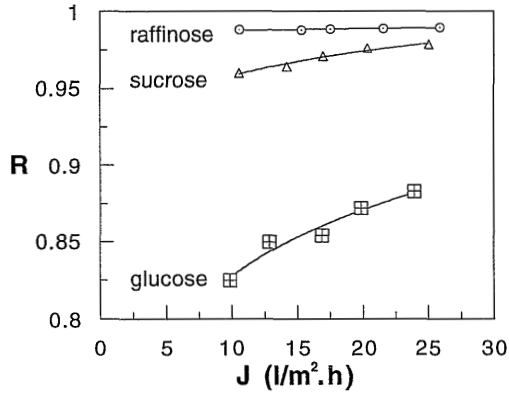

Figure 4.6: *Saccharide retentions as a function of the solvent flux for a CTA-LP membrane. Feed concentration: 2 g/l*

4.4.2 Retention measurements with dendrimer solutions

NF45 membrane

Unbuffered solutions
In case of the NF45 membrane the clean water flux that was determined in between retention measurements with dendrimer solution was almost equal to the clean water flux determined prior to the retention experiments.
The dependence of the retention on the concentration and on the solvent flux was investigated for DAB-dendr-$(CN)_8$. Neither the solvent flux nor the retention were significantly dependent on the concentration in the range of 0.5, 1.2 and 2.0 g/l. Therefore, retention measurements were carried out at one feed concentration.

The relation between solvent flux and retention for four different nitrile-terminated dendrimers (8CN, 16CN, 32CN and 64CN) is shown in Figure 4.7. Only the retention for the DAB-dendr-$(CN)_8$ was significantly lower than that of the other dendrimers. The extent of retention for this molecule was in the range of 0.85 and seems to increase with increasing solvent flux. For the other dendrimer molecules the retention seemed to increase with solvent flux as well, but some caution should be taken into account since the absolute error in the retention values is approximately 0.04. The pH for these solutions was in between 8.4 and 9.9, going from the highest to the lowest generation.

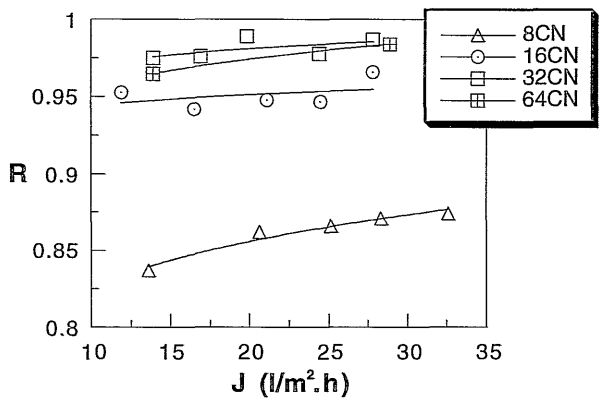

Figure 4.7: Retention of DAB-dendr-$(CN)_x$ as a function of the solvent flux for a NF45 membrane. pH=8.4-9.9

Figure 4.8 shows the retention for DAB-dendr-$(NH_2)_8$ and DAB-dendr-$(NH_2)_{16}$. The third generation of the amine-terminated dendrimers ($16NH_2$) showed a retention of 1. Therefore, experiments with higher generations were not carried out.

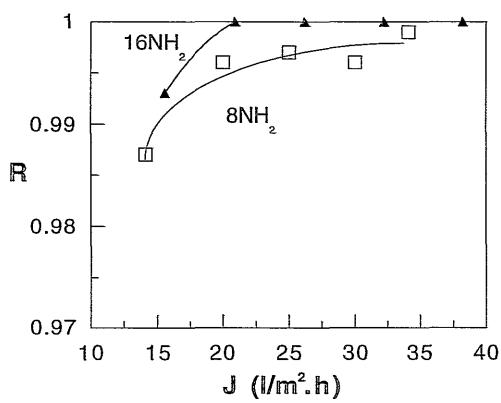

Figure 4.8: Retention of DAB-dendr-$(NH_2)_x$ as a function of the solvent flux for a NF45 membrane. pH≈10.6

The pH's of both solutions were approximately 10.6. Also in this case, it should be realized that the absolute error in the retention values is about 0.04.
Using a NF45 membrane, the retentions for the dendrimers with NH_2-endgroups are higher than for the CN-terminated dendrimers. This might be caused by the differences in size between the NH_2- and the CN-terminated dendrimers. According to Table 4.1 the size of an amine-terminated dendrimer of a certain generation is always larger than that of a nitrile-terminated one. Furthermore, it should be considered that the volume of the CN-terminated dendrimers was determined in acetone and not in water which was used in the retention measurements.

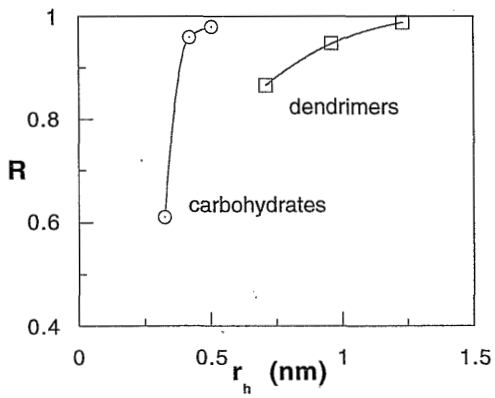

Figure 4.9: *Comparison of the retentions for different saccharides and CN-dendrimers for a NF45 membrane at a pressure difference of 5 bar.*

Figure 4.9 compares the retentions for four CN-terminated dendrimers as a function of their molecular size with the retentions for the various saccharides (glucose, sucrose and raffinose). Both experiments were carried out at the same pressure difference of 5 bar. The pH of the dendrimer solutions is about 9.5, whereas the pH of the saccharide solutions is about 6. As can be seen in this figure, the retentions for the saccharides are higher than those of the dendrimers, although it should be considered that the dendrimer size was not determined in water. Probably, these higher retentions for the saccharides are caused by differences in interaction between the membrane and the dendrimers, and between the membrane and the saccharides. Furthermore, the deformation of the saccharide and dendrimer molecules in a shear field may differ.

Buffered solutions
To investigate the influence of pH on the retention of dendrimers, experiments were carried out at pH=6 and pH=8. Prior to the retention measurements with buffered dendrimer solutions, solvent fluxes were measured of aqueous solutions containing the trisbuffer and the phosphate buffer (both without dendrimer). These measurements were carried out to investigate the influence of the presence of the buffer and that of the pH on the solvent flux. Although the solvent fluxes of both buffer solutions were about 20% lower than the pure water flux, the

flux decrease was considered small enough to carry out retention measurements with buffered dendrimer solutions. The differences in solvent flux between the solutions with pH=6 and pH=8 were negligible. The decrease of solvent flux might be caused by the adsorption of a secondary layer of buffer components at the membrane surface.

In case of the amine-terminated dendrimers a precipitate was formed when the buffer was added, which might be a reaction product between the dendrimer and the buffer, and no retention measurements were carried out with this solution.
In case of the nitrile-terminated dendrimers, retention measurements at pH=6 and a pressure difference of 5 bar showed, at least for the two smallest generations, a higher retention than for the unbuffered solution. This is shown in Figure 4.10, which compares the retentions of the dendrimers with the same hydodynamic radii (r_h) at different pH values.

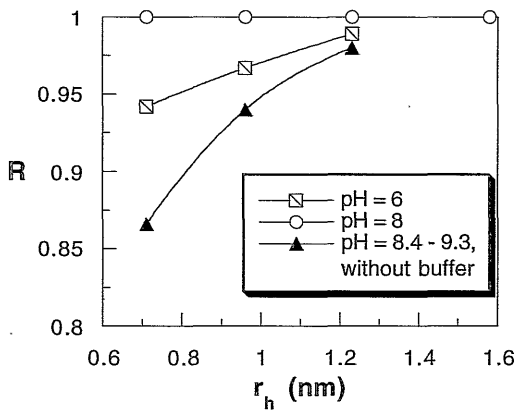

Figure 4.10: Comparison between retentions for different generations of CN-terminated dendrimers at different pH-values for a NF45 membrane. ΔP = 5 bar

Finally, retention measurements were carried out with buffered dendrimer solutions at pH=8 and a pressure difference of 5 bar. All CN-terminated dendrimers showed a retention of 1, i.e., a higher retention than in case of the unbuffered solution and than in the buffered solution at pH = 6. These results are shown in Figure 4.10 as well. The retention of the dendrimers in the buffered solutions may be affected by a possibly formed layer of buffer molecules.
The retention values of the amine-terminated dendrimers at pH = 8 showed an increase with increasing generation, i.e., hydrodynamic radius r_h, as plotted in Figure 4.11. The retention of the buffered dendrimer solution was lower than that of the unbuffered one. Probably, this may be caused by the pH of the solution. The natural pH of the amine-terminated dendrimers is 10.7, which means that in the buffered solution the pH is more than 2 pH points lower.
Addition of the trisbuffer to either the amine-terminated or the nitrile-terminated dendrimers showed a distinct difference. In case of amine endgroups the retention became lower by addition of the buffer, in case of the nitrile endgroups the retention became higher. Investigations with other membranes might give insight in the mechanism causing these differences.

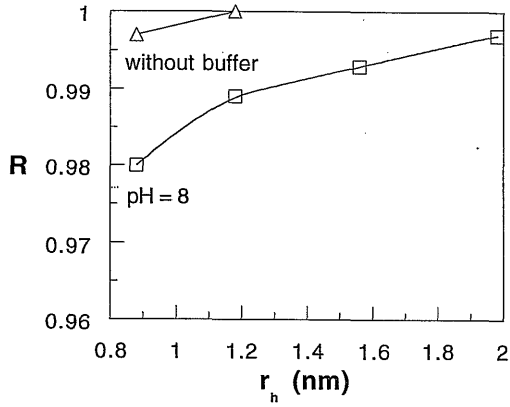

Figure 4.11: Comparison of the retentions for different generations of NH_2-terminated dendrimers at different pH's for a NF45 membrane. ΔP = 5 bar

Newkome and co-workers [14] showed that the size of their polyacid dendrimers was pH-dependent. Changing from low pH via neutral to basic (pH=3 → pH=7 → pH=13), the radius of the smallest dendrimer changed from 0.82 to 1.23 to 1.18 nm, respectively. These radii were determined by diffusion coefficients from 2D-NMR spectroscopy. The differences were even larger for higher generations of the dendrimer. Possibly, differences in dendrimer size at different pH play a role as well in our experiments.

CA30 membrane

Figure 4.12 shows the retention as a function of solvent flux for a CA30 membrane. As can be seen the membrane showed the highest retention of the largest dendrimer.

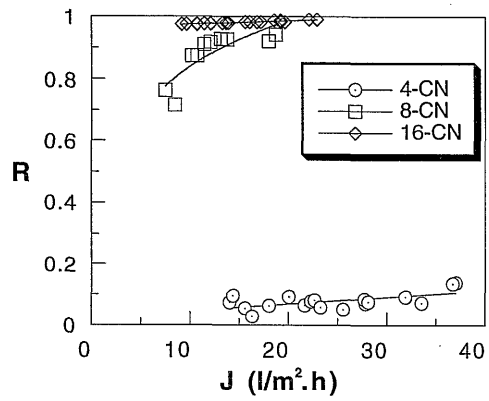

Figure 4.12: Retention of CN-terminated dendrimers as a function of the solvent flux for a CA30 membrane. (4CN: pH=7.3-7.5; 8CN: pH=9.1-9.6; 16CN: pH=9.6-9.9)

Figure 4.13 shows the difference in retention of a CA30 membrane between a 4-CN and a 4-NH_2 dendrimer solution. The retention of the dendrimer with 4 functional amine groups was much higher than that of the CN-terminated dendrimer. Probably, the differences in retention were partially caused by the size differences of the molecules and partially by different interactions between molecules and membrane.

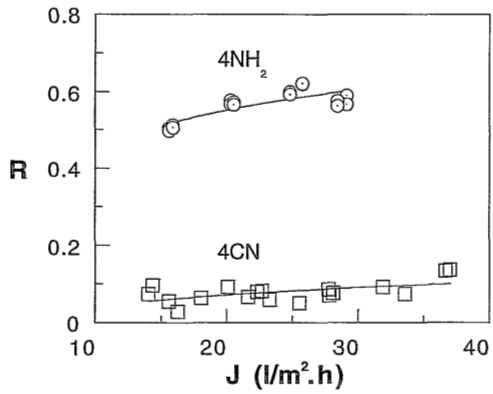

Figure 4.13: *Retention of CN and NH_2-terminated dendrimers with 4 functional endgroups as a function of the solvent flux for a CA30 membrane.(4CN: pH=7.3-7.5; 4NH_2: 10.8-11.3)*

Figure 4.14 shows the retention of a 4-NH_2 dendrimer solution as a function of the solvent flux at a pH value of 10.8-11.3 and at a pH value equal to 3. It can be seen that the retention becomes higher at the lower pH at a given solvent flux value. This might partially be explained by the protonation of the dendrimer at low pH, which may cause some enlargement of the molecule. Another explanation for the extremely high retention at pH=3 might be that the membrane has obtained a positive charge because of the low pH. Then, the high retention might be caused by an increase in the electrostatic repulsion from the membrane surface.

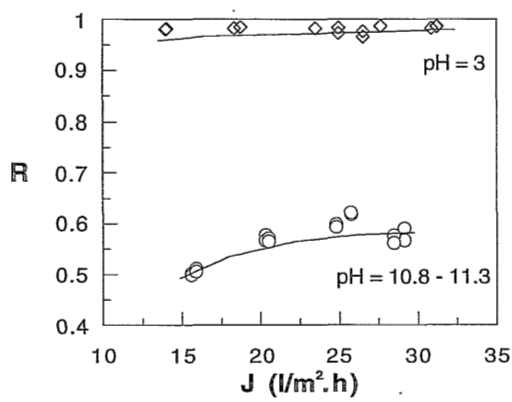

Figure 4.14: *Retention of 4-NH_2 dendrimer as a function of solvent flux for a CA30 membrane at pH = 3 and pH = 10.8-11.3*

Figure 4.15 shows a comparison between the retention of various CN-terminated dendrimers and the polysaccharides for the CA30 membrane. Like in case of the NF45 membrane, the retention of the dendrimers of comparable size is lower than that of the saccharides. Compared to the retention of raffinose, which is the largest saccharide molecule, the retention of the 4-CN dendrimer is very small. As the 4-CN dendrimer is only slightly charged, it is not clear what effects cause the large difference in retention between these solutes with equal size. Possibly, the dendrimer molecules show more deformation during the retention measurements than the saccharides, thereby causing a lower retention.

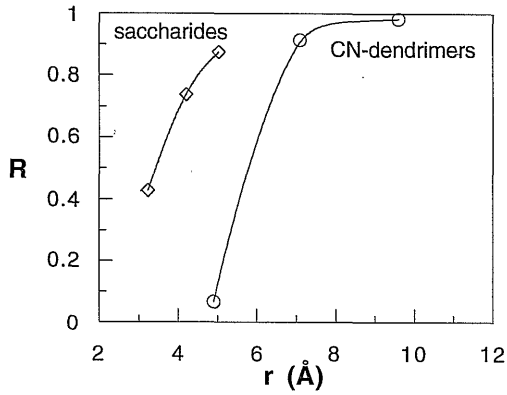

***Figure 4.15**: Comparison of the retentions for different saccharides and CN-dendrimers for a CA30 membrane at a pressure difference of 5 bar.*

ASP35 membrane

For the ASP35 membrane, the water fluxes in case of both the 4-CN and the 4-NH_2 dendrimer solutions decreased considerably compared to the pure waterflux, to about 20% of the initial extent.
Adjustment of the pH to 3 increased the water flux to the extent of the pure water flux before using filtering the dendrimer solutions as can be seen in Figure 4.16.
As shown in Chapter 3, the ASP35 membrane was characterized as a negatively charged membrane. In case of the basic dendrimer solutions, the positively charged dendrimers and the negatively charged membrane will interact strongly, what may result in the solvent flux decline. Possibly, the solvent flux increase at low pH values is caused by a decrease in dendrimer adsorption at the membrane surface because the surface charge of the membrane will be less (or no more) negative.

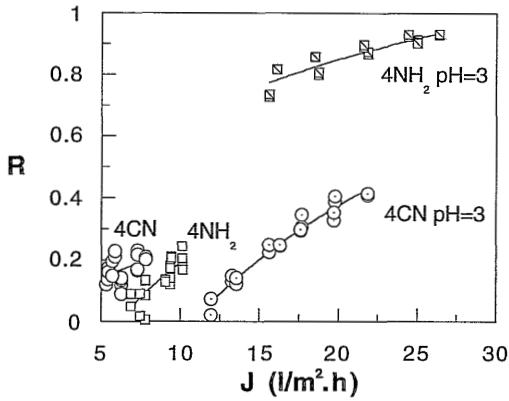

***Figure 4.16**: Retention of CN and NH_2-terminated dendrimers with 4 endgroups as a function of the solvent flux for a ASP35 membrane. 4CN: pH=7.3-7.7; 4NH_2: 9.2-10.3)*

PES10 membrane

Compared to the pure water flux of a PES10 membrane, the water flux of a DAB-dendr-$(CN)_8$ solution decreased to around 4% of the original value. For a DAB-dendr-$(CN)_{64}$ solution the solvent flux even approached zero. In both cases the stabilization of the water flux was very slow.

It was observed that the pure water flux, which was measured after a dendrimer retention measurement, reached after a certain period of time the same value as before the retention measurement.

For the DAB-dendr-$(CN)_8$ an apparent retention was found of -0.04, whereas for the retention of DAB-dendr-$(CN)_{64}$ an even more negative value was obtained, -0.60.

Both the solvent flux decline and the apparent negative retention seem to indicate a strong interaction between the dendrimers and the membrane. Like the ASP35 membrane, the PES10 membrane was classified as negatively charged (see Chapter 3). Its negative surface charge will attract the positively charged dendrimers, thereby causing an additional resistance to transport through the membrane.

UTC20 membrane

For the UTC20 membrane, the retentions for the smallest dendrimer (4-CN) were high, up to 0.97. The retentions for the 4-NH_2-terminated dendrimer and the 4-CN dendrimer solution at pH=3 were that high as well. No experiments were carried out with larger dendrimers.

γ-Al_2O_3 membrane

A γ-Al_2O_3 membrane was tested with DAB-dendr-$(NH_2)_8$, $(CN)_8$ and $(CN)_{16}$ solutions at an

applied pressure difference of 5 bar. The amine-terminated dendrimer showed a retention of 0.17. For the dendrimer with 8 CN endgroups, the retention was 0.10, for that with 16 endgroups 0.65. The water flux in the dendrimer retention experiments was as high as the pure water flux. This indicates that no modification of the γ-Al_2O_3 membrane occurred because of the high pH values of the dendrimer solutions. Since the pH values of the dendrimer solutions are around 11 and 9.4 for the 8-NH_2 and 8-CN solution, respectively, the γ-Al_2O_3 membrane will be negatively charged in these solutions. The pH value of the 16-CN solution is about 8, which is in the same range as the isoelectric point of Al_2O_3 that is reported to be in the pH range of 7-9. [15]. Therefore, the retention of this latter dendrimer can be caused only by size exclusion, in case of an uncharged membrane, or by a combination of size and electrostatic exclusion, in case of a positively charged membrane.

From the retention measurements with dendrimers it may be concluded that the lower generations of these molecules can be used for the characterization of nanofiltration membranes. However, it should be a first requirement to determine the exact sizes of these molecules within the solutions which are used for the retention measurements.
As mentioned before, the size of the dendrimers can be dependent on their environment. [14]. It was tried to measure the dendrimer size with Transmission Electron Microscopy (TEM) and Small Angle X-ray Scattering (SAXS) but none of these methods were successful. With TEM no individual dendrimer molecules could be observed. In case of SAXS the concentrations which were used in solution were too small for detection of the dendrimer size. The only result from the SAXS measurements was that the shape of even the largest dendrimers was not spherical.

4.5 CONCLUSIONS

The retention for (poly)saccharides seems to be determined by size effects. The higher the molecular weight of the solute, the higher the retention. An increase in the solvent flux through the membrane causes a higher retention.

Retention measurements with dendrimers showed an increasing retention with increasing dendrimer generation. For a NF45 membrane, the retention was independent of the concentration.
Dendrimers with different endgroups, CN or NH_2, showed for both the NF45 and CA30 membrane a much higher retention for the amine-terminated dendrimers than for the nitrile-terminated ones. Probably, differences in interactions between membrane and dendrimer cause the differences in retentions. At a pH of 3, where the dendrimers are thought to be fully protonated, the retention for a CA30 membrane was much higher than at a neutral pH of around 7.5. The membrane surface might have become slightly positively charged at that pH, resulting in the high retentions for the positively charged dendrimers.
In case of the NF45 membrane, the retention increased using buffer solutions for the nitrile-terminated dendrimers. In case of pH = 8, the dendrimer retention was 1, whereas for pH=6,

the retention is always above that of the unbuffered solution. This might be caused by differences in dendrimer size at the different pH values or by the formation of a layer of buffer molecules at the membrane surface. In case of the amine-terminated dendrimers the retention decreased for a solution which was buffered at a pH of 8.
Comparing the retention results of dendrimers and polysaccharides for the NF45 and the CA30 membrane, it appeared that, in case of approximately the same sizes, the dendrimer retention was lower compared to the saccharide.
The negatively charged membranes ASP35 and PES10 showed a high solvent flux decrease, when using the dendrimer solutions. Most probably, this is caused by the strong interaction between the negatively charged surface and the positively charged dendrimers.
Because no appropriate method was found to determine the size of the dendrimers in aqueous solutions at different pH values, the results of the dendrimer retention measurements were difficult to interpret in a quantitative way.

ACKNOWLEDGEMENTS

Mirjam Verbruggen is acknowledged for her preliminary analytical work on the dendrimers. Niklas Olsson is kindly acknowledged for the development of a method to analyse the dendrimer concentration and for retention measurements with dendrimers. Bart Velner is acknowledged for performing retention experiments with saccharide solutions. Finally, José Nolten is acknowlegded for performing retention experiments with both saccharide and dendrimer solutions.

SYMBOLS

c:	concentration	(mol/l)
D:	diffusion coefficient	(m^2/s)
f (λ):	wall correction factor for diffusive transport	(-)
g (λ):	wall correction factor for convective transport	(-)
J_S:	solute flux	(mol/m^2.s)
J_V:	solvent flux	(m/s)
L:	$= L_S/\Delta x$,	
	solute permeability coefficient corrected for the membrane thickness	(m/s)
L_V:	solvent permeability coefficient in two component system	(m^2/s.bar)
L_S:	solute permeability coefficient in two component system	(m^2/s)
p:	porosity	(-)
P:	pressure	(bar, N/m^2)
Pe:	Péclet-number	(-)
r:	radius	(m)
R:	retention	(-)
S:	hindrance factor	(-)

T:	temperature	(K)
x:	coordinate in flow direction	(m)
Δx:	membrane thickness	(m)
λ:	ratio of solute size and pore size	(-)
π:	osmotic pressure	(bar, N/m^2)
σ:	reflection coefficient	(-)
ϕ:	flow rate	(m^3/s)

subscripts:

D:	diffusive
f:	feed
F:	convective
p:	pore
p:	permeate
s:	solute
v:	solvent

REFERENCES

[1] Tsuru, T., Wang, X.-L., Nakao, S.I., Kimura, S., *Transport of neutral and charged solutes through nanofiltration membranes*, International Symposium on Fiber Science and Technology, Yokohama, Japan, 1994

[2] Kimura, S., Jitsuhara, I., *Transport through charged ultrafiltration membranes*, Desalination, 46 (1983) 407-416

[3] Sarrade, S., Rios, G.M., Carlès, M., *Dynamic characterization and transport mechanisms of two inorganic membranes for nanofiltration*, J. Membrane Sci., 97 (1994) 155-166

[4] Rautenbach, R., Gröschl, A., *Separation potential of nanofiltration membranes*, Desalination, 77 (1990) 73-84

[5] Spiegler, K. S., Kedem, O., *Thermodynamics of hyperfiltration (reverse osmosis): criteria for efficient membranes*, Desalination, 1 (1966) 311

[6] Nakao, S., *Membrane transport phenomena and ultrafiltration*, in: Encyclopedia of Fluid Mechanics; Vol. 2,4,5, ed. by N.K. Cheremisinoff, Gulf Publ. Comp., Houston, 1986, p. 987

[7] Bowen, W. R., Mukthar, H., *Characterisation and prediction of separation performance of nanofiltration membranes*, J. Membrane Sci., 112 (1996) 263-274

[8] Tomalia, D. A., *Starburst/cascade dendrimers: fundamental building blocks for a new nanoscopic chemistry set*, Adv. Mats., 6 (1994) 529-539

[9] Mekelburger, H.-B., Jaworek, W.,Vögtle, F., *Dendrimers, arborols, and cascade molecules: breakthrough into generations of new materials*, Angew. Chem., 31 (1992) 1571

[10] Issberner, J., Moors, R., Vögtle, F., *Dendrimers: from generations and functional groups to functions*, Angew. Chem., 33 (1994) 2413

[11] de Brabander- van den Berg, E., Meijer, E.W., *Poly(propylene imine) dendrimers: large-scale synthesis by hetereogeneously catalyzed hydrogenations*, Angew. Chem., 32 (1993) 1308

[12] O'Sullivan, D. A., *Dendrimers nearing availability for commercial evaluation*, Chem. Eng. News, 8 (1993) 20

[13] Atkins, P. W., Physical Chemistry, third ed., W.H. Freeman, New York, 1986

[14] Newkome, G. R., Young, J.K., Baker, G.R., Potter, R.L., Audoly, L., Cooper, D., Weis, C.D., Morris, K., Johnson, C.S., Jr., *Cascade polymers. pH dependence of hydrodynamic radii of acid terminated dendrimers*, Macromolecules, 26 (1993) 2394-2396

[15] Parks, G. A., *The isoelectric points of solid oxides, solid hydroxides and aqueous hydroxo complex systems*, Chem. Rev., 65 (1965) 177

APPENDIX II

Water permeabilities and sugar retentions

Membrane	Waterperm. ($l/m^2.h.bar$)	R (%) glucose (ΔP=5 bar)	R (%) sucrcose (ΔP=5 bar)	R (%) raffinose (ΔP=5 bar)
WFN0505	1.0	-	-	-
NF45	3.9	61	96	98
NF70	1.3	-	-	–
MPF21	6.6	14	93	99
MPF32	2.8	77	96	98
ASP35	4.3	7	30	42
SX01	2.1	-	-	-
SX10	2.8	-	-	-
HG01	3.7	-	-	-
HG19	1.2	-	-	-
BQ01	6.2	7	26	50
MX07	4.3	89	99	99
CTA-LP	2.3	89	97	98
TFCS	4.3	98	-	97
UTC60	2.2	92	94	92
UTC70	1.2	94	93	94
CA30	4.0	29	59	73
PES10	2.3	8	15	29
PVD1	2.0	-	-	-
Alumina	1.3	26	47	71

-: not determined

CHAPTER 5

Characterization of nanofiltration membranes by streaming potential measurements

ABSTRACT

Streaming potential measurements were carried out with various electrolyte solutions flowing along the membrane surface to investigate the influence of salt type and concentration on the zeta potential and the surface charge density of various polymeric nanofiltration membranes and a ceramic γ-Al_2O_3 membrane. The zeta potential decreased at increasing electrolyte concentration, while the kinetic surface charge density of the membranes increased. The polymeric membranes showed a negative zeta potential, while that of the ceramic membrane was positive. For some membranes the various electrolyte solutions used showed different zeta potentials, showing specific ionic adsorption, but for other membranes the zeta potential at the certain ionic strength did not depend on the type of salt.

The kinetic surface charge densities were generally the highest for sodium sulfate solutions compared to sodium and calcium chloride solutions.

The kinetic surface charge density was described by a Freundlich isotherm, which showed the influence of both the (fixed) membrane charge and the adsorption of ions on the surface charge. Generally, the fixed membrane charge was small compared to the charge density resulting from the adsorbed ions. The occurrence of this low membrane surface charge was confirmed by titration, which showed that the polymeric nanofiltration membranes contained negative charges, but only in small amounts.

5.1 INTRODUCTION

The separation of ions by nanofiltration membranes is thought to be achieved by both the size of the ions and by electrical interactions between membrane and ions. Whereas in Chapter 4 the influence of the size of the solutes on the separation was emphasized, this chapter will focus on the electrical interactions between membrane and ions, and more specific on the charges present at the membrane surface and on the ions at the interface.
As shown in Chapter 3, the charges at the membrane surface can exert repulsive forces on the ions in the feed, thereby causing a retention. To compare the effects of size and of charge on the separation features of nanofiltration membranes, the origin of the membrane charge must be identified and quantified.
The electrostatic interactions between membrane and ions can be investigated in different ways. Separation experiments have been performed, in which parameters like salt concentration and membrane flux have been changed, and these measurements were used for the estimation of the membrane charge [1-3]. The membrane charge density could be determined by membrane potential measurements [2,4,5]. Furthermore, electrical impedance measurements have been carried out giving information about the resistance to electrolyte transport through the membrane [6].
Streaming potential measurements is another technique to determine the membrane charge density [7-9]. In this chapter, the results of this technique will be described. When the streaming potentials are known, zeta potentials and kinetic surface charge densities of nanofiltration membranes can be estimated. The streaming potential measurements were carried out along the membrane surfaces, instead of through the membrane, with different types of ions at various concentrations. It is assumed that the charge density at the outer membrane surface is representative for that throughout the active toplayer.

5.2 THEORY

5.2.1 Membrane charge

Membranes that are put in contact with an aqueous electrolyte solution can obtain a charged surface by several mechanisms, such as the dissociation of fixed charged groups, the preferential adsorption of one type of ions or both mechanisms.
In case of polymeric membranes, charged groups are, e.g., carboxylic, amine and sulfonic groups. Ceramic membranes may contain ionizable groups as well. Most metal oxides are amphoteric, which means that they can either react as a weak acid or as a weak base, dependent on the pH [10]. Reactions that may take place at the surface are:

$$AlOH + H^+ \rightleftharpoons AlOH^+_2$$

$$AlOH \rightleftharpoons AlO^- + H^+$$

$$RCOOH \rightleftharpoons RCOO^- + H^+$$

$$RSO_3H \rightleftharpoons RSO_3^- + H^+$$

$$RNH_3 + H^+ \rightleftharpoons RNH_4^+$$

Membrane surfaces may also change the surface charge by adsorption of ions from the solution. If the adsorbing ions have a charge opposite to the surface, then adsorption is dominated by electrostatic attraction. Generally, it is not very easy to distinguish whether the charge on a surface is caused by reaction of surface groups or by adsorption.

5.2.2 Electrical double layer

If a surface is brought in contact with an electrolyte solution, an electrical double layer may be formed at the interface. In case of dissociation of chemical groups at the surface, the distribution of ions in the solution will be influenced. Near the surface, the majority of ions will have an electric charge opposite to the membrane charge, whereas further away from the surface, the amount of positively and negatively charges will be equal again. Since the system as a whole requires electroneutrality, the solution adjacent to the surface will carry the same amount of charges as present at the surface.
Helmholtz was one of the first who described electrical double layer phenomena. In his model it is assumed that the charge of the surface was compensated in one layer of counter-ions adjacent to the interface. The layer is assumed to be *fixed* near the interface. A schematic drawing of this model is shown in Figure 5.1(a).

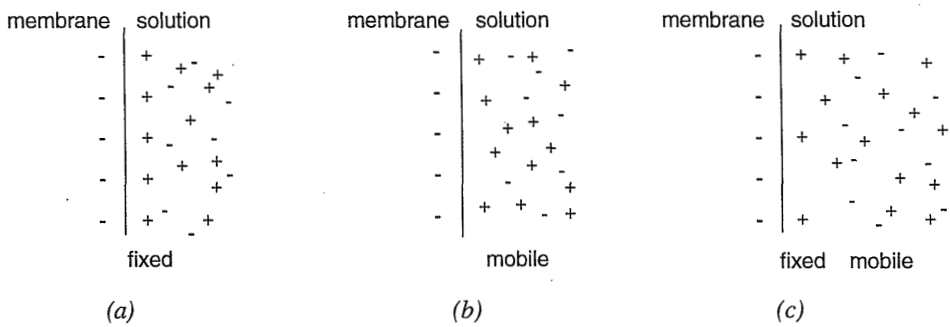

***Figure 5.1**: Schematic drawing of different double layer models, (a) Helmholtz model, (b) Gouy-Chapman model, (c) Stern model*

In the Gouy-Chapman model, see Figure 5.1(b), a statistical distribution of mobile ions in the solution is assumed, which obeys the Poisson-Boltzmann relation. One of the main problems with this model is that it treats the ions as point charges, which theoretically leads to very high

concentrations of ions in the vicinity of the charged surface. Furthermore, no ordering effects are taken into account. Stern combined the Helmholtz and the Gouy-Chapman model and assumed that the double layer existed of a layer of counter-ions which is fixed to the surface, the Stern layer, and a diffuse, mobile layer in which the ions are distributed according to the Poisson-Boltzmann relation, like in the Gouy-Chapman model. A schematic drawing of the Stern model can be seen in Figure 5.1(c).

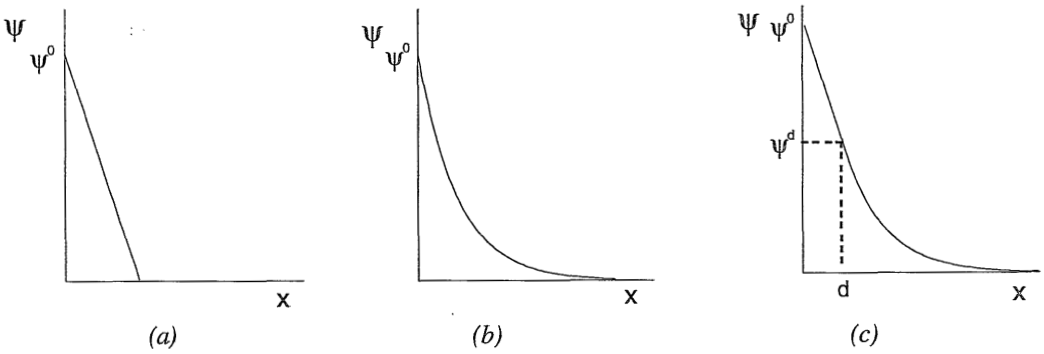

***Figure 5.2**: Schematic drawing of potential distributions as a function of the distance from the surface for (a) Helmholtz model, (b) Gouy-Chapman model and (c) Stern model. ψ^0 is the surface potential and ψ^d is the Stern potential.*

Double layer models may give insight in the potential distribution in a solution near a charged surface. Figure 5.2 shows the potentials, ψ, according to the various models as a function of the distance from the surface, x. The potential at the surface is called ψ^0. In the Helmholtz model, the double layer is considered to be equivalent to a parallel plate condenser, as shown in Figure 5.2(a), and therefore, the potential in the double layer decreases linearly with the distance. According to the Gouy-Chapman model, the potential in the double layer decreases exponentially and approaches to zero, see Figure 5.2(b). In the Stern model, a linear decrease of the potential occurs within the Stern layer having a thickness d. The potential at the Stern interface between the fixed and the diffuse part of the double layer is called ψ^d. Within the diffuse part of the double layer, the potential follows an exponential decrease according to the Gouy-Chapman model (Figure 5.2(c)).

In Figure 5.3 the model of Stern, which is the most realistic approach, is worked out in more detail. Here, different potentials are indicated: the surface potential, ψ^0, the potential at the Stern plane, ψ^d, and the electrokinetic or zeta potential, ζ. All these potentials are defined with respect to the potential at infinite distance from the surface. Although the surface potential is an important parameter, the potential at the Stern surface is more relevant. This potential is the actual potential influencing the behavior of the charged species. However, since the Stern-potential cannot be measured directly, consequently the electrokinetic or zeta potential is mostly used. The zeta potential represents the potential at the surface of shear between surface and

solution plane, at a plane close to the Stern layer. In literature it is very common to assume the Stern potential to be identical to the zeta potential [11]. This zeta potential (ζ) is shown in Figure 5.3 as well. The zeta potential can be determined by electrokinetic measurements, like streaming potential and streaming current measurements, electro-osmosis and electrophoresis.

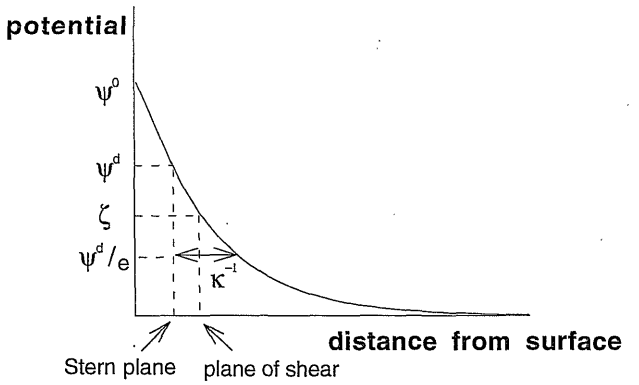

***Figure 5.3**: Schematic drawing of potential decrease as a function of the distance from the surface in an electrolyte solution*

The zeta potential is related to the phenomena that play a role between a charged surface and charged particles. The potential at the shear plane is determined by both the membrane surface potential and the fixed ions within the double layer and therefore, the zeta potential provides information on these two parameters.
The double layer thickness, κ^{-1}, is defined as the thickness of the diffuse layer, where the potential has decreased to a value of ψ^d/e, with e the natural number.

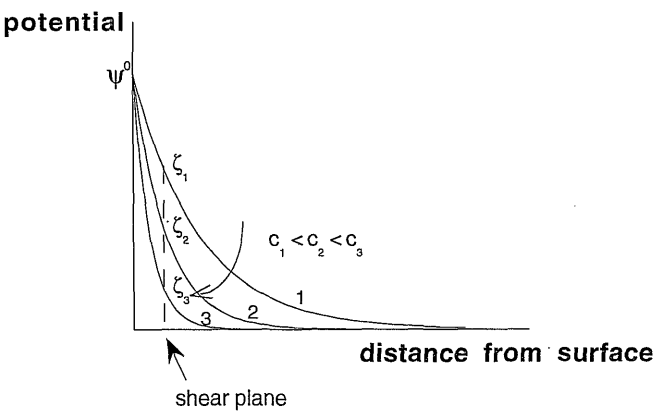

***Figure 5.4**: Schematic drawing of potential decrease as a function of the distance from the surface in electrolyte solutions with different concentrations, c*

Figure 5.4 shows the potential decrease as a function of the distance from the charged surface for electrolyte solutions with different concentrations. The concentration of solution 1 is lower

than that of 2, which is lower than that of 3. The higher the electrolyte concentration is, the higher the potential decrease within the solution will be, since more ions are present in the solution which may compensate the surface charge. This implies that the zeta potential will decrease with an increasing electrolyte concentration as well.

5.2.3 Streaming potential

Electrokinetic effects result from the influence of the hydrodynamic movement of one of the parts of the electrical double layer on the electric field, or vice versa, the influence of the electric field on the relative movement between parts of the double layer. In case of an interface between a solid surface and an adjacent solution two types of electrokinetic phenomena can be observed. Firstly, an electric field is applied which causes the movement of either the solution or the solid. The former phenomenon is called electro-osmosis, the latter electrophoresis. Secondly, movement of a charged surface relative to an adjacent electrolyte solution may cause an electric field. When the solution moves relative to the surface, a streaming potential will occur, whereas the movement of the solid within the solution is called the sedimentation potential. In this chapter the streaming potential will be elaborated into more detail.
By applying a hydrodynamic pressure on an electrolyte solution that is in contact with a charged capillary a flow of the solution will result which consequently causes a streaming potential. This streaming potential is the potential difference over the capillary at zero net current. Figure 5.5 schematically illustrates the origin of the streaming potential.

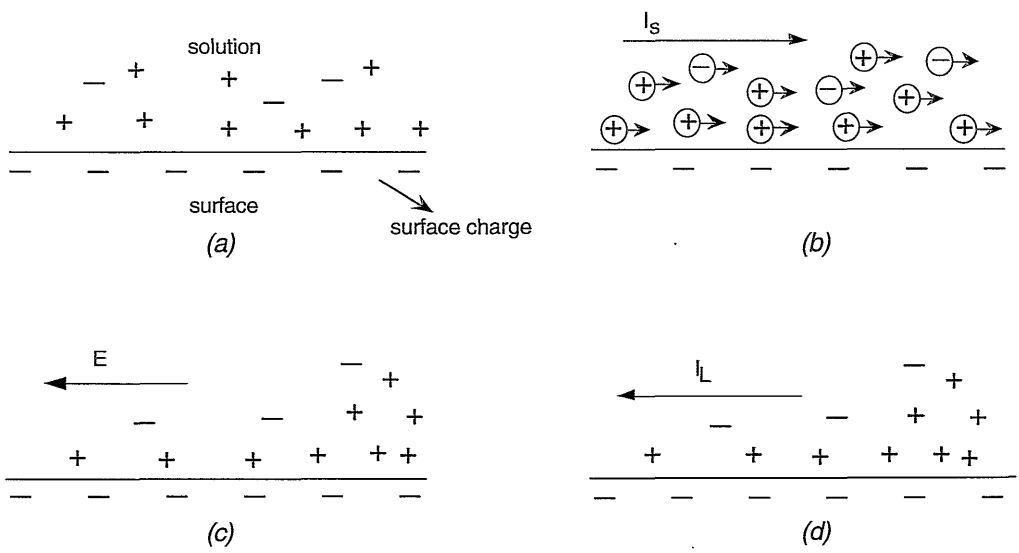

Figure 5.5: Schematic representation of the streaming potential. (a): double layer at charged surface, (b) generated streaming current, I_s, by a pressure applied, (c) accumulation of ions causing steaming potential, E, (d) induced leak current, I_L, by streaming potential. [12]

If a hydrodynamic force is applied on an electrical double layer, then a streaming current will be generated due to transport of counter-ions, which are present in the double layer (Figure 5.5(a) and (b)). The accumulation of counter charges downstream generates a streaming potential across the capillary (Figure 5.5(c)) which on its turn causes a conduction current through the capillary in the reverse direction (Figure 5.5(d)). In steady state, the streaming current equals the conduction current.
Measurement of a streaming potential can provide the zeta potential (ζ) and from this parameter the kinetic surface charge density (σ^d) at the hydrodynamic shear plane can be calculated. The streaming potential is defined positive for a higher potential at the high pressure side.

The relation between the streaming potential, ΔE_{str}, and the pressure difference applied, ΔP, is given by (e.g., [11,13]):

$$\frac{\Delta E_{str}}{\Delta P} = \frac{\varepsilon \zeta}{\eta (\lambda_0 + 2 \lambda_s / r)} \qquad \{5.1\}$$

where ζ is the zeta potential, ε the permittivity of the medium, η the viscosity, λ_0 the bulk conductivity, λ_s the surface conductivity and r the radius of the pore or capillary. In case of a channel, r is equal to half the width of a slit.
At electrolyte concentrations smaller than about 0.001M, the surface conductivity becomes important [13]. At concentrations above 0.001M, equation {5.1} reduces to:

$$\frac{\Delta E_{str}}{\Delta P} = \frac{\varepsilon \zeta}{\eta \lambda_0} \qquad \{5.2\}$$

In case of smaller concentrations, when the surface conductivity plays a role, equation {5.1} should be applied. Because it is difficult to measure the surface conductivity directly, the actual resistance of the electrolyte solution, R_{exp}, across the slit or pore can be measured. By comparing this value with the resistance that can be calculated from experiments at high concentrations, R_{th}, where the surface conductivity can be neglected, equation {5.1} can be written as [13]:

$$\frac{\Delta E_{str}}{\Delta P} = \frac{\varepsilon \zeta}{\eta \lambda_0} \frac{R_{exp}}{R_{th}} \qquad \{5.3\}$$

Equation {5.1} to {5.3} can be applied when the thickness of the double layer, κ^{-1}, is much smaller than the radius of the pore or half the width of the slit through which the solution streams.
The streaming potential theory has been derived for the case of a perfectly smooth surface, while in case of membrane surfaces some roughness will always be present. Although in principle, the inner regions of the double layer could only be described in a correct way by an extended characterization of the membrane interface, we will assume the membrane surface to

be smooth.

Streaming potential measurements can be carried out through a membrane and along a membrane surface. Mostly, streaming potential measurements are performed through porous membranes. In that case an electrical double layer is formed by the charged membrane pore walls and the adjacent electrolyte solution. By comparison of the streaming potential of various membranes, for instance before and after adsorption of protein or other species, changes in the pore characteristics have been determined [14-16]. Streaming potential measurements along surfaces can be determined by fixing two charged surfaces opposite to each other at a certain distance, thereby creating a slit with charged walls. Hereby, the surface characteristics of a membrane can be measured (see, e.g., [12,17,18]).
For both types of streaming potential measurements, through and along membranes, equations {5.1} to {5.3} can be applied.
Two problems should be considered when streaming potential measurements through pores are carried out with nanofiltration membranes. Since nanofiltration membranes are not isotropic, it should be confirmed that the streaming potential which is measured through the membrane is the streaming potential of the active toplayer only and not of the support layer that does not contribute to the separation. Furthermore, the theoretical interpretation of the streaming potential through nanofiltration membranes is very difficult, because the Helmholtz-Smoluchowski equation can only be used when κ^{-1} is much smaller than the radius of the pore. If pores are present in nanofiltration membranes, their radius will be around 1 to 2 nm, whereas the double layer thickness in a mono-mono-valent electrolyte solution with a molarity of 0.1M is about 1 nm. At lower concentrations it becomes even larger, so the Helmholtz-Smoluchowski equation cannot be used anymore.
Streaming potential measurements along a nanofiltration membrane provide information on the surface characteristics which are thought to be representative for the active toplayer of the membrane. Because of this argument and the problems with the streaming potential measurements through nanofiltration membranes, streaming potential measurements were carried out along the membrane surface.

Various origins of charge can be observed with respect to a charged membrane and an electrolyte solution. When adsorbing ions are present in the Stern layer, three different contributions to the total charge of the system can be distinguished. Firstly, the fixed charges at the membrane surface, Q^0, secondly, the charges of the Stern layer, Q^S, and finally, the charges within the diffuse part of the electrical double layer, Q^d. Since electroneutrality is required, the total charge of the electrical double layer equals zero.
Assuming that the diameter of the pore or the width of the slit through which the solution is streamed is much larger than the double layer thickness, κ^{-1}, the relation between the surface charge density (σ) of each of the layers can be written as:

$$\sigma^0 + \sigma^S + \sigma^d = 0 \qquad \{5.4\}$$

The surface charge density is not always confined to an infinitely thin layer, but can have a certain thickness. This may, for instance, be the case for the membrane surface charge density, σ^0, which can be located somewhere near the membrane surface. The surface charge density of the diffuse part of the double layer, σ^d, is the total charge present within a column with a certain area normal to the membrane surface. For a flat surface, the surface charge density at a distance x from the surface can be written as:

$$\sigma^d(x) = \int_x^\infty \rho(x)\,dx \qquad \{5.5\}$$

where $\rho(x)$ is the space charge density at a place x normal to the surface.
From this equation, it can be derived that the surface charge density at a plane at a distance x from the surface equals [11]:

$$\sigma(x) = -\varepsilon\kappa\psi(x)\frac{\sinh\left(\frac{zF}{2RT}\psi(x)\right)}{\frac{zF}{2RT}\psi(x)} \qquad \{5.6\}$$

with ε being the permittivity of the medium, κ the reciprocal Debije length, $\psi(x)$ the potential distribution as a function of distance x, z the valency, R the gas constant, T the temperature and F the Faraday constant.
For a solution containing a mono-mono-valent electrolyte, the surface charge density at the shear plane, σ^d, or the kinetic surface charge density, with a potential equal to ζ can be written as:

$$\sigma^d = -\varepsilon\kappa\zeta\frac{\sinh\left(\frac{F}{2RT}\zeta\right)}{\frac{F}{2RT}\zeta} \qquad \{5.7\}$$

which reduces for small potentials ($\psi \lesssim 50$ mV) to:

$$\sigma^d = -\frac{\varepsilon\zeta}{\kappa^{-1}} \qquad \{5.8\}$$

The Debije length, κ^{-1}, can be calculated according to:

$$\kappa^{-1} = \sqrt{\frac{\varepsilon RT}{2F^2 I}} \qquad \{5.9\}$$

with $I = 0.5\sum_i z_i^2 c_i$,

with I being the ionic strength, z_i the valency and c_i the concentration of species i.

In case of electrolyte solutions containing ions with different valencies, the kinetic surface charge density can be obtained from [11]:

$$\sigma^d = -(\text{sign}\,\zeta)\sqrt{2\varepsilon c R T}\sqrt{\nu_+ \exp\left(-\frac{z_+ F}{R T}\zeta\right) + \nu_- \exp\left(-\frac{z_- F}{R T}\zeta\right) - \nu_+ - \nu_-} \qquad \{5.10\}$$

with ν the stoichiometric number, z_+ and z_- the valency of the cation and the anion, respectively, and (sign ζ) the positive or negative sign of the ζ-potential.

5.3 EXPERIMENTAL

5.3.1 Streaming potential measurements

The set-up to determine streaming potentials was almost identical to that described by Van Wagenen and Andrade [19]. With this set-up, streaming potentials can be measured along a surface.
Figure 5.6 shows a schematic drawing of the cell which was manufactured by Mr. van Beek from the Agricultural University of Wageningen (The Netherlands). The membrane samples are glued upon glass plates (microscope slides). The dimensions of the membrane samples are 76 * 26 mm.

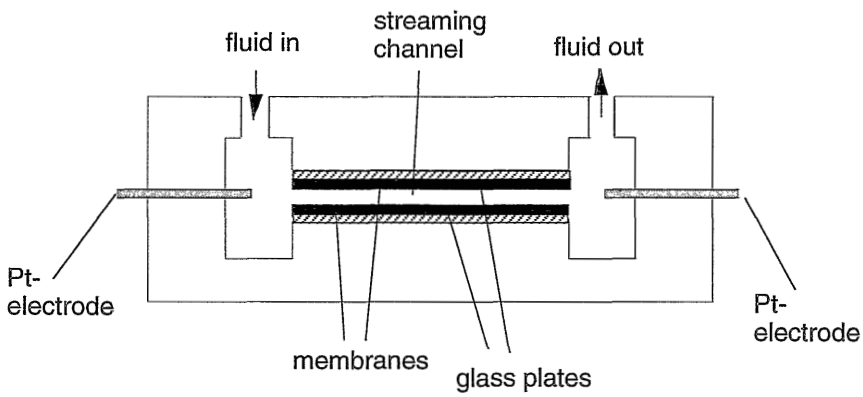

Figure 5.6: Schematic illustration of the streaming potential cell

The cell consists of two Plexiglas parts containing sample channels that hold the glass slides with the membranes glued on top. Clamps hold both cells parts together. Under the glass slides silicon rubber sheets can be applied to prevent leakage at the interface between cell and glass slide. The cell parts are separated by a Teflon sheet which serves two functions: spacing between sample plates and leak prevention. In case of polymeric membranes this was 200 μm

thick, whereas in case of ceramic membranes a 50 μm thick sheet was used. Platina black electrodes are inserted into the chambers at both ends of the cell.
The driving pressure can be applied in both directions and consequently the electrolyte solution can pass through the channel from the left to the right or from the right to the left. The pressure difference was varied in the range of 0 to 0.25 bar and was monitored with an accuracy of 0.01 bar. Streaming potential measurements were repeated at least six times by measuring at decreasing pressure.
The streaming potential was measured using a digital multimeter (Simpson, Model 464, Simpson Electric Company, Elgin), which had an internal impedance of 10 GΩ.
The concentrations of the electrolyte solutions used were in the range of 10^{-5} to 0.01 M for the three salts used: NaCl, $CaCl_2$ and Na_2SO_4 (Merck, p.a.). The streaming potentials were measured from low to high concentration. For every electrolyte fresh membranes were used.
Electrolyte conductance was measured by a conductivity meter (Microprocessor Conductivity Meter LF 537, WTW). The pH of the electrolyte bulk solutions was measured by a pH meter (691 pH Meter, MetrOhm). Demineralized water filtered by a Milli-Q-Plus unit (conductivity 60 nS/cm) was used as solvent.
The temperature of the system was kept at 20-23°C and the pH of the electrolyte solutions was kept at 6 ± 0.3.

5.3.2 Titration

The polymeric membranes that were used for the streaming potential measurements were titrated to determine the concentration of fixed charges in the membrane or the ion exchange capacity. Therefore, the toplayer and, in some cases, an intermediate layer were separated from the supports of these membranes. The toplayer and intermediate layer were used for titration.
50 mg of the membrane was immersed in water, and subsequently, the polymer was titrated by a 0.01M NaOH solution. The titrations were carried out with a MetrOhm 716 DMS Titrino automatic titration set-up.
No blanc titrations were carried out, so only the total amount of acidic groups was determined. Titration is a bulk technique by which the space charge density of the material is obtained, contrarily to the streaming potential measurements by which the surface charge density can be obtained.

5.3.3 Membranes

The following commercially available polymeric nanofiltration membranes were used for this research: ASP35 (Advanced Membrane Technology), NF45 (Dow-FilmTec), CTA-LP (Fluid Systems), UTC90 (Toray) and a ceramic γ-Al_2O_3 membrane. The γ-Al_2O_3 membrane was prepared on a glass plate. This plate was dipped in a boehmite-PVA sol (see Chapter 3), dried and then calcined at 600°C. For the γ-Al_2O_3 membrane only some measurements were carried out.
According to the information of the manufacturers, the ASP35, NF45 and UTC90 membranes are weakly negatively charged membranes at a pH of 6, whereas the CTA-LP membrane is

non-charged. The ASP35 membrane is made of polysulfone, the NF45 and UTC90 membranes are interfacially polymerized polyamide membranes and the CTA-LP membrane is a cellulose triacetate membrane. The γ-Al_2O_3 membrane has a positive charge at this pH.

5.4 RESULTS

5.4.1 Titration

The concentrations of acidic groups of the four polymeric membranes determined by titration are shown in Table 5.1. These experiments showed that the membrane surface charge density is only small when compared to values reported for the titration of charged ultrafiltration, charged composite reverse osmosis and ion exchange membranes, which had ion exchange capacities of 1.08 mmol/g, 1 mmol/g and 0.6 to 2.8 mmol/g, respectively [2,20,21]. The concentrations of fixed charged groups at the nanofiltration membrane surfaces are 10 to 300 times smaller. The relative error in the concentration of acidic groups is about 1%.

Table 5.1: Concentrations of fixed charge and formal membrane surface charge densities at several polymeric nanofiltration membranes determined by titration

membrane	acidic groups (mmol/g)	σ_0 (A.s/m^2)
ASP35	0.108	371
NF45	0.017	37.7
UTC90	0.040	78.7
CTA-LP	0.014	54.6

The surface charge density was calculated by multiplying the acid concentration by the mass per area of the toplayers of each of the membranes. By calculating the membrane surface charge density in this way, it is assumed that all acidic groups are concentrated at the surface of the membrane. The surface charge density obtained by titration will be indicated by the term *formal* surface charge density.

5.4.2 Streaming potential measurements

The streaming potential measurements showed that the streaming potential increased with increasing pressure and decreasing electrolyte concentration. This is in agreement with the theoretical considerations. If a higher pressure is applied, the accumulation of counter charges downstream will be larger as schematically shown in Figure 5.4, and consequently, the streaming potential which compensates this accumulation will be larger as well. In case of a concentration increase, the thickness of the double layer will diminish, which results in a smaller streaming potential. An example of a streaming potential measurement can be seen in

Figure 5.7, where the streaming potential is plotted as a function of the pressure difference applied for various NaCl concentrations for a NF45 membrane.

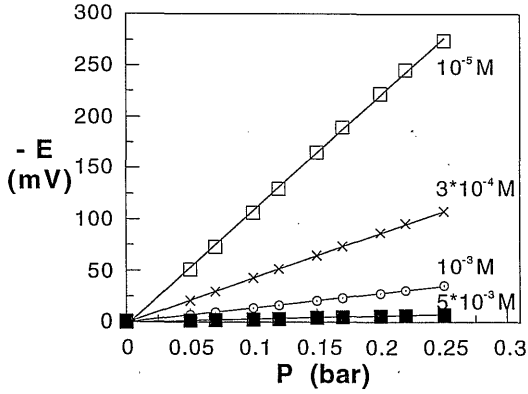

Figure 5.7: *Streaming potential as a function of the applied pressure for different concentrations of NaCl. Membrane: NF45*

The streaming potentials found for all polymeric membranes were negative, whereas those of the γ-Al_2O_3 membrane were positive at a pH of 6. The ASP35 membrane was characterized as a negatively charged membrane, according to the salt retention measurements described in Chapter 3. In case of non-specific ion adsorption, a negative surface charge mostly will show a negative streaming potential. The NF45, CTA-LP and UTC90 membranes were characterized neither as negatively charged nor as positively charged membranes, based on the salt rejection measurements. Their negative streaming potentials seems to concur with the negative streaming potential observed for uncharged polymeric films and membranes as reported before [7,22].
For the γ-Al_2O_3 membrane the positive streaming potential was in accordance with the results from the retention measurements, described in Chapter 3, indicating a positively charged surface for this membrane at a pH of 6.

The use of different electrolytes of identical ionic strength resulted in different streaming potentials. By equation {5.3}, the corresponding zeta potentials were calculated. The Figures 5.8 and 5.9 show the zeta potentials for four polymeric membranes. The zeta potentials were all negative and showed a decrease with an increase in ionic strength, because the potential in a concentrated electrolyte solution will decrease faster (like schematically shown in Figure 5.4).
For the ASP35 membrane, the zeta potentials measured for the sulfate solution were lower than those measured for the sodium and calcium chloride solutions, whereas the values for both chloride solutions were comparable. For the NF45 membrane, the highest zeta potentials were measured with a Na_2SO_4 solution. The zeta potentials measured with NaCl were lower, whereas those measured with $CaCl_2$ were the lowest. The zeta potentials measured for the CTA-LP membrane showed very similar results for the various salts, which might be caused by comparable interactions of the three electrolyte solutions with this membrane. In case of the

UTC90 membrane, the zeta potentials for the various salts were comparable as well, although the zeta potential at low concentrations of the calcium chloride solution was much higher compared to the other electrolytes.

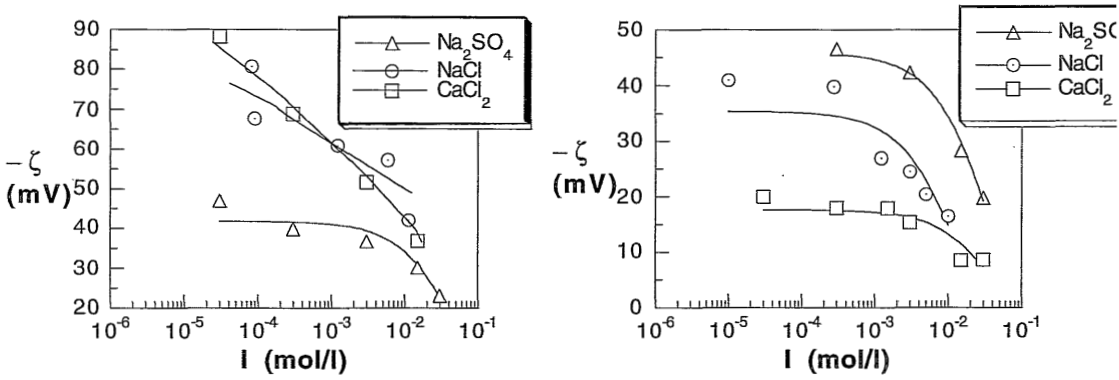

Figure 5.8: *Zeta potentials for a ASP35 (a) and a NF45 membrane (b) measured with different electrolyte solutions at various concentrations*

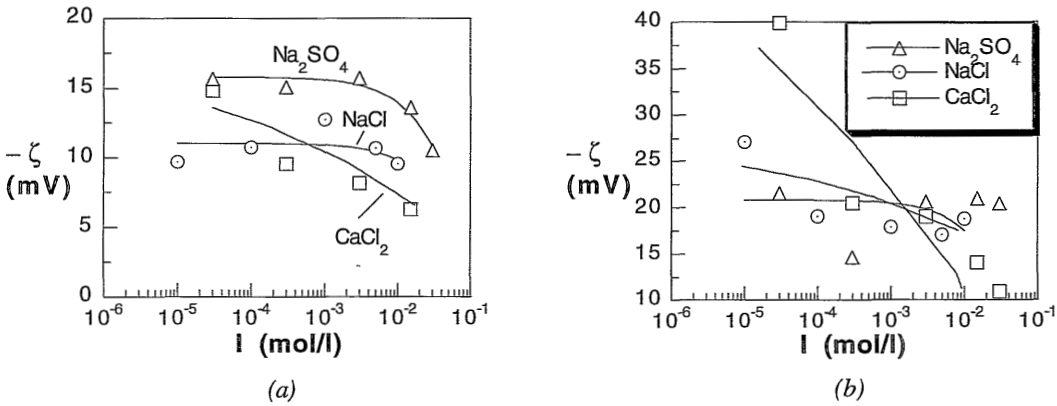

Figure 5.9: *Zeta potentials for a CTA-LP (a) and a UTC90 membrane (b) measured with different electrolyte solutions at various concentrations*

The interpretation of the zeta potentials measured along the membrane surfaces may have been complicated by the swelling behavior of the membrane toplayer as well. This effect may influence the decrease of the electrical potential in another way than the kinetic effects that play a role, like the position of the shear plane. Differences in swelling may be accomplished by different types of electrolytes and by different concentrations. A highly swollen toplayer can, for instance, contain more ions than a slightly swollen layer, which may result in a steeper

potential decline within the swollen layer for the former case. Since the shear plane will be located at more or less the same distance from the outer surface for both layers, the zeta potential will be smaller for the highest swollen toplayer. In literature this was observed for dialysis membranes, for which the membranes with the highest degree of hydrophylicity, i.e., the highest swelling, showed the lowest zeta potential [18].

The kinetic surface charge densities calculated from the streaming potential measurements by equations {5.7} and {5.10} are shown in Figure 5.10. For the various electrolytes a comparison is made between the different polymeric membranes. As can be seen from this figure, the kinetic surface charge densities of the membranes increased with increasing electrolyte concentration. The surface charge density of the ASP35 membrane was the highest, whereas the surface charge densities of the other three membranes were much lower, with CTA-LP being the lowest. The difference between the membranes was most distinct at high electrolyte concentrations.

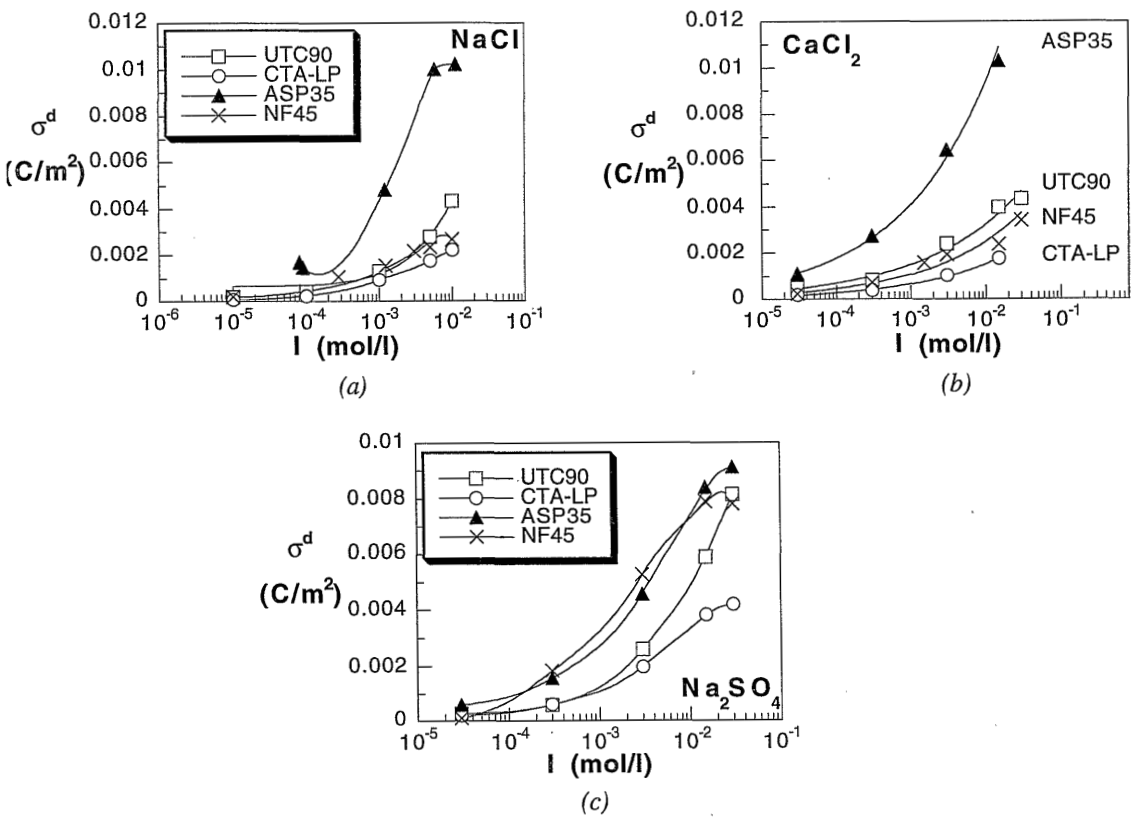

Figure 5.10: *Kinetic charge density for different polymeric nanofiltration membranes measured with different electrolyte solutions at various concentrations. (a) NaCl, (b) $CaCl_2$, (c) Na_2SO_4*

The surface charge densities measured with NaCl (Figure 5.10 (a)) were almost identical to the kinetic surface charge densities measured with $CaCl_2$.The surface charge densities measured with Na_2SO_4 were very similar for the ASP35 and the NF45 membrane. The surface charge density of the UTC90 membrane strongly increased at ionic strengths higher than 3 mM. Again, the CTA-LP membrane showed the lowest kinetic surface charge density.
When comparing the kinetic surface charge densities shown in Figure 5.10 for the various electrolytes at the same ionic strength, the surface charge densities determined with sodium sulfate were higher than those with the chloride solutions for all polymeric membranes except for the ASP35 membrane. Most probably, this is caused by differences in interaction between the membrane material and the sodium sulfate and the chloride solutions. Later in this chapter, the differences between the kinetic charge densities determined with the various electrolytes will be discussed in more detail.
As shown in Figure 5.10, the kinetic surface charge density became higher with increasing electrolyte concentration. Since the extent of this surface charge density increased, consequently, the sum of the surface charge density of the membrane and that of the Stern plane should become more negative, to obey the electroneutrality condition of the system (equation {5.4}). Since the membrane charge density is assumed to be constant, the Stern surface will become more negative with increasing electrolyte concentration, which may be caused by the adsorption of anions [12,18,23,24].
To describe the adsorption of ions at the Stern plane, adsorption isotherms can be used, by which the number of adsorbed ions can be determined. For this purpose, the Freundlich adsorption isotherm can be applied, which describes adsorption at heterogeneous surfaces like those of membranes, i.e., which have different regions at the membrane surfaces with different adsorption energies. It is an empirical isotherm that relates the surface charge density and the concentration of adsorbed ions with a power law [9]:

$$\sigma^S (c_-) = a\, c_-^b \qquad \{5.11\}$$

with a and b being constants and c_- the concentration of anions in solution. Although the Freundlich isotherm is an empirical relation, several authors have tried to correlate the constants a and b to parameters like the number of adsorption sites at the membrane surface and the mean Gibbs' free energy of adsorption [7,9,25].

The total charge density at the membrane surface, the Stern plane and the shear plane can be obtained by combination of equations {5.4}, {5.11} and {5.7} for a mono-mono-valent electrolyte solution and {5.4}, {5.11} and {5.10} for an asymmetric electrolyte solution, respectively:

electrolyte solution containing mono-mono-valent salt:

$$\sigma^0 + a\, c_-^b - \varepsilon \kappa \zeta \frac{\sinh \left(\frac{F}{2RT} \zeta \right)}{\frac{F}{2RT} \zeta} = 0 \qquad \{5.12\}$$

electrolyte solution containing ions with different valencies:

$$\sigma^0 + a\, c_-^b - (\operatorname{sign}\zeta)\sqrt{2\varepsilon c R T}\sqrt{\nu_+ \exp\left(-\frac{z_+ F}{R T}\zeta\right) + \nu_- \exp\left(-\frac{z_- F}{R T}\zeta\right) - \nu_+ - \nu_-} = 0 \qquad \{5.13\}$$

In the derivation of these equations, the difference between the Stern plane and the shear plane is not accounted for. It might be possible to obtain an expression for the surface charge density of the layer in between these two planes by the division of the Stern layer in an inner and out Helmholtz plane, but this would complicate the calculations in a tremendous way [26]. Furthermore, it should be realized that the membrane surface charge is assumed to be constant. This assumption will be discussed later in this chapter.

To discriminate between the actual charge of the membrane and the adsorbed charges, equations {5.12} and {5.13} were fitted to the experimental data, assuming the kinetic surface charge as the sum of the membrane surface charge and the adsorbed charge according to the Freundlich isotherm. As an example Figure 5.11 shows the kinetic charge density of a ASP35 membrane as a function of the anion concentration for a NaCl, a Na_2SO_4 and a $CaCl_2$ solution. The solid line within this figure is drawn according to equation {5.4} in combination with equation {5.11}. It was possible to fit the kinetic surface charge densities to the anion concentrations for all combinations of membranes and electrolytes in the same way as shown in Figure 5.11, except for the Na_2SO_4 solution in case of the NF45 membrane.

For the ASP35 membrane, the various electrolytes showed the same kinetic charge density at a certain anion concentration. The other three membranes showed a difference between the relation of the kinetic charge density and the anion concentration for the chloride and the sulfate solutions, indicating different adsorption characteristics of both anions. The relation between the charge density and the anion concentration was equal for both sodium and calcium chloride solutions. Since the anion for both electrolytes is chloride, this is in accordance with the observation that adsorbing anions within the Stern layer cause the increase in the kinetic surface charge density.

Table 5.2 summarizes the results of the fitting of the three parameter model, according to equation {5.12} and {5.13}. The surface charge densities calculated for the membrane surfaces are in the range of $-7.0*10^{-4}$ to $8.9*10^{-5}$ A.s/m^2, which are small compared to the values of the determined kinetic charge densities as shown in Figure 5.10. Since the fitted values of the membrane surface charge densities are small and dependent on the types of electrolyte used, no conclusions will be drawn from these data. It can be concluded that in case of a constant membrane surface charge density, the kinetic surface charge density of the membrane increases because of the adsorption of anions in the Stern layer.

When comparing the results for the adsorption of chloride and sulfate, the values of parameter a were higher for sulfate adsorption in case of the CTA-LP and the UTC90 membrane, whereas for the ASP35 membrane, this parameter was equal for the adsorbing anions.

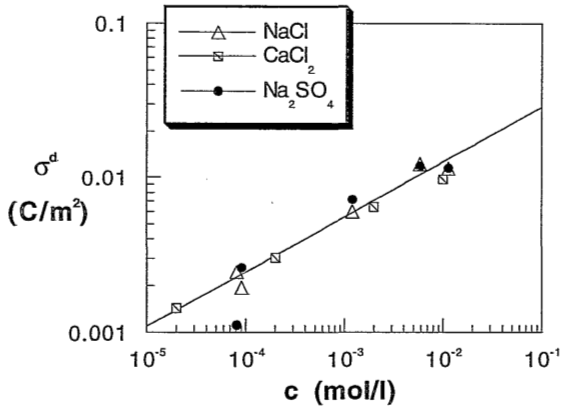

Figure 5.11: *Kinetic surface charge density of a ASP35 membrane as a function of the anion concentration in case of different electrolyte solutions. The line is fitted according to equations {5.12} and {5.13}*

Table 5.2: *Parameters a and b and the membrane surface charge density, σ_0, for different nanofiltration membranes calculated from equations {5.12}/{5.13}*

	σ_0 (C/m^2)	- a (*10^{-3}A.s.m/mol)	b (-)
membrane: **ASP35**			
$NaCl/CaCl_2/Na_2SO_4$	$-3*10^{-5}$	0.066	0.36
membrane: **NF45**			
$NaCl/CaCl_2$	$-4*10^{-4}$	0.015	0.37
membrane: **CTA-LP**			
$NaCl/CaCl_2$	$7*10^{-5}$	0.024	0.50
Na_2SO_4	$-5.0*10^{-5}$	0.040	0.45
membrane: **UTC90**			
$NaCl/CaCl_2$	$-4*10^{-5}$	0.022	0.40
Na_2SO_4	$8.9*10^{-5}$	0.104	0.52

According to Calvo and Benavente the ratio between parameter a and the valence of the anion can be linearly related to the amount of adsorption sites present at the membrane surface [25], [9]. In that case, the amount of adsorption sites of the CTA-LP membrane is equal for chloride and sulfate ions, while for the ASP35 membrane the amount of adsorption sites for the sulfate ions is half that for the chloride ions. In the former case, a sulfate ion might occupy one adsorption site, like a chloride ion, whereas in latter case, the sulfate ion occupies two adsorption sites, where the chloride ion needs only one. The energetically most favorable configuration will depend on the membrane material. In case of the UTC90 membrane, the amount of adsorption sites is higher for the sulfate ions than for the chloride ions. It is not clear yet how this might be explained on a microscopic level.
Following the approach of Calvo, the parameter b is inversely proportional to the mean Gibbs' free energy of adsorption, which is negative for all cases calculated in this chapter [9,25]. As can be seen the differences between the parameters b determined for chloride and sulfate adsorption are not very high in case of the ASP35 and CTA-LP membrane, which are the membranes showing the highest and the lowest kinetic charge density, respectively. This indicates the importance of the amount of adsorption sites for the adsorption isotherm.
Comparing the chloride adsorption for the different membranes, it can be seen that for the ASP35 membrane both the high amount of adsorption sites, related to a high value of parameter a, and the high negative value of the mean free energy of adsorption, related to a small value of b, resulted in high kinetic surface charge densities. The main difference between the NF45 and the ASP35 membrane was the smaller amount of adsorption sites for the former, whereas the CTA-LP and UTC90 membrane showed both less adsorption sites and smaller negative adsorption energies, which lead to less ionic adsorption.
The interpretation of the constants a and b from the Freundlich isotherm in terms of adsorption sites and adsorption energy, like shown in the previous section, should only be done with great care. Although this interpretation relates the constants of the power law with physical parameters, the empirical basis of the Freundlich isotherm should always be considered.

The main assumption to interpret the increase of the kinetic surface charge density in terms of electrolyte adsorption is that the increase is only caused by the increasing amount of adsorbed charge, whereas the membrane surface charge is assumed to be constant as a function of the electrolyte concentration. Following this approach, the influence of the dissociation rate of the acidic groups in the membrane is neglected. It is, for instance, known that the pK_a values of the ionizable groups of polyelectrolytes can change with ionic strength [27,28]. Marinsky showed that the pK_a values of polyacrylic acid changed drastically when changing the electrolyte concentration [27].
No experiments have been carried out to check the hypothesis that for the membranes used the dissociation constant of the acidic groups is not influenced by the ionic strength. Most probably, in case of the sulfonic acid groups, the dissociation rate will be independent of the ionic strength. However, if carboxylic groups are present, like in case of the interfacially polymerized polyamides, then the pK_a value may range roughly from 4.5 to 7, i.e., from completely dissociated to almost fully undissociated.
However, no conclusions can be drawn concerning the influence of the acidic groups with

respect to the charge density. Depending on the kind of ionizable groups present at the membrane surface and on the mean Gibbs' free energy of adsorption, the kinetic surface charge density will probably be influenced by either the dissociation rate of the charged groups or by the adsorption of ions at the surface or by a combination of each.

The large differences between the values of the formal surface charge densities determined by the titrations and the kinetic surface charge densities of the streaming potentials measurements may result from the fact that titration is a bulk technique, whereas in case of the streaming potential measurements the surface characteristics (and in fact the characteristics of the shear plane) are determined, which depend on the membrane material and the ions used [29]. Because in case of titration all charged groups present in the sample are attributed to the surface, the formal surface charge density will always be higher the value obtained from the streaming potential measurements when only the charges present at the surface are measured. Furthermore, the bulk properties of membranes can be considerably different from those at the surface as shown by Takagaki and co-workers [30].
When calculating the kinetic surface charge density by equation {5.6} and {5.9}, one of the main assumptions is that the Stern plane equals the shear plane. However, the shear plane may be located at a distance further away from the surface than the Stern plane. Then, the charge of the diffuse part of the double layer which is in between the Stern and the shear plane is not accounted for. This results in an underestimation of the sum of the surface charge density of the membrane surface and that of the Stern layer, explaining partly the lower membrane surface charge density determined with the streaming potential measurements.

5.5 CONCLUSIONS

The streaming potential measurements showed that both streaming and zeta potentials decreased with increasing salt concentration. For all polymeric membranes the zeta potential determined was negative, whereas for the ceramic membrane a positive value was found.
The zeta potentials measured with different electrolytes of the same ionic strength were almost identical for the CTA-LP membrane and for the UTC90 membrane as well. The interpretation of zeta potential data was complicated by the influence the swelling behavior of the membrane may have.
The surface charge densities were the highest for the ASP35 membrane and the lowest for the CTA-LP membrane. Furthermore, for all membranes both chloride solutions gave comparable results for the kinetic surface charge densities, whereas the surface charge density determined with sodium sulfate was remarkably higher than that with the chloride solutions for all membranes except the ASP35 membrane.
Assuming the kinetic surface charge to be equal to a constant membrane surface charge density and a surface charge density of the Stern layer that could be described by a Freundlich isotherm, the calculated surface charge density at the membrane surfaces investigated was small and especially at higher electrolyte concentrations it was negligible compared to the adsorbed

charges. Anion adsorption seemed to be the major contribution to the surface charge density. (In almost all cases anion adsorption could be described with a Freundlich adsorption isotherm.) Titration showed that the membrane space charge density was small, in the order of 10 to 100 times smaller than the values reported in literature for charged ultrafiltration and reverse osmosis membranes.

ACKNOWLEDGEMENTS

Bert Damink is acknowledged for his experimental work on the streaming potential measurements and for our fruitful discussions, Maikel van Bree and José Nolten for their experimental work. Simona Mesaric is acknowledged for starting up the streaming potential measurements and for her preliminary experimental work, Peter Paauw for his preliminary experiments. Dr. Ab van der Linde (LUW) is acknowledged for the help concerning the experimental procedures for the streaming potential measurements and Marcel Minor (LUW) for the discussion on the theoretical interpretation. In this Dr. Thonie van den Boomgaard was also very helpful.
Wim Lengton (Analytical Department) is acknowledged for the titration of the membranes.

SYMBOLS

a:	constant	(A.s.m/mol)
b:	constant	(-)
c:	concentration	(mol/l)
E:	potential	(V)
F:	Faraday constant	(A.s/mol)
I:	ionic strength	(mol/l)
I:	current	(A)
P:	pressure	(N/m^2, bar)
Q:	charge	(A.s)
r:	radius, half width	(m)
R:	gas constant	(J/K.mol)
R:	resistance	(Ω)
T:	temperature	(K)
x:	coordinate normal to surface	(m)
z:	valency	(-)
ε:	dielectric constant	(A.s/V.m)
ζ:	zeta potential	(V)
η:	viscosity	(Pa.s)
κ^{-1}:	Debije length	(m)
λ:	conductivity	(Ω^{-1}/m)
ν:	stoichiometric number	(-)
ρ:	space charge density	($A.s/m^3$)

σ:	charge density	($A.s/m^2$)
ψ:	potential	(V)

subscripts:

d:	diffuse
exp:	experimental
L:	leak
s:	surface
s, str:	streaming
S:	Stern
th:	theoretical
-:	anion
+:	cation
0:	bulk

superscripts:

0:	at membrane surface
d:	diffuse
S:	Stern

REFERENCES

[1] Jitsuhara, I., Kimura, S., *Rejection of inorganic salts by charged ultrafiltration membranes made of sulfonated polysulfone*, J. Chem. Eng. Jap., 16 (1983) 394

[2] Tsuru, T., Nakao, S.I., Kimura, S., *Effective charge density and pore structure of charged ultrafiltration membranes*, J. Chem. Eng. Jap., 23 (1990) 604

[3] Wang, X.-L., Tsuru, T., Togoh, M., Nakao, S.I., Kimura, S., *Evaluation of pore structure and electrical properties of nanofiltration membranes*, J. Chem. Eng. Jap., 28 (1995) 186-192

[4] Kimura, Y., Lim, H.-J., Iijima, T., *Membrane potentials of charged cellulosic membranes*, J. Membrane Sci., 18 (1984) 285-296

[5] Takagi, R., Nakagaki, M., *Membrane potential of separation membranes as affected by ion adsorption*, J. Membrane Sci., 71 (1992) 189

[6] Benavente, J., Jonsson, G., *Transport of Na_2SO_4 and $MgSO_4$ solutions through a composite membrane*, J. Membrane Sci., 80 (1993) 275

[7] Hernández-Gimenez, A., Martínez, L., Gomez, M.V., *Concentration dependence of the adsorbed charges and the zeta potentials on the walls of neutral and charged microporous membranes*, J. Coll. Int. Sci., 158 (1993) 429

[8] Hernández, A., Martínez, F, Martin, A., Prádanos, P., *Porous structure and surface charge density on the walls of microporous alumina membranes*, J. Coll. Int. Sci., 173 (1995) 284-296

[9] Benavente, J., Hernández, A., Jonsson, G., *Proper and adsorbed charges on the surfaces of the polysulfonic support of a composite membrane from electrokinetic phenomena*, J. Membrane Sci., 80 (1993) 285

[10] Alami-Younssi, S., Larbot, A., Persin, M., Sarrazin, J., Cot, L., *Rejection of mineral salts on a gamma alumina nanofiltration membrane. Application to environmental process*, J. Membrane Sci., 102 (1995) 123-129

[11] Lyklema, J., Fundamentals of Interface and Colloid Science, Vol. II: Solid-fluid interfaces, Academic Press, London, 1995

[12] Elimelech, M., Chen, W.H., Waypa, J.J., *Measuring the zeta (electrokinetic) potential of reverse osmosis membranes by a streaming potential analyzer*, Desalination, 95 (1994) 269

[13] Hunter, R. J., Zeta potential in colloid science. Principles and applications, Academic Press, London, 1981

[14] Nyström, M., Lindström, M., Matthiasson, E., *Streaming potential as a tool in the characterization of ultrafiltration membranes*, Colloids and Surfaces A, 36 (1989) 297-312

[15] Nyström, M., Pihlajamäki, A., Ehsani, N., *Characterization of ultrafiltration membranes by simultaneous streaming potential measurements and flux measurements*, J. Membrane Sci., 87 (1994) 245

[16] Causserand, C., Nyström, M., Aimar, P., *Study of streaming potentials of clean and fouled ultrafiltration membranes*, J. Membrane Sci., 88 (1994) 211

[17] Jacobasch, H.-J., Schurz, J., *Characterization of polymer surfaces by means of electrokinetic measurements*, Prog. Coll. Pol. Sci., 77 (1988) 40-48

[18] Werner, C., Jacobasch, H.-J., Reichelt, G., *Surface characterization of hemodialysis membranes based on streaming potential measurements*, J. Biomats. Sci., Polymer ed., 7 (1995) 61-76

[19] Wagenen, R. A., van, Andrade, J.D., *Flat plate streaming potential investigations: hydrodynamics and electrokinetic theory*, J. Coll. Int. Sci., 76 (1980) 305

[20] Ikeda, K., Nakano, T., Ito, H., Kubota, T.,Yamamoto, S., *New composite charged reverse osmosis membrane*, Desalination, 68 (1988) 109

[21] Sata, T., *Modification of ion exchange membranes*, J. Coll. Int. Sci., 44 (1973) 393-406

[22] Wagenen, R. A., van, D.L. Coleman, King, R.N., Triolo, P., Brostrom, L., Smith, L.M., Gregonis, D.E., Andrade, J.D., *Streaming potential investigations: polymer thin films*, J. Coll. Int. Sci., 84 (1981) 155

[23] Bowen, W. R., Mukthar, H., *Characterisation and prediction of separation performance of nanofiltration membranes*, J. Membrane Sci., 112 (1996) 263-274

[24] Takagi, R., Kashima, S., Gotoh, K., Tagawa, M., Nakagaki, M., *Adsorption of halogen ion on cellulose acetate membrane determined by membrane potential*, ICOM '96, Yokohama, Japan, 1996, p. 189

[25] Calvo, J. I., Hernández, A., Prádanos, P., Tejerina, F., *Charge adsorption and zeta potential in Cyclopore membranes*, J. Coll. Int. Sci., 181 (1996) 399-412

[26] Börner, M., Jacobasch, H.-J., Simon, F., Churaev, N.V., Sergeeva, I.P., Sobolev, V.D., *Zeta potential measurements with fibre plugs in 1:1 electrolyte solutions*, Colloids and Surfaces A, 85 (1994) 9-17

[27] Marinsky, J. A., *A Gibbs-Donnan-based interpretation of the sensitivity of the measurable acid dissociation properties of poly(acrylic acid) to concentration levels of salt and polyelectrolyte*, J. Phys. Chem., 96 (1992) 6484-6487

[28] Bloomfield, V., Carpenter, I.L., *Biological polyelectrolytes*, in: Polyelectrolytes, ed. by M. Hara, Marcel Dekker, New York, 1993

[29] Howell, J. A., Nyström, M., *Fouling phenomena*, in: Membrane processes in bioprocessing. Theory and applications, ed. by J.A. Howell Sanchez, V., Field, R.W., Blackie Academic & Professional, London, 1993, p. 203-241

[30] Takagi, R., Tagawa, M., Gotoh, K., Nakagaki, M., *Variation of membrane charge of Nylon 6 with pH*, J. Membrane Sci., 92 (1994) 229-238

CHAPTER 6

Retention measurements: comparison of theory and experiments

ABSTRACT

The theoretical description of the transport of both saccharides and ions through nanofiltration membranes is compared with experimental data.

Saccharide retentions can be described well by phenomenological flux equations for a solution consisting of a solvent and a solute, resulting in a specific permeability and reflection coefficient for each combination of membrane and saccharide.

The extended Nernst-Planck equation in combination with the Donnan equilibrium has been used to model the flux-retention experiments for the salt solutions. The numerical calculations resulted in a good agreement between theory and experimental data and acceptable values for the fixed charge densities have been determined. The effective membrane thicknesses calculated were higher than those observed by Scanning Electron Microscopy. The occurrence of negative retentions of the chloride ions in a chloride/sulfate mixture was described adequately by the model. The negative retentions of sodium ions in a sodium/calcium mixture could not be described appropriately.

6.1 INTRODUCTION

The experimental results of retention measurements with salt solutions, saccharides and dendrimers were discussed in Chapter 3 and 4. In this chapter the results of the phenomenological models as described in Chapter 2 will be compared to the experimental retention data. In the case of the dendrimers both size and actual charge are not well defined and, therefore, the theoretical interpretation of the retention data will be restricted to the saccharide and the salt retention experiments.
Firstly, the theoretical predictions and the experimental results for the retention measurements with the saccharides will be presented and, secondly, the comparison for retention measurements with the salt solutions will be shown.

6.2 EXPERIMENTAL

The retention measurements which will be discussed here were carried out with saccharide and electrolyte solutions. The retention measurements were carried out in a stirred cell, whereas the hydrostatic pressure difference applied was in the range of 3 to 7 bar. Ultrapure water was used as solvent.
In case of the saccharide solutions, glucose, sucrose and raffinose (Merck, p.a) were used with a concentration of 1 or 2 g/l.
The electrolyte retention measurements were carried out with NaCl, $CaCl_2$, Na_2SO_4 and with mixtures of NaCl/$CaCl_2$ and NaCl/ Na_2SO_4. The concentrations used were 0.001, 0.005 and 0.01M.
The membranes used for the saccharide retention measurements were the CTA-LP (Fluid Systems), ASP35 (Advanced Membrane Technology), NF45 (FlmTec), UTC90 (Toray) and CA30 (Hoechst Celanese) membrane, those for the electrolyte retention measurements CTA-LP, ASP35, NF45, UTC90 and UTC70 membranes (Toray) and a ceramic γ-Al_2O_3 membrane.

6.3 RESULTS

6.3.1 Saccharide retention measurements

The experimental data for the flux-dependent retention measurements with saccharide solutions were fitted with equation {4.4} to obtain values for the reflection, σ, and solute permeability coefficient, L:

$$R = \frac{\sigma (1 - e^{Pe})}{1 - \sigma e^{Pe}} \qquad \{6.1\}$$

with $Pe = - J_v \frac{(1 - \sigma)}{L}$, and with R being the retention, σ the reflection coefficient, Pe the Péclet number and J_v the solvent flux.

The experimental data for a CA30 membrane are shown in Figure 6.1, whereas the corresponding theoretical data are represented by the curves in this figure. As can be seen from this figure, a good agreement was found between the experimental data and the theoretical retention data as predicted by the phenomenological equations.

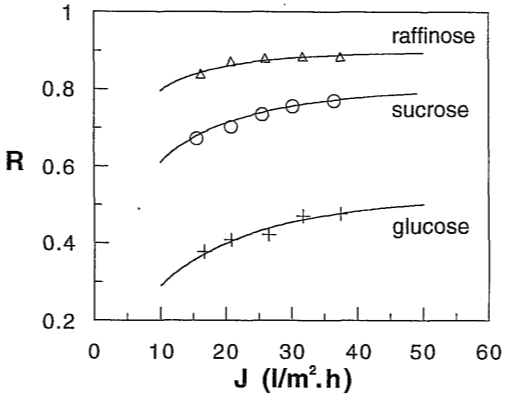

Figure 6.1: *Saccharide retention as a function of the solvent flux for CA30 membrane (Δ, O, +: experimental data; solid line: theoretical fit)*

The flux-dependent saccharide retention measurements were carried out with the membranes CTA-LP, ASP35, NF45, UTC90 and CA30. For all membranes the reflection coefficient increased in the following sequence: σ (glucose) < σ (sucrose) < σ (raffinose), whereas the solute permeability coefficient decreased: L (glucose) > L (sucrose) > L (raffinose). The mean values of these parameters are shown in Table 6.1. In case of the ASP35 membrane the retention data were too scattered to be interpreted. The reason for these scattered results is still unclear.

Table 6.1: *Reflection and solute permeability coefficients determined for several saccharides for different nanofiltration membranes*

	CTA-LP		NF45		UTC90		CA30	
	σ (-)	L (m/s)	σ (-)	L (m/s)	σ (-)	L (m/s)	σ (-)	L (m/s)
glucose	0.892	4.35e-7	0.881	5.53e-7	0.936	4.99e-8	0.548	3.18e-6
sucrose	0.981	1.05e-7	0.984	1.71e-7	0.994	2.22e-8	0.799	1.22e-6
raffinose	0.992	2.85e-8	0.984	1.02e-8	0.957	2.72e-9	0.883	4.56e-7

The differences between the membranes based on glucose retentions are illustrated in Figure 6.2. The lower retention for the saccharides for the CA30 membrane is caused both by a low reflection coefficient and a high permeability coefficient. In case of the UTC90 membrane, the high retention is affected by a high reflection coefficient and a low solute permeability. The differences between the CTA-LP and the NF45 membrane are only small.

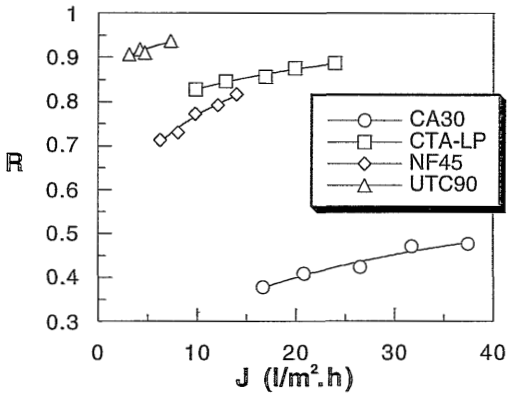

Figure 6.2: Glucose retention as a function of the solvent flux for different nanofiltration membranes (□, ◇, Δ, O: experimental data; solid line: theoretical fit)

The reflection and solute permeability coefficient were related to the ratio of solute radius and pore radius which was used in the steric hindrance model, according to equations {2.29} and {2.30}. A combination of these equations results in a membrane pore radius. By a combination of the equations {2.27}, {2.29} and {2.30}, the retention, R, can be described as:

$$R = \frac{(1 - e^{Pe})(1 - g(\lambda) S_F)}{1 - (1 - g(\lambda) S_F) e^{Pe}} \qquad \{6.2\}$$

with

$$Pe = - \frac{g(\lambda) S_F}{f(\lambda) S_D D (\varepsilon / \Delta x)} J_v \qquad \{6.3\}$$

and with $f(\lambda)$ and $g(\lambda)$ being the wall correction factors for diffusive and convective transport respectively, S_D and S_F the steric hindrance factors for diffusive and convective transport, $\lambda = r_s / r_p$ with r_s the radius of the solute and r_p the radius of the pore, p the porosity and Δx the membrane thickness. The ratio of the porosity and the membrane thickness, $p/\Delta x$, was determined by solvent permeability measurements:

$$\frac{p}{\Delta x} = J_v \frac{8 \tau \eta}{r_p^2 \Delta P} \qquad \{6.4\}$$

with τ being the tortuosity of the membrane, which was assumed to equal unity, and η the viscosity of the solvent.

Since the relations for the wall correction and steric hindrance factors (equations {2.1}, {2.2}, {2.3} and {2.6}) are valid for $\lambda < 0.8$, it was tried to fit only the data of the CA30 membrane to the equations {6.2} and {6.3}. By minimizing the difference between the theoretical and the experimental retention values, a value of 0.723 nm for the pore size of the CA30 membrane was found. Except for determining one common pore size for all saccharides, it was also tried to find the best pore radius for each of the saccharides.

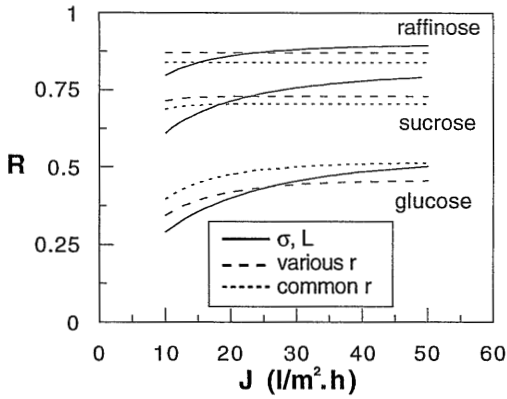

Figure 6.3: *Theoretical saccharide retentions as a function of the solvent flux for CA30 membrane*

However, as can be seen from the combinations of the Figures 6.2 and 6.3, neither the fitting of the flux-retention data with only one value of the pore radius, nor with various values of the pore size for the different saccharides resulted in a good correlation between the retentions calculated with this model and the experimental data. The solid lines in this figure are those which have been calculated with the reflection and permeability coefficients according to equation {6.1} and which showed a good agreement with the experimental data as illustrated by Figure 6.1. The curves with the small dashes are calculated with a common pore radius and those with the larger dashes are calculated with a specific pore radius for each saccharide. As can be seen from Figures 6.2 and 6.3, the agreement between the experimental results and the theoretical predictions according to equations {6.2} and {6.3} was poor, for both a common or a variable pore radius. This may result from the invalidity of the equations for the wall hindrance factors and wall friction factors which were derived for systems consisting of much larger pores and much larger solutes compared to the system investigated here [1]. Furthermore, the validity of the pore concept in this approach can be questioned.

6.3.2 Electrolyte retention measurements

Single salt solutions

The diffusion coefficients of the ions, the sign of the fixed charge density of the membrane, the permeate concentration of the ions and the solvent flux were input parameters used for the calculations by the set of equations {2.30} to {2.37}, which will be shown in this chapter. These calculations resulted for a certain membrane-electrolyte solution system in a corresponding membrane charge, a membrane thickness, a concentration profile within the membrane, an electrical gradient and in two Donnan potentials at either side of the membrane. An example of the concentration gradients of the sodium and chloride ions in a negatively charged nanofiltration membrane is shown in Figure 6.4. These profiles were calculated by the extended Nernst-Planck equation as presented in Chapter 2. The membrane has a fixed charge density of 5.4 $*10^{-2}$ mol/l, whereas the electrolyte feed concentration is 1.53 $*10^{-3}$ mol/l. The concentrations within the membrane are shown on a logarithmic scale. The concentration of the co-ion within the membrane is very small, whereas that of the counter-ion nearly equals the membrane fixed charge concentration. The decrease of the sodium concentration across the membrane cannot be observed on the logarithmic scale used in this figure. The distribution of ions between membrane and solution were calculated with the equation for the Donnan equilibrium (equation 2.37).

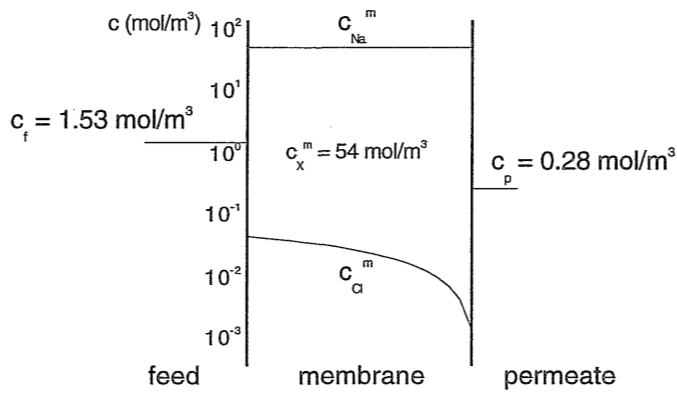

Figure 6.4: *Concentration gradients of Cl^- and Na^+ in a negatively charged membrane with a fixed charge of 0.054 mol/l.*

To calculate the theoretical curves, the chemical diffusion coefficients of the sodium and chloride ions were assumed to be $0.84*10^{-9}$ and $1.503*10^{-9}$ m^2/s, respectively. An overview of the diffusion coefficients of each of the ions is shown in Table 6.2. These, effective, diffusion coefficients, $D_{eff,\,i}$, for the components i were calculated by multiplying the bulk diffusion coefficients of the ions, $D_{bulk,\,i}$, by the diffusive steric hindrance factors, $K_{i,d}$, which were found in literature [2]:

$$D_{eff,\,i} = K_{i,d}\, D_{bulk,\,i} \qquad \{6.5\}$$

The steric hindrance factor for diffusion was assumed to be equal to that in a pore with a radius of 1 nm.

Table 6.2: *Ionic diffusion and diffusive hindrance coefficients used in the numerical calculations*

	$D_{bulk,i}$ (10^{-9} m^2/s)	$K_{i,d}$ (-)	$D_{eff,\,i}$ (10^{-9} m^2/s)
Na^+	1.33	0.633	0.84
Cl^-	2.03	0.740	1.50
Ca^{2+}	0.92	0.543	0.50
SO_4^{2-}	1.06	0.553	0.59

The experimental and theoretical retentions of a 0.001M NaCl solution are shown in Figure 6.5 as a function of the solvent flux for four nanofiltration membranes. The curves represent the calculated values while the points are the experimental values. For all membranes the experiments have been performed at the same hydrostatic pressures. The highest solvent flux was achieved at a pressure difference of 7 bar.

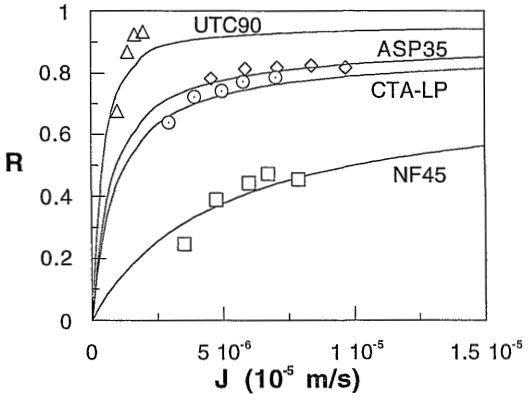

Figure 6.5: *Experimental and theoretical values for retention of a 0.001M NaCl solution as a function of the solvent flux. Theoretical curves (solid lines) have been calculated by equations {2.30} to {2.37}*

The values of the membrane charge and membrane thickness determined by equations {2.30} to {2.37} for six membranes for an 0.001M NaCl solution are shown in Table 6.3. The calculations were carried out assuming a negative membrane charge for the polymeric membranes and a positive charge for the ceramic membrane. It should be realized that the values determined for the membrane thicknesses and charges are effective parameters.

When the calculated membrane charge density and thickness from this table are compared with the resulting retentions as shown in Figure 6.5, it can be seen that both the smaller membrane thickness and the lower membrane charge contribute in case of the NF45 membrane to the lower NaCl retention. The high retention of the UTC90 membrane is mainly due to the high membrane charge.

Table 6.3: *Calculated membrane thickness and membrane charge for different nanofiltration membranes in case of 0.001M NaCl solution*

membrane	Δx (10^{-5} m)	c_X^m (mol/l)
ASP35	3.26	- 0.054
NF45	1.47	- 0.020
CTA-LP	3.60	- 0.034
UTC90	4.12	- 0.215
UTC70	11.2	- 0.088
γ-Al_2O_3	5.78	+ 0.025

The calculated membrane thickness and charge depend on the diffusion coefficients of the ions used. For the calculated retentions it was assumed that the diffusion coefficients of the sodium and chloride ion were equal in all membranes.
The membrane thicknesses calculated can be compared to the membrane thicknesses which were observed by Scanning Electron Microscopy (SEM). Because the NF45, UTC90, UTC70 and γ-Al_2O_3 membrane are composite membranes, the thickness of the toplayer of these membranes can be determined relatively easily. According to the SEM measurements, the toplayer thicknesses of these membranes are 0.35, 1.2, 4.8 and 8 μm, respectively. These values are much smaller than the membrane thicknesses calculated. This difference in membrane thickness may result from the fact that the calculated thickness is an effective parameter, which comprises different factors for the resistance of solute transport, like for instance the resistance of the support layer and the membrane tortuosity. Furthermore, the choice of the diffusion coefficient of the ions will influence the calculated membrane thickness as well. The ASP35 and CTA-LP membrane were not considered because it was difficult to determine the thickness of the active layer of these asymmetric membranes.

The influence of the diffusion coefficients on the calculated membrane thickness and charge is shown in Table 6.4, for a NF45 membrane and a 0.001M NaCl solution. The thickness and the charge of the membrane were calculated for diffusion coefficients of the chloride and sodium ion which were both 10% higher and 10% lower than their original values. As can be seen, a lower diffusion coefficient causes a lower calculated membrane charge and a higher membrane thickness.
When interpreting the membrane charges and thicknesses calculated by the model, this influence of the diffusion coefficients on these parameters should be considered. For instance,

in case of the UTC90 membrane, it might be that the value of the membrane charge is affected by the ionic diffusion coefficients. Since this membrane is tighter than the other membranes investigated, as can be concluded from Figure 6.5, the hindrance of diffusion may be higher and, therefore, the effective diffusion coefficient smaller. Then, consequently, the membrane charge will be lower as well.

Table 6.4: *Influence of the diffusion coefficients of the ions on the calculated membrane thickness and membrane charge for NF45 membrane*

D	Δx (10^{-5} m)	c_X^m (mol/l)
D	1.5	0.020
1.1* D	1.0	0.031
0.9* D	2.3	0.012

The calculated retention curves for NaCl solutions with different feed concentrations and a CTA-LP membrane are shown in Figure 6.6. Both the membrane charge and membrane thickness resulting from these calculations increased with increasing electrolyte concentration. The same behavior was observed for other combinations of membrane-electrolyte solution. The increase in the membrane charge with increasing electrolyte concentration seems to be analogous to the increase in the kinetic surface charge density with increasing salt concentration which was found by the streaming potential measurements shown in Chapter 5, although in that case surface charge densities were determined and in this case space charge densities. In literature, this phenomenon has been observed by several authors (e.g., [2,3]). However, it is not clear how the ionic concentration could influence the membrane thickness, so this is just a result of the fitting procedure. To improve the insight in the calculation procedure, the calculations of the membrane thickness and membrane charge were then performed in two stages. Firstly, for a certain electrolyte concentration the membrane charge and membrane thickness were determined. Secondly, the mean value of the membrane thickness was calculated for a specific electrolyte in case of different concentrations and the corresponding membrane charges were determined. The curves calculated with a fixed value of the membrane thickness and a variable value of the membrane charge at different NaCl concentrations are shown in Figure 6.6 as well, showing reasonable agreement with the experimentally determined values. The mean effective membrane thickness for the CTA-LP membrane was found to be $5.47*10^{-5}$ m, whereas the negative membrane charge varied from 0.026 to 0.099 mol/l with increasing electrolyte concentration.
Since the CTA-LP membrane has an asymmetric structure, most probably the properties of this membrane, like the charge density, are functions of the membrane cross-section. Therefore, the calculated parameters should be considered as effective values, which can be assigned to membrane with a symmetric structure and a homogeneously distributed membrane space charge density.

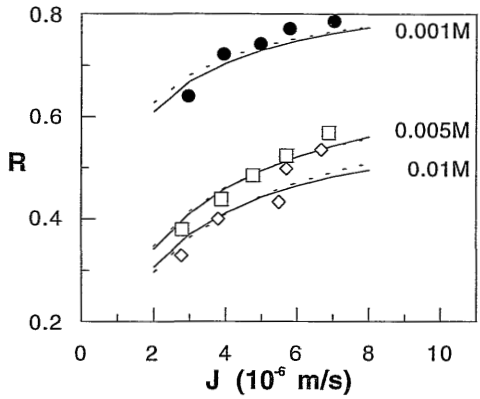

Figure 6.6: *NaCl retention as a function of the solvent flux for different electrolyte concentrations. Membrane: CTA-LP. Solid lines: calculation with variable membrane charge and membrane thickness, dashed lines: calculation with variable membrane charge and constant membrane thickness*

For the ASP35 membrane, the flux-retention curves of NaCl and $CaCl_2$ solutions were compared (Figure 6.7). As can be seen from this figure, the agreement between the calculated curves and the experimental data is good. The membrane thickness and membrane charge determined for 0.001M NaCl and $CaCl_2$ solutions were almost equal at the same feed concentration. The calculated negative membrane charge for the NaCl solution was 0.054 mol/l, the membrane thickness was $3.3*10^{-5}$ m. In case of $CaCl_2$, these parameters were 0.064 mol/l and $3.6*10^{-5}$ m, respectively. The difference in Donnan potential was the main difference between the behavior of the two solutions and this will have a large impact on the retention. The Donnan potential of the NaCl solution at the feed solution-membrane interface was about -95 mV, whereas in case of the $CaCl_2$ solution it was -43 mV. Because of the small concentration gradient within the membrane the calcium concentration at the permeate side is not much lower than that at the feed side, which results in a Donnan potential of -46 mV. For the sodium chloride solution, the concentration decrease of the ions within the membrane is much higher, which results in a calculated Donnan potential at the permeate side of -138 mV. This large difference in Donnan potential between the two interfaces caused the larger decrease of the sodium ion concentration and resulted in a high retention compared to that of the calcium ions.

However, the agreement between membrane parameters calculated from retention measurements with different electrolytes was not found for all membranes. For instance, in case of a UTC90 membrane, the membrane charge and the membrane thickness determined for a 0.001M NaCl solution differed significantly from that for a 0.001M Na_2SO_4 solution. Both the membrane charge and the membrane thickness were more than twice as high in the former case (NaCl: negative membrane charge: 0.215 mol/l, thickness $4.1*10^{-5}$ m; Na_2SO_4: negative membrane charge: 0.075 mol/l, thickness $2.0*10^{-5}$ m).

The calculation of the membrane charge and membrane thickness for the NF45 and CTA-LP

membrane and a $CaCl_2$ solution resulted in negative membrane charges which were higher than 1 mol/l. These are very high values that differ significantly from the values determined from the NaCl retention measurements as shown in Table 6.3. However, it should be mentioned that these membranes had $CaCl_2$ and Na_2SO_4 retentions which were higher than that of NaCl, which cannot be explained assuming a negatively charged membrane.

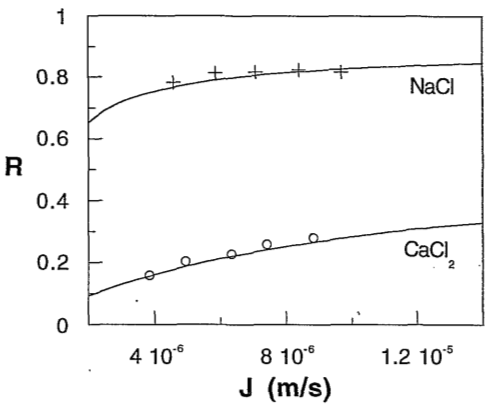

Figure 6.7: *NaCl and $CaCl_2$ retentions as a function of the solvent flux. Concentration: 0.001M. Membrane: ASP35. Solid lines are drawn according to the numerical model*

Salt mixtures

The model which was outlined in Chapter 2 was used to interpret the experimental data for the retention measurements with the anion and cation mixtures.
Figure 6.8 shows schematically the concentration profiles of sodium, chloride and sulfate ions within a negatively charged membrane.

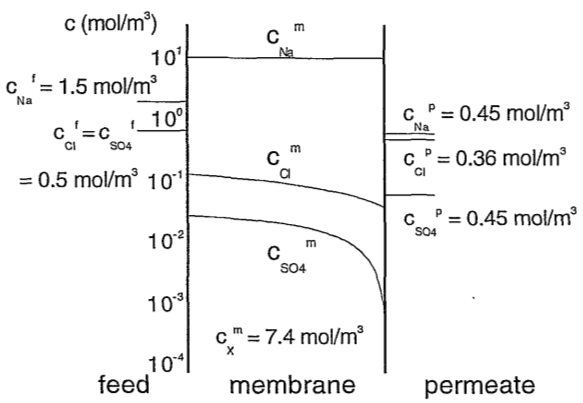

Figure 6.8: *Concentration gradients of sodium, chloride and sulfate ions in a negatively charged membrane and in adjacent solutions*

The membrane has a fixed charge of 0.0074 mol/l, whereas the feed contains 0.0005M NaCl and 0.0005M Na_2SO_4. As can be seen from Figure 6.8, the concentration of bivalent sulfate in the membrane is much lower than that of the other co-ion which has a lower valency, i.e., the chloride ion. This difference is caused by the Donnan potential which induces a larger concentration decrease at the membrane-solution interface in case of a multi-valent co-ion. The decrease of the sodium ion concentration across the membrane cannot be observed because of the logarithmic scale.

The experimental results of retention measurements with anion mixtures, performed with a UTC90 membrane, are shown in Figure 6.9. The chloride and sulfate ion retentions were determined for different compositions of the feed mixture. For these experiments the overall anion concentration was 0.01M, while changing the ratio of the chloride and sulfate ions.

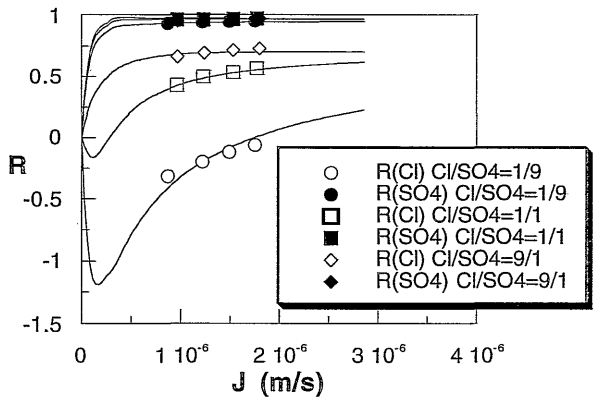

Figure 6.9: Cl^- and SO_4^{2-} retention as a function of the solvent flux for different ionic compositions in a $NaCl/Na_2SO_4$ mixture. Membrane: UTC90. Overall anion concentration: 0.01M. Solid lines are calculated.

The curves are drawn according to the set of equations presented in Chapter 2. As can be seen from Figure 6.9, the retentions of both chloride and sulfate ions could be described well by this model. Even the negative retentions of the chloride ions were predicted adequately. Differences in the relative contributions of the convective, diffusive and electric potential induced fluxes to the overall fluxes of the ions cause the minima in the flux-retention curves for the chloride ions. At low solvent fluxes the diffusive and electric potential induced fluxes determine the overall transport of ions, whereas the convective flux becomes the most important part at high fluxes.
To gain insight in the phenomenon of negative retention, chloride ion concentration profiles within the membrane have been calculated for anion mixtures with two different ratios of chloride and sulfate ions, 1/1 and 1/9, respectively. The overall anion concentration was 0.01M. As can be seen in Figure 6.10 (a), the chloride ion retention is positive for the former case, whereas it is negative for the latter case.

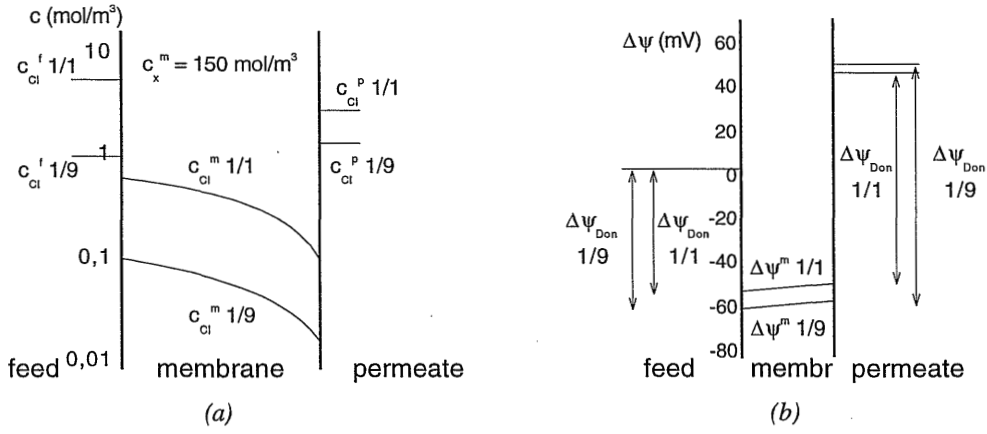

Figure 6.10 *(a): Concentration gradients of chloride ions in a negatively charged membrane and in adjacent solutions for an anion mixture with a molecular ratio of 1/1 and 1/9 chloride/sulfate. Total anion concentration: 0.01M. (b): Corresponding potentials with $\Delta\psi_{Don}$ the Donnan potential and $\Delta\psi^m$ the potential difference within the membrane*

The negative fixed charge density was chosen to be 0.150 mol/l and the membrane thickness $1*10^{-4}$ m.

The potential profiles for these two ratios are shown in Figure 6.10(b). For both ratios 1/1 and 1/9 chloride/sulfate the Donnan potentials between the permeate side and the membrane were higher, -100 and -104 mV, respectively, than those between the feed side and the membrane which were - 56 and - 64 mV, respectively. The negative Donnan potentials cause a decrease of the chloride ion concentration in the membrane compared to that in the feed. The higher Donnan potential at the permeate side of both mixtures is caused by the decrease of the ion concentration across the membrane. For the ion ratio chloride/sulfate 1/9, the higher Donnan potential at the feed side is caused by the higher concentration of sulfate ions, which increases the Donnan potential for a negatively charged membrane as has been shown in Chapter 2. The electric field within the membrane is constant as mentioned before. The potential over the membrane had a positive sign and was more or less equal for both chloride/sulfate ratios, i.e., 3.7 mV. As Figure 6.10 shows, the concentration of chloride ions in the permeate will be higher than that in the solution, i.e., a negative solute retention will be found.

For the cation mixtures the description of the experimental flux retention data was more difficult than for the anion mixtures. Figure 6.11 shows the experimentally and theoretically determined retentions of the sodium, calcium and chloride ions for the ASP35 membrane in case of an overall cation concentration of 0.01M and a Na^+/Ca^{2+} ratio of 1/9.

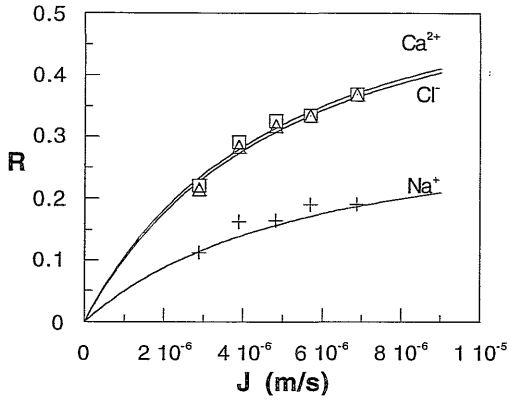

Figure 6.11: *Na^+, Ca^{2+} and Cl^- retention as a function of the solvent flux. Membrane: ASP35. Overall anion concentration: 0.01M, ratio Na^+/ Ca^{2+}: 1/9. Solid lines are calculated*

The negative fixed membrane charge density determined was 0.735 mol/l and the membrane thickness 5.2 $*10^{-5}$ m. This membrane charge density is much higher than that determined for a 0.001M NaCl solution as shown in Table 6.3. An explanation for this discrepancy cannot be given yet.

The model correctly described the retentions of the different ions of this mixture and predicted the retention of the calcium ions to be higher than that of the sodium ions. This result was different from that of the retention of sodium and calcium ions in a single salt solution, where the calcium ion retention was lower than that of the sodium ions (see Figure 6.7). The Donnan potentials determined for the experiments as shown in Figure 6.11 were about -48 mV at the feed side and -52 mV at the permeate side. The potential drop in the membrane was about 3 mV. The potentials across the membrane are shown in Figure 6.12(b).

The higher retention for the calcium ions is mainly determined by the difference in Donnan potential at the feed and at the permeate side. The higher Donnan potential at the permeate side, which is caused by the lower electrolyte concentration in the membrane at the permeate side, affects the relative concentration decrease for the calcium ions diffusing from feed to permeate phase more than that for the sodium ions. This is a result of the higher valency of the calcium ion (the solute distribution can be written as: $\frac{c^m}{c^0} = \exp\left(-\frac{z F}{R T}\Delta\psi_{Don}\right)$, see Chapter 2).

Figure 6.12(a) shows the concentration profiles of the sodium, calcium and chloride ions within the membrane. Because of the negative membrane charge, the concentrations of both calcium and sodium ions were higher within the membrane than in the solution. The concentrations of both cations remain more or less constant across the membrane thickness.

The calculation of the membrane charge for other combinations of a membrane and a cation mixture sometimes resulted in unrealistic high values of this parameter, such as a negative membrane charge of 6.3 mol/l. As observed before, the membrane charge is influenced by the choice of the diffusion coefficients. When these are lower than the values used in this thesis, the corresponding membrane charge will be lower as well.

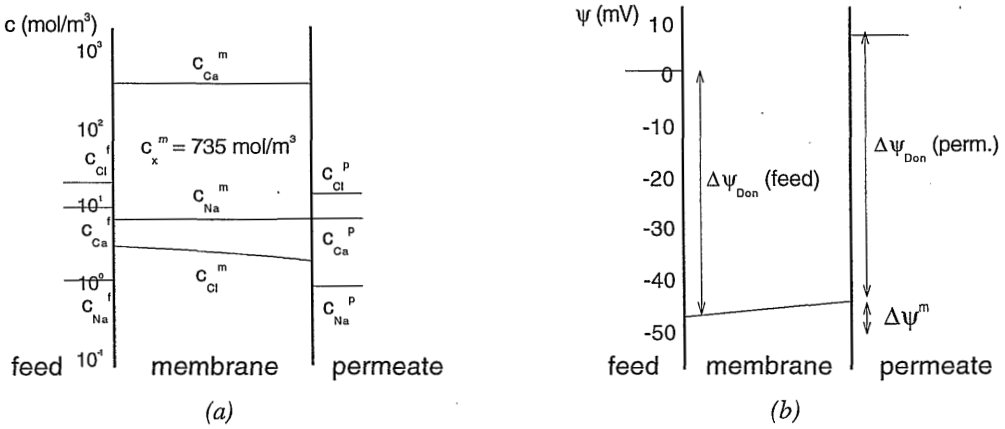

***Figure 6.12**(a): Concentration gradients of sodium, calcium and chloride ions in a negatively charged membrane and in adjacent solutions. Overall anion concentration: 0.01M, ratio Na^+/ Ca^{2+}: 1/9. (b): Corresponding potentials, with $\Delta\psi_{Don}$ the Donnan potential and $\Delta\psi^m$ the potential difference within the membrane*

In case of the cation mixtures, negative retentions of sodium ions were observed (see for instance Fig 3.11), like for chloride ion in case of the anion mixtures. However, these negative retentions could not be described adequately by the model as presented in Chapter 2. It is not clear yet what causes the discrepancy between the model and the experimental results for this specific case.

To achieve a negative retention for a positively charged ion within a negatively charged membrane, the concentration gradient of this ion in the membrane should be higher than the difference between the changes in concentration at either side of the membrane which are caused by the Donnan potentials. Since the Donnan potential at the permeate side will be larger than that at the feed side, because of the lower electrolyte concentration at the permeate side in the membrane, the concentration gradient in the membrane should be positive:

$$\frac{d\, c_i^m}{d\, x} > 0 \qquad \{6.4\}$$

so

$$\frac{J_v}{P_i^m}\left(K_{i,c}\, c_i^m - c_{i,p} \right) - \frac{z_i F}{R T} c_i^m \frac{d\, \psi^m}{d\, x} > 0 \qquad \{6.5\}$$

(see equation {2.29}). In case of a negative membrane charge, the sodium ion concentration in the membrane will be higher than that in the permeate, so the first term at the left-hand side of equation {6.5} will be positive. Because the second term at the left-hand side will be positive as well, this means that a positive concentration gradient will result if the first term is larger than the second term. Only in that case, a negative retention may result.

6.4 CONCLUSIONS

The relation between the retention of saccharides and the solvent flux could be described very well by the phenomenological relations for a system consisting of one solvent and one solute. The calculated reflection coefficients of the various saccharides increased with increasing molecular weight of the molecules, whereas their permeability coefficient decreased. It was not possible to relate the reflection coefficient and the permeability coefficient to a membrane pore size, since the pore model used did not describe the experimental results adequately.
The extended Nernst-Planck equations resulted in good agreement between the theoretical and experimental retentions for both single salt solutions and salt mixtures. The calculations resulted in negative fixed membrane charge densities of 0.215 to 0.02 mol/l for the polymeric nanofiltration membranes investigated and a positive fixed charge density of 0.025 mol/l for the ceramic γ-Al_2O_3 membrane. The calculated effective membrane thicknesses were in the range of $1*10^{-5}$ to $1*10^{-4}$ m. These thicknesses are rather high compared to those observed by SEM, which may result from the fact that effective thicknesses have been calculated, which include different factors that cause resistance to solute transport. The values of the membrane charge and thickness calculated are dependent on the diffusion coefficients of the ions used.
The negative retention of the chloride ions in a mixture with sulfate could be described well by the extended Nernst-Planck equation. Furthermore, the model predicted a higher retention for the calcium ions than for the sodium ions in a cation mixture in the case of a negatively charged membrane. The same retention behavior was experimentally found.
The negative retentions of sodium ions in a cation mixture could not be explained.

ACKNOWLEDGEMENTS

Jeroen Boom is kindly acknowledged for the programming of the numerical procedure to calculate the Nernst-Planck equation and the discussions on this topic. Prof. A. Yaroshchuk and Carla Koopman are acknowledged for the discussions on the topic of the interpretation of salt retention measurements.

SYMBOLS

c:	concentration	(mol/l)
D:	diffusion coefficient	(m^2/s)
F:	Faraday constant	(C/mol)
f (λ):	wall correction factor for diffusive transport	(-)
g (λ):	wall correction factor for convective transport	(-)
J_v:	solvent flux	(m/s)
$K_{i,d}$:	diffusive coupling coefficient	(-)
L:	$= L_s/\Delta x$, solute permeability coefficient corrected for the membrane thickness	(m/s)

L_s:	solute permeability coefficient in two component system	(m^2/s)
p:	porosity	(-)
P:	pressure	(bar, N/m^2)
Pe:	Péclet-number	(-)
r:	radius	(m)
R:	gas constant	(J/mol.K)
R:	retention	(-)
S:	hindrance factor	(-)
T:	temperature	(K)
Δx:	membrane thickness	(m)
z:	valence	(-)
η:	viscosity	(Pa.s)
λ:	ratio of solute size and pore size	(-)
σ:	reflection coefficient	(-)
τ:	tortuosity	(-)
ψ:	potential	(V)

subscripts:

D:	diffusive
Don:	Donnan
eff:	effective
f:	feed
F:	convective
i:	species i
p:	pore
p:	permeate
s:	solute
X:	fixed membrane charges

superscript:

m:	membrane (phase)

REFERENCES

[1] Nakao, S., *Membrane transport phenomena and ultrafiltration*, in: Encyclopedia of Fluid Mechanics; Vol. 2,4,5, ed. by N.K. Cheremisinoff, Gulf Publ. Comp., Houston, 1986, p. 987

[2] Bowen, W. R., Mukthar, H., *Characterisation and prediction of separation performance of nanofiltration membranes*, J. Membrane Sci., 112 (1996) 263-274

[3] Tsuru, T., Nakao, S.I., Kimura, S., *Effective charge density and pore structure of charged ultrafiltration membranes*, J. Chem. Eng. Jap., 23 (1990) 604

CHAPTER 7

Conclusion: comparison of characterization techniques for nanofiltration membranes

ABSTRACT

In this thesis various techniques have been described to characterize nanofiltration membranes. This final chapter is aimed to relate and compare these different methods.

Parameters calculated from electrolyte retention measurements were compared with experimentally determined properties, such as the Donnan potential with the zeta potential and the calculated charge density with the titrated charge density.

The influence of the electrolyte concentration on the membrane charge density was shown for both the streaming potential and the electrolyte retention measurements.

Finally, the electrolyte retentions measured for four polymeric nanofiltration membranes were compared and related to experimentally determined properties, like the kinetic surface charge density, the titrated charge density, the glucose retention and the solvent permeability.

7.1 INTRODUCTION

The characterization of membranes gives insight in the transport mechanism of solutes through a membrane and may give information about the relation between structure and separation properties.
In case of nanofiltration membranes, a variety of membrane structures exist. Charged as well as uncharged, porous as well as solvent-swollen, polymeric as well as ceramic, and all these different membranes may have comparable separation performances. For each of the membranes a certain combination of exclusion effects and transport phenomena determines the solute transport and separation.
When the characteristics of different nanofiltration membranes are compared, it should be realized that these membranes may have very different morphologies. Therefore, the characterization of nanofiltration membranes can be carried out preferably by methods which determine performance related properties. Membrane parameters, like fixed charge density and thickness, may then be estimated from these characterization methods, such as the electrolyte retention measurements as was shown in Chapter 6. However, this does not imply that characterization methods which determine membrane structural parameters, like pore size and pore size distribution, are not suitable for nanofiltration membranes. For instance, in case of permporometry, the pore size distribution of a membrane is measured. However, when the pore size is smaller than 2 nm or the membrane does not have any fixed pores because of its network morphology, no pore sizes can be calculated using capillary condensation theories. This is different from the calculation of pore sizes from, for instance, the saccharide retention measurements as shown in Chapter 6. In this case, membrane pores were assumed to be present, but this does not imply that the membrane really should have pores to achieve this separation.

In this thesis several characterization methods for nanofiltration membranes have been used, like saccharide and electrolyte retention measurements, titration and streaming potential measurements. In this final chapter, these characterization methods will be compared. Firstly, the Donnan potentials which were calculated from the electrolyte retention measurements will be compared with the zeta potentials determined by the streaming potential measurements. Secondly, the membrane charge measured by titration will be related to the calculated values from the retention measurements. Furthermore, the dependence of the membrane charge on the electrolyte concentration will be investigated for the streaming potential and electrolyte retention measurements. Finally, the results of the salt retention measurements will be compared to the charge densities as calculated from the streaming potential measurements. The results of the saccharide retention measurements will be included in this discussion as well.

7.2 DONNAN AND ZETA POTENTIALS

In a stationary situation, different equilibria exist between solutes in the bulk solution and in

the membrane. When ions in combination with a charged membrane are considered, a Donnan equilibrium exists between the ions in the bulk and the mobile ions in the membrane. This Donnan equilibrium is both dependent on the membrane charge and on the concentration and kind of electrolyte. Furthermore, an equilibrium distribution exists between the ions in the solution and the ions adsorbed at the membrane surface. These phenomena are influenced by the adsorption energies of the ions at the surface and by electrostatic interactions between membrane surface and ions. Because of these adsorbed ions, the membrane may behave in the same way as if these adsorbed charges would have been fixed charges, therefore, influencing the Donnan equilibrium.

Not only different distribution equilibria near the membrane-solution interface can be distinguished, but also different potentials, which correspond to these distribution equilibria. Two important potentials near this interface are the Donnan potential and the zeta potential. The former can be situated exactly at, or a little inside, the membrane, whereas the latter lies at the shear plane between the fixed and the diffusive part of the double layer, just at a small distance from the membrane surface within the solution. The Donnan potential provides information on the electric charges inside the membrane, whereas the zeta potential mainly gives information on the charge at the membrane surface. In Figure 7.1, the potential distribution within a membrane and the adjacent electrolyte solutions is schematically shown. The Donnan potential reflects the unequal ionic distribution between the membrane and the bulk solution in case of a charged membrane and represents the resulting potential difference. The zeta potential is induced by the ionic distribution within the solution near a charged surface and equals the potential difference between the potential at the shear plane of membrane and electrolyte solution and that of the bulk.

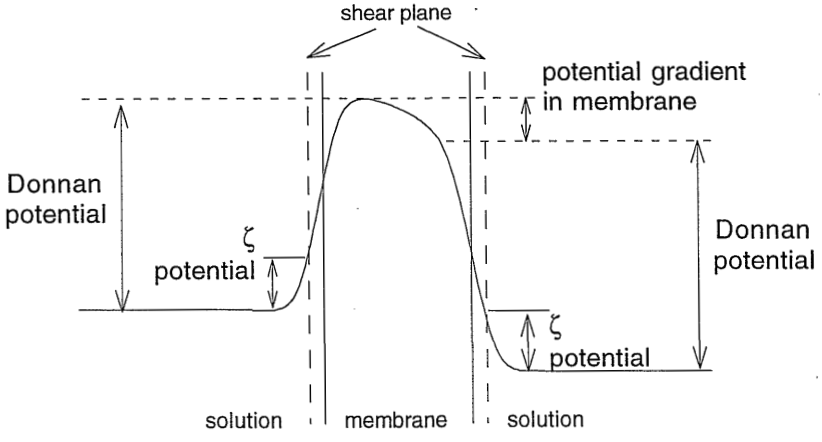

Figure 7.1: *Schematic drawing of the potential distribution in a membrane-electrolyte solution system, showing the zeta (ζ) and Donnan potentials ($\Delta\psi_{Don}$)*

Figure 7.2 shows the Donnan and zeta potentials for a ASP35 membrane in contact with NaCl solutions of various concentrations. Both potentials were negative in the concentration range

investigated and both decrease with increasing electrolyte concentration. The Donnan potential is always higher than the zeta potential, which indicates that a higher charge will be present within the membrane than at the shear plane between membrane and electrolyte solution. Since the potential within the Stern-layer will decrease because of adsorbed ions in this layer (as can be seen from Figure 5.3), it is expected that the Donnan potential would be higher than the zeta potential.

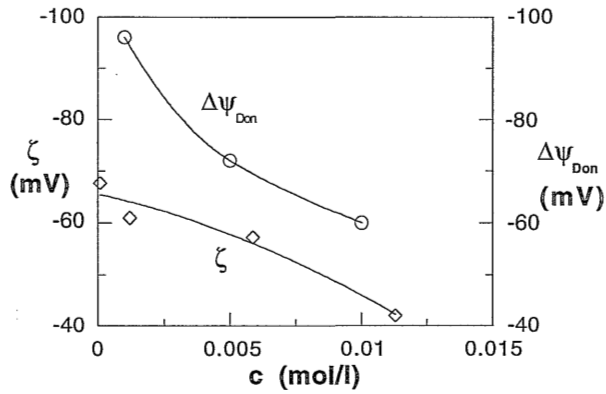

Figure 7.2: *Donnan, $\Delta\psi_{Don}$, and ζ potentials as a function of the NaCl feed concentration for a ASP35 membrane*

For the other membranes and electrolyte solutions investigated the sign of the Donnan and zeta potential was always the same, i.e., negative for the polymeric membranes and positive for the ceramic membrane. However, the difference between both potentials for these membranes was even more pronounced than for the ASP35 membrane.

The difference between the Donnan and the zeta potential, which was in most cases more than 50 mV, showed the large discrepancy between the potential which is measured just outside the membrane and the potential which influences the ionic distribution over membrane and electrolyte solution. If the calculated values of the Donnan potentials are correct (they are influenced by the choice of the ionic diffusion coefficients), then it can be concluded that the zeta potentials do not show a good agreement with the potential within the membrane. In that case, electrokinetic measurements by which zeta potentials are obtained do not seem a very appropriate technique to determine the (Donnan) potential of nanofiltration membranes which influences the ion selectivity.

Of course, it should be considered that the calculation of the membrane charge from the retention measurements results in a charge which is assumed to be homogeneously distributed over the membrane, so no differences in charge density are thought to exist as a function of the membrane thickness. This can be a cause of the differences between zeta and Donnan potential. Differences between the charges at the surface and charges inside the membrane, i.e., between the zeta and the Donnan potential, were shown by Takagi and co-workers as well [1]. They attributed these differences to the different mechanisms to may play a role at the surface or

within the membrane, for instance, the dissociation of ionic groups that may cause the surface charge, or adsorption of ions that can influence the effective charge within the membrane.

7.3 MEMBRANE CHARGE

Membrane charge can result from two factors, i.e, from the fixed charged groups present in the membrane material and from the adsorption of ions within the membrane or at the membrane surface. Titration experiments and retention measurements with low concentrations of electrolytes give insight in the first phenomenon and information on the bulk properties of the membrane may be obtained. Ionic adsorption can be investigated by the determination of the membrane charge as a function of the electrolyte concentration.

7.3.1 Titrated and calculated membrane charge density

The bulk membrane charge density was determined by two different characterization methods. By titration experiments the membrane charge was measured directly. It gives the concentration of acidic groups of the various polymeric membrane materials. In case of the electrolyte retention measurements, the membrane charge was calculated from the experimental data. The membrane charge density which was calculated for a 0.001M NaCl solution was compared to the results of the titration measurements. The membrane charge determined for the lowest electrolyte concentration used in the retention measurements was chosen, since ion adsorption at the membrane surface was thought to be minimal. The results of the membrane charge determination of both methods are summarized in Table 7.1.
The density of most polymers is around 1 kg/dm^3.
As can be seen from this table, the order of magnitude of the membrane space charge density is equal for the titration and the retention experiments. However, only in case of the NF45 membrane the values are more or less comparable. The membrane charge density of the UTC90 membrane calculated from the retention measurements is very high compared to the titration results, which may be affected by the (high) ionic diffusion coefficients used in the calculation. The difference between the membrane charge density of the ASP35 membrane and that of the

Table 7.1: *Membrane charge density, c_X^m, determined by titration and by retention measurements with 0.001M NaCl*

membrane	c_X^m (mol/kg) (titration)	c_X^m (mol/l) (retention)
ASP35	0.108	0.054
NF45	0.017	0.020
UTC90	0.040	0.215
CTA-LP	0.014	0.034

CTA-LP and NF45 membranes determined by titration is larger than that in case of the retention measurements.

Comparing the results for the titration and the retention measurements, it should be realized that in case of titration all ionizable groups have been determined, whereas in case of the retention measurements the amount of charged groups at pH = 6 has been obtained. Therefore, the membrane charge density obtained by titration was expected to be higher than that obtained from the retention measurements. However, this is not the case for three of the membranes shown in Table 7.1. Possibly, the estimation of the ionic diffusion coefficients within the different membranes causes this discrepancy.

7.3.2 Membrane charge density and electrolyte concentration

Both streaming potential measurements and electrolyte retention measurements resulted in membrane charges which were measured at different electrolyte concentrations. In case of the streaming potential measurements the surface charge density (amount of charges per area) at the shear plane was measured, whereas in case of the retention measurements the space charge density was calculated (amount of charges per volume).
The increase of the surface charge density at the shear plane between membrane and electrolyte solution was assumed to be enhanced by an increase in ion adsorption with increasing salt concentration (see Chapter 5). This ion adsorption could be described, in almost all cases, by a Freundlich isotherm. In case of the electrolyte retention measurements the membrane space charge could be determined for only three concentrations. These membrane charges are shown in Figure 7.3 as a function of the electrolyte concentration for some membrane-electrolyte systems.

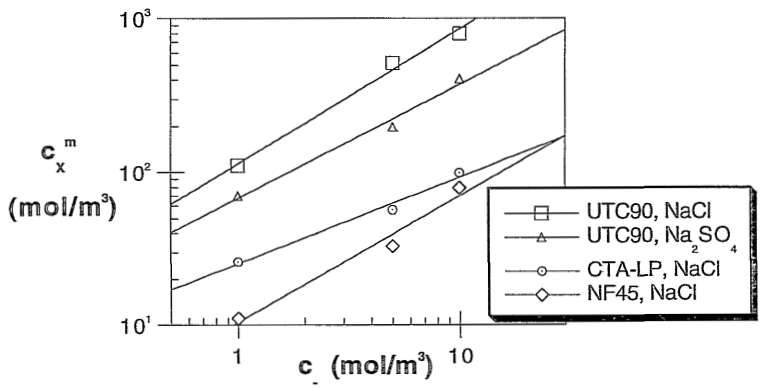

Figure 7.3: *Membrane charge densities, c_X^m, as a function of the anion concentration, c, for different nanofiltration membranes and different electrolytes. The lines refer to values calculated by equation {7.1}*

As can be seen from Figure 7.3, the membrane charge density increased with increasing

concentration. Since the negative charge of the membrane became higher, it was assumed that the anions adsorbed at the membrane material. Like in case of the surface charge densities calculated from the streaming potential measurements, it was tried to relate the anion concentration with the membrane charge by a Freundlich isotherm :

$$c_X^m = a\, c_-^b \qquad \{7.1\}$$

with c_X^m the membrane charge, c_- the anion concentration and a and b being constants. In this case it was assumed that all charges present in the membrane were adsorbed charges. It should be realized that describing the charge densities in terms of ion adsorption, the influence of the ionic strength on the dissociation rate of the acidic groups in the membrane has been neglected. The lines in Figure 7.3 are drawn according to this equation. Because only three membrane charge densities were calculated from the retention measurements, it is difficult to draw conclusions about the agreement between the Freundlich isotherm and the experimental relation of the anion concentration and the membrane charge. Therefore, the constants a and b for the Freundlich isotherm in this case will not be compared to those calculated from the streaming potential measurements. From these two types of membrane charge densities it should be considered that the streaming potential measurements result in *surface* charge densities, whereas in case of the retention measurements *space* charge densities are calculated.
Moreover, a comparison between these two membrane charge densities would have been difficult, since the assumptions which were used to describe both, i.e., the increase of the kinetic surface charge density and that of the calculated membrane charge density, as a function of the electrolyte concentration were different. In case of the kinetic surface charge density, the membrane charge density was assumed to be constant, whereas the variation in the kinetic surface charge density was attributed to ion adsorption at the surface. In case of the calculated membrane charge density, as shown in Figure 7.3, it was assumed that the membrane charge was homogeneously distributed over the membrane. The overall membrane charge density varies with the electrolyte concentration because ion adsorption is assumed to occur everywhere in the membrane and not only at its surface. Therefore, the surface and the space charge density can only be adequately compared, if the assumptions concerning ion adsorption are equal for both charge densities.

7.4 ELECTROLYTE RETENTION

The membrane charge and membrane thickness as calculated from electrolyte retention measurements can give an indication for the differences in separation behavior between the membranes investigated. When the membrane charge and thickness are known, the contributions of the convective, the diffusive and the electric transport to the overall solute transport can be determined. However, since the ionic diffusion coefficients were assumed to be identical in all membranes, the influence of the ionic size on the separation was not explicitly taken into account. Because some diffusive hindrance was expected, the effective diffusion

coefficients which were used in the model calculations were smaller than the ones within solution. In this section the electrolyte retentions of the ASP35, UTC90, NF45 and CTA-LP membranes will be compared and possible explanations for the differences in behaviour will be given based on the kinetic charge densities as determined from the streaming potential measurements, the titrated membrane charges, the saccharide retentions and the solvent permeabilities.

ASP35 and UTC90 membrane

When comparing the retention of an 0.001M NaCl and Na_2SO_4 solution for the ASP35 and the UTC90 membrane, it can be seen from Table 7.2 that the UTC90 membrane shows both a higher NaCl and a higher Na_2SO_4 retention. The retentions were measured at the same hydrostatic pressure difference, ΔP = 7 bar. The difference in retention between NaCl and Na_2SO_4 might be attributed to the higher charge for this membrane as can be seen from Table 7.1.

Table 7.2: *NaCl and Na_2SO_4 (0.001M) retentions for ASP35 and UTC90 membrane*

	ASP35	UTC90
R (NaCl)	0.82	0.93
R (Na_2SO_4)	0.90	0.98

By comparing the glucose retentions and the kinetic surface charge densities which were determined by the streaming potential measurements with the electrolyte retentions, an alternative explanation for the higher retention of the UTC90 membrane could be found. In this way, the membrane charges calculated from the electrolyte retention measurements, which are influenced by the choice of the ionic diffusion coefficients, are not considered.
The kinetic surface charge densities determined for the UTC90 membrane were lower than those for the ASP35 membrane, as shown in Chapter 5, which indicated that charge effects were smaller for the UTC90 than for the ASP35 membrane. Since the solvent permeability was much lower for the UTC90 than for the ASP35 membrane (L_v (ASP35) = 4.3 l/m^2.h.bar; L_v (UTC90) = 2.3 l/m^2.h.bar), differences in the hindrance of solute transport were assumed to influence the electrolyte separation for the UTC90 membranes more strongly. This is supported by the retention measurement with glucose that showed a much higher value for the UTC90 membrane (R > 0.85) than for the ASP35 membrane (R < 0.15). Figure 7.4 shows the retention for the various saccharides for both membranes as a function of their radius. As a comparison the range of ionic radii is shown in this figure as well. Although the radii of the ions are much smaller than those of the saccharides, it can be seen from this figure, that most probably, the steric hindrance of solute transport will be smaller in case of the ASP35 membrane than for the UTC90 membrane. This implies a higher ion diffusion coefficient in the ASP35 membrane. Therefore, the high retention of NaCl and Na_2SO_4 of the UTC90

membrane may be the result of both size and charge effects, although the size effects seem to be most important. The electrolyte retention of the ASP35 membrane will be influenced more by charge than by size effects. The very low retention for $CaCl_2$ for this negatively charged membrane, R (0.001M $CaCl_2$) < 0.30, and the larger influence of the electrolyte concentration on the retention seem to indicate the relatively small importance of the size of the hydrated ions.

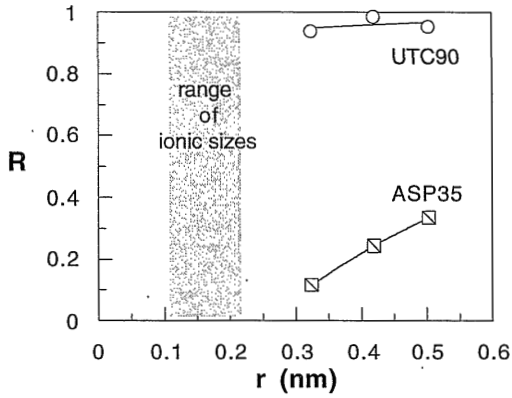

Figure 7.4: *Retention of saccharides as a function of their radius for a ASP35 and a UTC90 membrane. The range of sizes of the hydrated ions investigated is indicated by the shaded area.*

ASP35, CTA-LP and NF45 membrane

The membrane charge densities for the CTA-LP and NF45 membrane were always smaller than that of the ASP35 membrane, irrespective of the characterization method used. The saccharide retentions of the former membranes were much higher than those of the ASP35 membrane. Therefore, it was concluded that size effects for electrolyte separation were more important, whereas charge effects were less important in case of the CTA-LP and the NF45 membrane compared to the ASP35 membrane. This qualitative conclusion was supported by the salt retention measurements given in Chapter 3, which characterized the ASP35 membrane as a negatively charged membrane and the other two membranes as membranes for which both size and charge effects determined the salt separation.

UTC90, CTA-LP and NF45 membrane

The main factor influencing the high salt retention for the UTC90 membrane, compared to the CTA-LP and NF45 membrane, seems to be the low solute transport rate through this membrane. The low glucose permeability (see Table 6.1) for the UTC90 membrane is an indication for this low salt transport, whereas the low solvent permeability which was determined by the pure water flux measurements shows a large resistance for membrane transport as well. The different membrane charges determined by the different characterization techniques provide no information on the relative influence of the membrane charge on the

electrolyte retention for these membranes.

CTA-LP and NF45 membrane

For the NF45 membrane, a large difference was found between the retention of NaCl and $CaCl_2$ and Na_2SO_4 (see Table 7.3). For the CTA-LP membrane these differences are much smaller. It is not clear yet what causes this difference between these membranes. Neither the membrane charges which were determined by the different techniques, nor the retention measurements with the saccharides or the solvent permeabilities showed a distinct difference for the CTA-LP and the NF45 membrane, although the differences in NaCl retention are obvious.

Table 7.3: *NaCl , $CaCl_2$ and Na_2SO_4 (0.001M) retentions for NF45 and CTA-LP membrane*

	R(NaCl)	R($CaCl_2$)	R(Na_2SO_4)
NF45	0.52	0.90	0.91
CTA-LP	0.79	0.88	0.99

7.5 CONCLUSIONS

The characteristics of the nanofiltration membranes investigated in this work were compared with each other in this chapter.
The Donnan potentials calculated from the electrolyte retention measurements and the zeta potentials which resulted from the electrokinetic measurements showed that the Donnan potentials were always higher than the zeta potentials. Both the Donnan and the zeta potential had a negative charge for the polymeric membranes, whereas they were positive for the γ-Al_2O_3 membrane. Both potentials decreased with increasing electrolyte concentration.
The membrane charge densities calculated from the electrolyte retention measurements and those determined by titration were of the same order of magnitude. Differences between these values may result from the chosen value of the diffusion coefficients of the ions which influence the membrane charge density calculated from the retention measurements. The membrane charge density for both the retention and the streaming potential measurements showed an increase with increasing electrolyte concentration, which could be described in both cases with a Freundlich isotherm. However, since only three concentrations were investigated for the retention measurements, no conclusions could be drawn from this relationship.
The electrolyte retention for the ASP35 membrane was mainly attributed to the influence of electrostatic interactions between ions and the membrane. In case of the UTC90, CTA-LP and NF45 membrane, the solute size effects were thought to determine the separation. The UTC90

membrane showed the highest salt retention of the membranes compared, which was due to a low solvent and solute permeability.

SYMBOLS

a,b:	constant	(-)
c:	concentration	(mol/l)
r	radius	(m)
R:	retention	(-)
ζ:	zeta potential	(V)
ψ:	potential	(V)

subscripts:

Don: Donnan

X: fixed membrane charges

-: anion

superscripts:

m: membrane

REFERENCES

[1] Takagi, R., Tagawa, M., Gotoh, K., Nakagaki, M., *Variation of membrane charge of Nylon 6 with pH*, J. Membrane Sci., 92 (1994) 229-238

Levensloop

Marjo Peeters werd op 17 juli 1967 geboren in Stramproy. In 1985 haalde ze haar Gymnasium diploma aan het Bisschoppelijk College in Weert en aansluitend begon ze met haar studie Chemische Technologie aan de Universiteit Twente. Na het behalen van haar propaedeuse in september 1986 werd de studie Chemische Technologie gecombineerd met de bovenbouw-studie Wijsbegeerte van Wetenschap, Technologie en Samenleving. De studie Chemische Technologie werd in 1992 afgerond met een afstudeeronderzoek op het gebied van karakterisering van ultrafiltratiemembranen voor niet-waterige oplossingen bij dr. M.H.V. Mulder binnen de onderzoeksgroep Membraantechnologie. In 1993 werd haar studie Wijsbegeerte van Wetenschap, Technologie en Samenleving afgesloten met een afstudeer-scriptie bij de vakgroep Filosofie van Wetenschap en Samenleving onder leiding van prof. dr. A. Rip. Hierin werd de technologieontwikkeling van een nieuw type membraan bij het bedrijf Delair beschreven. In februari 1993 startte zij haar promotieonderzoek op het gebied van de karakterisering van nanofiltratiemembranen. Het in dit proefschrift beschreven onderzoek werd uitgevoerd onder leiding van prof. dr. ir. H. Verweij van de vakgroep Anorganische Materiaal-kunde en prof. dr. H. Strathmann van de vakgroep Membraantechnologie aan de Universiteit Twente.

ISBN 978-3-86509-157-7